7-2015

Modeling Radiation Heat Transfer for Building's Cooling and Heating Loads: Considering the Role of Clear, Cloudy, and Dusty Conditions in Hot and Dry Climates

Salem Ahmed Algarni
University of Arkansas, Fayetteville

Recommended Citation

Modeling Radiation Heat Transfer for Building's Cooling and Heating Loads: Considering the Role of Clear, Cloudy, and Dusty Conditions in Hot and Dry Climates

Modeling Radiation Heat Transfer for Building's Cooling and Heating Loads: Considering the
Role of Clear, Cloudy, and Dusty Conditions in Hot and Dry Climates

A dissertation submitted in partial fulfillment
of the requirements for the degree of
Doctor of Philosophy in Mechanical Engineering

by

Salem A. Algarni
King Khalid University
Bachelor of Engineering in Mechanical Engineering, 2007
Oklahoma State University
Master of Science in Mechanical and Aerospace Engineering, 2010

July 2015
University of Arkansas

This dissertation is approved for recommendation to the Graduate Council.

_____
Dr. Darin W. Nutter
Dissertation Director

_____   _____
Dr. Rick J. Couvillion   Dr. Uchechukwu C. Wejinya
Committee Member   Committee Member

_____   _____
Dr. Larry A. Roe   Dr. Chase E. Rainwater
Committee Member   Committee Member

Abstract

The influence of transient factors such as sky long wave radiation exchange and atmospheric aerosols (i.e., smog, and dust – made up of sand, clay, and silt) are not carefully considered in current building design and simulation models. Therefore, the research objective was to better understand and account for such variables, resulting in improved radiative predictive capabilities, especially important for hot and dry climates under different sky conditions including clean, cloudy, and dusty. Overall, results of this dissertation provided a better prediction method for sky long wave radiation exchange with a building's roof and the impact of dust accumulation on energy use, especially for poorly and uninsulated residential buildings. The two most significant results for this study were (1) a new absorptivity model was introduced in an effort to relate a building's exterior roof solar and thermal properties (absorptivity, reflectivity, and emissivity) to monthly averaged dust accumulation, and (2) a new dusty sky temperature model was introduced as a function of atmospheric aerosol optical depth to better account for dust impact on sky temperature prediction.

Acknowledgements

First of all, I would like to praise *Allah* for providing me with strength and endurance to complete this project. Additionally, I would like to express my appreciation to everyone who provided me with the help to complete this project.

One of the most important contributions towards my success was the chair of my committee, Professor Darin Nutter. His guidance and patience as well as providing excellent and stimulating environments were outstanding in my educational development. Though I consider his friendship most endearing, his proficient knowledge and wisdom provided me with motivation and confidence. His dedication to his work and availability to his students are remarkable qualities that proved successful in my journey.

Committee members Professors Rick Couvillion, Larry Roe, Uchechukwu Wejinya, and Chase Rainwater were outstanding through my progression. The committees' valuable collaboration has been a helpful asset and contribution in the overall project.

Thanks to my home university, King Khalid University, for the financial support. The study would not have existed without their support. Thanks to all my friends and people of the Islamic Society of North West Arkansas for advice, suggestions, and the good times that we had together.

I would like to express the deepest gratitude to my parents and family back home whom always are offering me unconditional love and unlimited support.

Last, but certainly not least, special thanks to my wife for her support throughout the entire journey: her encouragement, sacrificing, and understanding.

Dedication

To my wife, son and daughter.

Table of Contents

List of Figures

List of Tables

List of Publications

Algarni, S., Nutter, D., 2013. Geospatial Representation of the Residential Energy Use in Saudi Arabia. Proceedings of the 2013 ASME Early Career Technical Conference (ECTC), April 4–6, Tulsa, Oklahoma, USA.

Algarni, S., Nutter, D., 2015. Survey of Sky Effective Temperature Models Applicable to Building Radiant Heat Transfer., ASHRAE *Transactions*, vol. 121, part 2-in press.

Algarni, S., Nutter, D., 2015. Effect of Clouds and Dust Storms on the Sky Radiation Exchange for Buildings Located in Hot-Dry Climates, Science and Technology for the Built Environment, 21(4):403–412.

Algarni, S., Nutter, D., 2015. Influence of Dust Accumulation on Building Roof Thermal Performance and Heat Gain, Energy and Buildings-in press.

1. Introduction

Heating, ventilating, and air-conditioning (HVAC) design models are used to estimate necessary equipment capacity and the expected system energy use. To do this, thermo-physical relationships are used to predict various heat transfer phenomena. Historically, incident solar radiation effects have not been studied as much as other building heat transfer interactions, such as conduction and convection. Consequently, the influence of transient factors such as sky long wave radiation exchange and atmospheric aerosols (i.e., smog, and dust – made up of sand, clay, and silt) are not carefully considered in current building design and simulation models. Therefore, the main objective of the research described in this dissertation is to better account for such variables, resulting in improved radiative predictive capabilities, especially important for hot and dry climates.

In order to accomplish the dissertation main objective, the following "built-up" topics were investigated: (1) understanding building characteristics for those existing in hot and dry climates; (2) studying current sky long wave radiation temperatures models and the primary factors which influence the temperature calculations; (3) quantifying the impact of sky radiative cooling on building roof thermal behavior considering the role of clear, cloudy and dusty sky conditions; and (4) investigating the influence of dust accumulation on building transient variables under the conditions of hot-dry climates. These "built-up" studies are briefly described below and depicted in Figure 1.1.
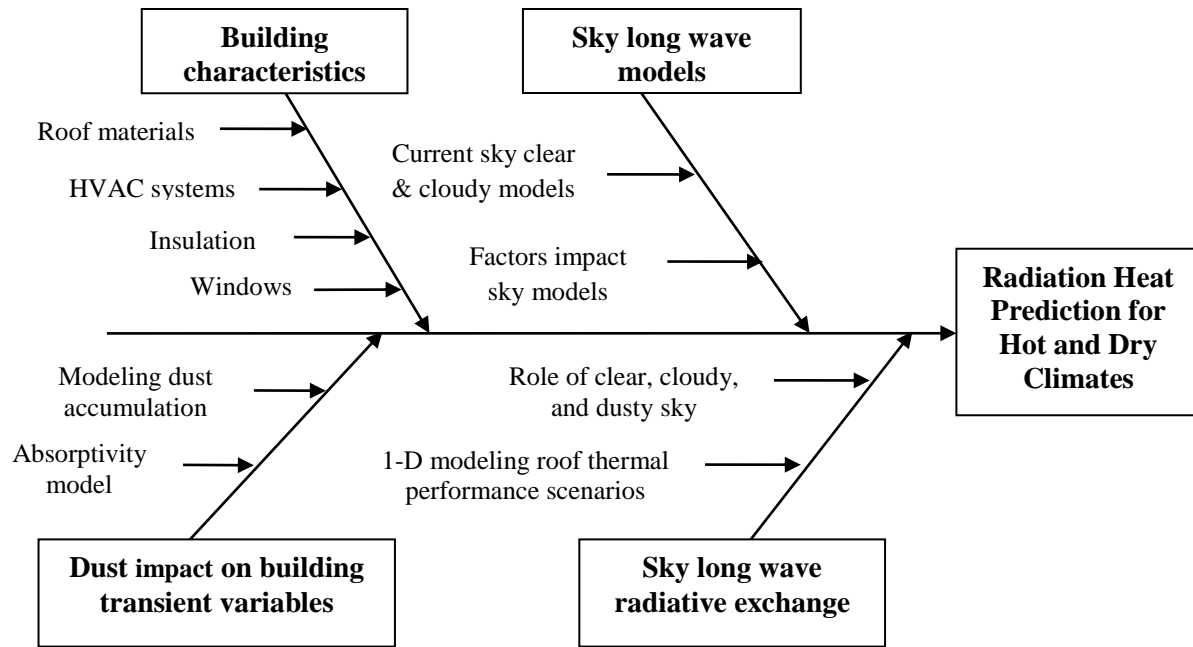
Figure 1.1 Overview of related parameters and topics needed to improve the current predictive capability of building simulation programs for hot and dry climates

1.1. Building characteristics

An understanding of the 'big picture' was sought. In extreme hot and dry climates, excessive heat causes an occupant thermal discomfort. Therefore, buildings consume a substantial portion of energy due to the high demand on cooling [1]. For example, in a hot and dry site such as Saudi Arabia, about 76% of generated electric energy is used for operating residential, governmental and commercial buildings. Moreover, about half of the total consumption is used for the residential sector [2] compared to 22% in USA [3]. The residential sector's high consumption is due to the inefficient buildings, high cooling loads, and harsh climate in this area of the world. Therefore, an understanding of building heat transfer elements is very essential.

2

Considering that the residential sector is a major energy consumer, the limitations of previous studies, and the rapid growth in the energy demand, it can be concluded that more comprehensive energy system studies are needed. Therefore, a simulation study was performed for common residential buildings in Saudi Arabia, an extreme hot and dry climate. The building energy simulation program known as eQuest (v. 3.64) was used to model representative building base cases, which were compared to potential energy efficiency improvements.

1.2. Sky long wave radiation models

During summertime conditions, heat gain through a building's exterior surface includes various forms of absorbed incident solar radiation, long wavelength radiation exchange, and absorbed heat via convection. For many years, the conventional method to account for these three energy interactions has been to incorporate an effective outdoor air temperature known as the 'sol-air' temperature [4, 5]. The sky long wave radiation exchange is mainly a function of the sky effective temperature. In particular, radiative cooling is a result of heat loss by long wave radiation emission towards the sky, where the sky can be used as a heat sink for exterior surfaces of buildings.

To better quantify the influence of sky long wave radiation exchange on a building's external surface, an accurate sky effective temperature should be considered. Therefore, this chapter provides a comprehensive review of existing sky temperature models, both clear and cloudy, from the available literature. The models were categorized by data input requirements and computational approaches. The model results were demonstrated under various climate conditions. For selected models, a comparison of hourly sky radiation exchange from a horizontal surface was provided.

1.3. Clouds and dust storms impact in hot-dry climates

In many extremely hot and dry climate areas, such as the Middle East and North Africa, a horizontal roof is the most common building roof type. Regardless of building orientation, the outside roof surfaces are exposed to external environmental conditions. Solar radiation, outdoor air temperature, sky long wave radiation, and other factors strongly affect the inside comfort of the building and the cooling equipment capacity. Therefore, properly estimating the cooling and heating loads depends on an accurate consideration of these influential factors.

As a result, this chapter attemptes to numerically quantify the influence of sky radiative cooling effects on building roof thermal behavior under the conditions of extreme hot-dry climates. A one-dimensional transient heat transfer model was developed to evaluate the effect of sky radiative exchange. Numerical calculations were performed by the implicit finite difference method and applied to the extreme hot-dry climate of Riyadh, Saudi Arabia. Aerosols impact on total solar radiation was captured by implementing the ASHRAE 2013 Clear Sky model [6]. Moreover, newly available sky temperature measurements of Saudi Arabia were compared with published sky models to assess the best fit model. Furthermore, a dusty sky temperature model was proposed using the Aerosol Optical Depth (AOD). The impacts of sky temperature on the cooling load gained though non-insulated and insulated roofs were also studied. Finally, the impact of sky radiative exchange was also evaluated in four other extreme hot-dry global; Alice Springs, Australia; Jaisalmer, India; Khartoum, Sudan; and Phoenix, AZ, United States.

1.4. Influence of dust accumulation

In arid climates, dust storms are very common. Deserts in Africa, the Middle East and Asia are the main sources of such storms. Within the United States, the High Plains area has moderate

aerosol (dust) concentration levels. Consequently, dust accumulation on a building's roof can occur in and near these extremely hot and dry locations. Because dust has a relatively high absorptivity, accumulated dust on a roof's surface will increase the overall absorptivity, resulting in more absorbed solar radiation into the building. Therefore, investigating the influence of dust on a building's roof solar absorptivity is the main objective of this chapter.

In particular, the influence of dust accumulation on horizontal surface's (e.g., building roof) absorptivity and annual heat gain were studied. A correlation between roof solar absorptivity and dust accumulation was introduced as a function of dust deposition. In addition, dust deposition was modeled to predict the monthly and annual dust accumulation on a building's roof using a more accurately calculated solar absorptivity. Furthermore, the study covered parameter sensitivity and overall impact analysis of solar absorptivity with annual building heat gain.

Since the dissertation consists of four published/publishable articles under the supervision of the dissertation director, Professor Darin Nutter, the dissertation is constructed in the "Published/Publishable Articles" format consistent with the University of Arkansas Graduate School Guide formatting requirements. Each article represents a unique chapter in this dissertation. Chapter 2 is a conference paper presented at and published in ASME Early Career Technical Conference [7] titled "Geospatial Representation of the Residential Energy Use in Saudi Arabia". Chapter 3 is a technical paper that will be presented in ASHRAE 2015 Annual Conference and published in ASHRAE Transactions [8] titled "Survey of Sky Effective Temperature Models Applicable to Building Envelope Radiant Heat Transfer". Chapter 4 is a journal paper published in Science and Technology for the Built Environment [9] titled "Effect of Clouds and Dust Storms on the Sky Radiation Exchange for Buildings Located in Hot-Dry

Climates". Chapter 5 is a journal paper submitted to Energy and Buildings [10] titled "Influence

of Dust Accumulation on Building Roof Thermal Performance and Heat Gain". Chapter 6 is the

dissertation conclusion that summarizes the articles' findings.

1.5. References

[1] Ben Cheikh, H., Bouchair, A., 2004. Passive cooling by evapo-reflective roof for hot dry climates. *Renewable Energy* 29(11):1877–1886.

[2] Saudi Electric Company. 2012. Annual Report. Riyadh, Saudi Arabia.

[3] U.S. Energy Information Administration, 2012, Annual energy review.

[4] Kuehn, T.H., Ramsey, J.W., Threlkeld, J.L., 1998. *Thermal Environmental Engineering*. Third ed. New Jersey: Prentice Hall.

[5] ASHRAE. 1989. *1989 ASHRAE Handbook—Fundamentals*. Atlanta: ASHRAE.

[6] ASHRAE. 2013. *2013 ASHRAE Handbook—Fundamentals*. Atlanta: ASHRAE.

[7] Algarni, S., Nutter, D., 2013. Geospatial Representation of the Residential Energy Use in Saudi Arabia. Proceedings of the 2013 ASME Early Career Technical Conference (ECTC), April 4–6, Tulsa, Oklahoma, USA.

[8] Algarni, S., Nutter, D., 2015. Survey of Sky Effective Temperature Models Applicable to Building Envelope Radiant Heat Transfer, ASHRAE *Transactions*, vol. 121, part 2-in press.

[9] Algarni, S., Nutter, D., 2015. Effect of Clouds and Dust Storms on the Sky Radiation Exchange for Buildings Located in Hot-Dry Climates, Science and Technology for the Built Environment, 21(4):403–412.

[10] Algarni, S., Nutter, D., 2015. Influence of Dust Accumulation on Building Roof Thermal Performance and Heat Gain, Energy and Buildings-in press.

2. Geospatial Representation of the Residential Energy Use in Saudi Arabia

2.1. Abstract

One-half of the total electrical energy use in Saudi Arabia is consumed by the residential building sector. This is a higher portion than other countries due to the inefficient buildings and the harsh climate of Saudi. In this study, the most common residential buildings types (apartment, traditional house, and villa) were modeled. eQuest 3.64, a building energy simulation program, was used to model representative building base cases and compared to potential energy efficiency improvements. Results showed that for a typical housing unit, adding insulation and a higher efficiency air conditioning unit has the potential to reduce overall energy use by 38% and the cooling energy consumption by 52%. Furthermore, geospatial modeling techniques were applied to characterize energy intensity and consumption by regions. The results of this work are the beginning of an effort to better understand and to identify potential ways of reducing energy use across the Kingdom of Saudi Arabia.

2.2. Introduction

In Saudi Arabia, buildings consume a substantial portion of energy. About 76% of the generated electric energy is used for operating residential, governmental and commercial buildings. As shown in Figure 2.1, half of the total consumption is used for the residential sector [1], compared with 22% in USA [2]. Moreover, the residential electric consumption in the last decade has increased sharply by more than 94% [1].

7
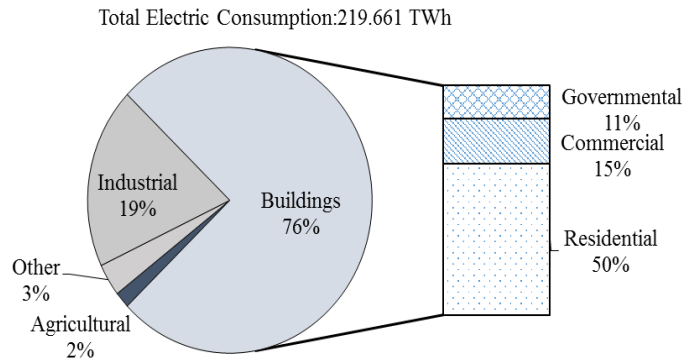
Figure 2.1 Electric energy consumption by sectors in Saudi Arabia in 2011

In fact, there are several factors that have led to high residential energy consumption. First, the low priced electrical energy, which is subsided by Saudi government, has caused public attitudes and behavior toward reducing personal energy use in the home to be very limited. Second, the harsh climate of Saudi which is considered 'hot-and-dry' in the country's interior and 'hot-and-humid' in coastal areas, requires significant space cooling-related energy use. Third, the residential building envelopes are not constructed in an energy efficient manner. For example, about 70% of residential buildings have no insulation in the walls or roof [3]. Fourth, the typical residential air conditioning system has a very low minimum energy efficiency ratio (EER) of 7.5. Therefore, up to 73% of the energy used in buildings is consumed by AC systems [4]. Lastly, the high annual population growth (2.9 % [5]), the large family size, and the rapid economic growth have resulted in an average annual increase in electricity usage of 4.9% during 1999-2009. It was reported that 1.65 million new residential building units (which represents

39% of the total existing units) will be built by 2015 in order to meet the rapid growth demand [6], resulting in increased total energy use and more frequent power shortages (especially during the summer peak hours).

As compared to the US residential energy consumption survey (RECS) [7], very little data are available, in the public domain, regarding Saudi residential buildings. In fact, only limited total energy consumption data are available, either on a whole country or regional basis. Compared to other Gulf Cooperation Council countries (GCC), which have similar climate conditions and culture, Saudi Arabia is the largest in population and total electricity consumption. In fact, it accounts for more than the half of the GCC's total electric consumption. Table 2.1 provides a comparison of GCC electricity consumption and cost.

Table 2.1 GCC electricity consumption and cost [8]

GCC-Country	Population in 2009 (M)	Electricity consumption (TWh) in 2008	Electricity consumption per cap (kWh/cap) in 2009	Electricity consumption by residential sector (%) in 2008	Residential electricity price (US¢/KWh) in 2008
Saudi Arabia	25.39	181.098	7,842	53	1.2
Kuwait	2.80	45.233	16,673	48	0.7
Bahrain	0.79	9.719	13,625	54	0.8
Oman	2.85	11.317	5,457	56	2.5
Qatar	1.41	18.387	16,353	45	2.2
UAE	4.60	86.260	17,296	35	5.2

Several studies have been performed on potential energy efficiency improvements for this region. They could be classified into two groups: "early studies" (published in late 1980s and 1990s) and "experimental/simulation studies". The early studies generated weather data for selected Saudi cities. The completed weather data sets are primarily used by building energy

simulation programs. Said and Kadry [9] attempted to generated the weather year data for five Saudi cities (Riyadh, Jeddah, Dhahran, Hail, and Khamis-Mushayt) of 22 years data (1970-1991). Said et al. [10] described the Saudi climate conditions for 20 cities including the monthly ambient temperature, degree-day base temperature and summer and winter outdoor design temperature. The experimental and simulation studies have been conducted on selected housing units in a few Saudi cities. These studies showed that enhancing the building envelope characteristics would contribute in a high energy savings. Ahmed [11] simulated a two story-house in Dhahran (hot-and-humid) by using the DOE-2.1E. His results showed that adding sufficient insulation to both walls and roof saved 42% of the total annual energy. The impact of different thermal insulation on single residential house in Riyadh (hot-and-dry) was investigated by AL-Homoud, [12], where 24% to 46% saving on annual energy use was achieved. A set of recommendations and guidelines for sustainable future Saudi residential housing was presented by Taleb and Sharples [13]. Although these studies were important, they were limited to only a few cities in Saudi (due largely to the lack of weather data needed to fully simulate the country wide impact). Furthermore, these studies concentrated on the building thermal load without paying attention to air-conditioning system efficiency or performance. Moreover, window air condition systems were not considered in most studies, although they represent about 70% of residential cooling systems in the current housing units and 56% of the current market volume in Saudi [3].

Considering that the residential sector is a major energy consumer, the limitations of previous studies, and the rapid growth in the energy demand, it can be concluded that more comprehensive energy system studies are needed. In this paper, the building energy simulation program known as eQuest 3.64 [14] was used to model all residential building types in Saudi

(apartment, traditional house, and villa). Including a typical base case model, a test matrix of various building envelope and air-conditioning system efficiencies was created and simulated. Next, the results were used to predict energy intensities and total electrical consumption for the country. Each were calculated and discussed based on building types and characterized by regions. After creating the necessary spatial data, the residential building energy intensities and consumptions were geospatially mapped for the country by using commercially available Geographic Information Systems (GIS) software package (ArcGIS 10.1) [15]. The primary objective of this study was to gain an understanding of residential energy use in Saudi Arabia and the influence of various energy-related building and system factors.

2.3. Methodology

2.3.1. Simulation model use

An annual hourly analysis was conducted by using a building energy simulation program known as eQuest version 3.64. Each building model had four major inputs categories: hourly weather data, building envelope, building equipment, and schedules. The following is a short description of the data gathered for the study and how it was used.

2.3.2. Hourly weather data

Fifteen (15) typical meteorological year (TMY3) weather data sets were used to cover all Saudi climate conditions and investigate the impact of the climates on consumption, as shown in Table 2.2.

11

2.3.3. Building envelope

Information on design parameters such as walls, roof, construction materials, windows and general dimensions. For the base case, the building envelope model inputs were selected based on the most common buildings in the country [16].

2.3.4. Building equipment and schedules

Data on building equipment (air-conditioning systems, lighting, hot water system,…) and schedules (occupancy, lighting, plug loads,…). For the base case, equipment and schedules was obtained through a questionnaire survey conducted on the housing unit's owners [17-19].

2.3.5. Energy monthly consumption data

The Saudi Electric Company (SEC) is the main supplier of electricity service to residential consumers. SEC provides an account number for each consumer and through that number, the last 12 months of electricity consumption bill can be obtained [20]. The electricity was assumed to be the main source of energy since propane is sparsely used for some cooking equipment.

2.3.6. National buildings data

Information on classification of housing units, their numbers, and average floor areas were collected. In general, the main types of dwellings in Saudi are apartments, traditional houses, and villas [16]. Due to the lack of data, a typical floor area for the three types in the capital city of Saudi, Riyadh, was assumed for the rest of housing across the country [21].

Table 2.2 Test Saudi cities corresponding to weather data used in simulation

City	Region	Elevation (ft)	Location Latitude (N)	Longitude (E)	Housing Units % (2007)
Abha	Asir	7217.8	18.13	42.30	7.11
Al-Majaridah		1523.0	19.13	41.92	
Arar	Northern Border	5747.0	30.98	41.03	0.92
Buraydah	Al-Qaseem	2010.6	26.33	43.97	4.16
Najran	Najran	4324.3	17.29	44.70	1.74
Al-Aqiq	Al-Bahah	5160.3	20.26	41.68	1.60
Dammam	Eastern	20.0	26.39	49.98	13.45
Hafar Al-Batin		1011.8	28.43	45.98	
Jazan	Jazan	54.1	16.89	42.55	4.45
Hail	Hail	3308.0	27.51	41.68	1.88
Jeddah	Makkah	53.0	21.59	39.17	29.59
Medina	Al-Madinah	1994.8	24.46	39.62	6.71
Riyadh	Al-Riyadh	2037.0	24.71	46.72	24.25
Tabuk	Tabuk	2457.4	28.55	36.61	2.95
Skaka	Al-Jouf	1962.6	30.04	40.21	1.19

2.3.7. *Total energy consumption*

Three base case models were created. Each model was validated by comparing its monthly energy consumption results for a year to the actual electric bills for existing buildings. Then efficient building envelopes and air conditioning systems were investigated and compared with the base cases for energy improvements. The simulation test matrix is shown in Table 2.3.

Table 2.3 Simulation test matrix

Factor	Description
Air conditioning EER	7.5, 8.5 (base case), and 11
Window Area %	10, 15 (base case), 20, and 30
Window type	Double-glazed clear glass (base case), double-glazed with low emissivity glass
Insulation	Insulated walls and roof, no insulated walls and roof (base case)
Combination	Insulated wall-roof and EER 11, non-insulated walls and roof and EER 8.5 (base case)

In the simulation test matrix, 9 parametric studies were investigated including a base case design. Furthermore, building orientations were investigated. However, the effect of different building orientations on the simulation results was found to be negligible (<0.1%). Annual energy use, HVAC energy use and energy use intensity (EUI) were calculated, compared and the possible savings scenarios were shown and discussed.

For each Saudi region, the total energy consumption of each building type was determined by multiplying the compute energy intensity times the regional total building type floor area. Then the total consumption of the three residential units types were added to represent the total regional consumption, as given in the following equation [22].

$$E_{region} = \sum_{i=1}^{N} \left(A_i \sum_{j=1}^{M} EUI_j \right) \qquad (1)$$

Where E_{region} is the total energy consumption for a given region (kWh), A_i is the floor space (ft^2), EUI_j is the energy use intensity (Btu/hr-ft^2), N is the number of buildings, and M is the number of buildings types.

The sum of the 13 Saudi regions was added to represent the country's total residential energy consumption. The Saudi total energy consumption was then validated by comparing it to the published data of the Saudi Electricity Company (SEC) [1]. Figure 2.2 shows a summary of the simulation and calculation process. The process is repeated using all combinations of the three building models, 15 weather climates, and 9 building configurations, resulting in a total of 405 simulation runs.

Simulation Inputs

eQuest

Compare model and actual building total
monthly consumptions deviation

No

Calibrate

$\Delta \leq 8\%\ast$

Yes

Calculate *EUI*

$$E_{region} = \sum_{i=1}^{N}\left(A_i \sum_{j=1}^{M} EUI_j \right)$$

$$E_{country} = \sum_{1}^{13} E_{region}$$

$$E_{country} \Leftrightarrow E_{SEC}$$
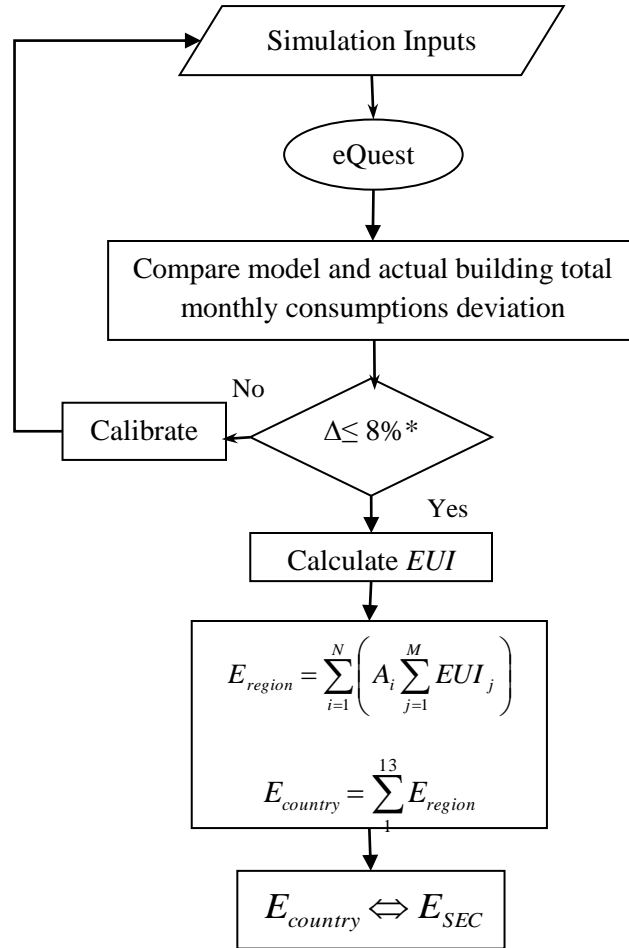
*An 8% difference was used, which is less than the standard "10%" [22].

Figure 2.2 Flow chart of simulation and calculation process

2.3.8. *GIS energy analysis*

The regional residential building energy intensities and consumption were then geospatially

mapped by using a commercially available Geographic Information Systems (GIS) software

package (ArcGIS 10.1). In general, GIS is a computer system that can collect, store, analyze, and

present different kinds of geographic data. The GIS was produced by the Environmental Systems

Research Institute. For this study, acquiring the necessary spatial data was quite challenging. In Saudi, residential spatial data is not available for public use. Its use is limited to organizations like the national Saudi postal system and the ministry of Municipal and Rural Affairs [MOMRA]. So for this analysis, high level spatial data was produced by digitizing the online MOMRA map [23]. For the digitizing process, the MOMRA map was converted to vector digital data by tracing all the lines/points of the residential area images of Saudi.

2.4. *Building description*

As previously stated, Saudi housing can generally be classified into three types: apartments, traditional houses and villas. Representative residential buildings, based on actual buildings are described in Table 2.4 Similarly, the basic buildings schedules of occupancy, lighting, office equipment, miscellaneous equipment, and air conditioning are given in Table 2.5.

Table 2.4 Base cases buildings characteristics

Characteristic	Apartment	Traditional House	Villa
Location	Jeddah, Saudi Arabia	Al-Majaridah-Asir, Saudi Arabia	Madinah, Saudi Arabia
Orientation	Front elevation facing north	Front elevation facing north-east	Front elevation facing south
Floor dimensions	29.53×27.89×11.4 ft	55.77×52.49×11.5 ft	52.49×45.93×11.4 ft
Doors type	Wood	Steel, Polyurethane core	Wood
Window Type	Double Clear 1/8 in		
Window Area	15% glazed of wall area		
Occupancy	4 people	6 people	7 people
Roof	6 in filled concrete slab +1 in Cement mortar inside	6 in filled concrete slab +1 in Cement mortar inside	1 in Asphalt+ 6 in filled concrete slab +1 in Cement plaster inside

	1 in Cement mortar outside +6 in hollow concrete block +1 in Cement mortar inside	1 in Cement mortar outside +6 in hollow concrete block +1 in Cement mortar inside	1 in Cement plaster outside +6 in hollow concrete block +1 in Gypsum plastering
Wall	1 in Cement mortar outside +6 in hollow concrete block +1 in Cement mortar inside	1 in Cement mortar outside +6 in hollow concrete block +1 in Cement mortar inside	1 in Cement plaster outside +6 in hollow concrete block +1 in Gypsum plastering
Floor	4 in concrete slab earth contact	4 in concrete slab earth contact	6 in concrete slab earth contact + 2 in polystyrene
Operation	24 hours with various schedule for lighting and equipment		
Lighting Power Density	0.080 W/ ft^2	0.070 W/ ft^2	0.070 W/ ft^2
Equipment Power Density	0.098 W/ ft^2	0.080 W/ ft^2	0.102 W/ ft^2
Hot water	3 gallons/person/day		
HVAC	Window Air conditioning cooling only, 18000 BTU/hr, EER 8.5		
Thermostat set point	75 F		

Table 2.5 Basic building schedules used in simulations

	Hours	Apartment		Tradition house		Villa	
		Weekdays (Sat.-Wed)	Weekends (Thu & Fri)	Weekdays (Sat.-Wed)	Weekends (Thu & Fri)	Weekdays (Sat.-Wed)	Weekends (Thu & Fri)
Building operation	1-24	24 hours low operation entire year					
Occupancy	1-7	100%	60%	100%	100%	100%	100%
	8-14	15%	20%	30%	50%	40%	50%
	15-21	30%	40%	60%	90%	50%	80%
	22-24	90%	60%	100%	100%	100%	100%
Lighting	1-7	5%	10%	5%		10%	
	8-14	10%	10%	50%		50%	
	15-21	90%	50%	60%		70%	
	22-24	70%	50%	5%		10%	
Refrigerator	1-24	100%					
Office and miscellaneous equipment	1-7	5%	5%	5%	5%	5%	5%
	8-14	5%	40%	30%	50%	50%	50%
	15-21	75%	60%	60%	90%	70%	80%
	22-24	15%	25%	5%	5%	5%	5%
Air conditioning	1-24	100%					

2.5. Results, validation, and analysis

2.5.1. Models results

Simulation results for the three base cases building types models and the actual building's electrical use are shown in Figures 2.3, 2.4 and 2.5, along with the distribution of yearly energy consumption of end-use equipment. On an annual basis, each building's simulation results were found to be very close to the actual annual electricity bills. For the monthly simulation calculations, most models showed a lower rate during summer months (6, 7 and 8) and were in better agreement during the rest months of the year. On average for all three models, space cooling was found to have the highest portion of 62%, lights and equipment were 13%, and 15%, respectively. Smaller portions were consumed by the refrigerator (6%) and water heating (3%). Overall, the country's annual energy consumption difference between simulations results and actual was 11.7 %. Shortage of the country's average building floor area data and variation in buildings operation schedules are considered the major causes.
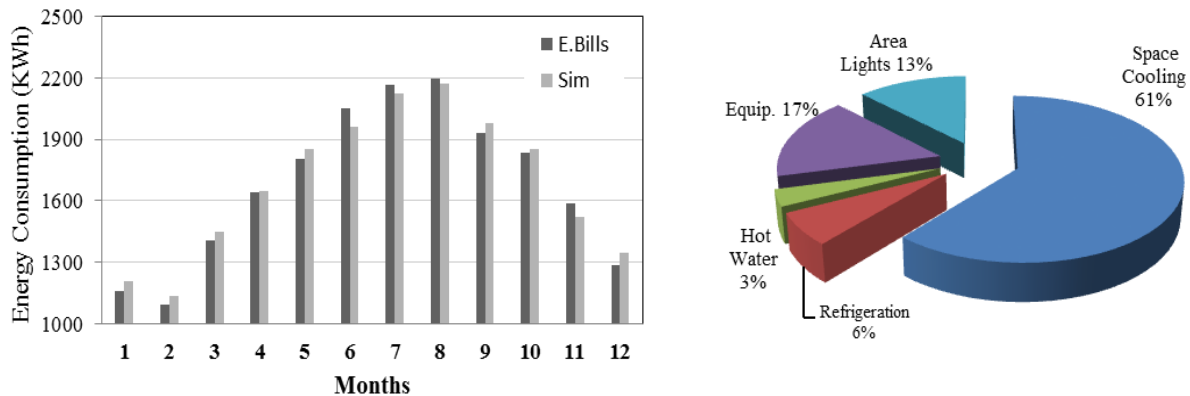
Figure 2.3 Comparison between electricity bills and energy simulation results in apartment base model-*Jeddah* with the distribution of yearly energy consumption of end-use equipment

18
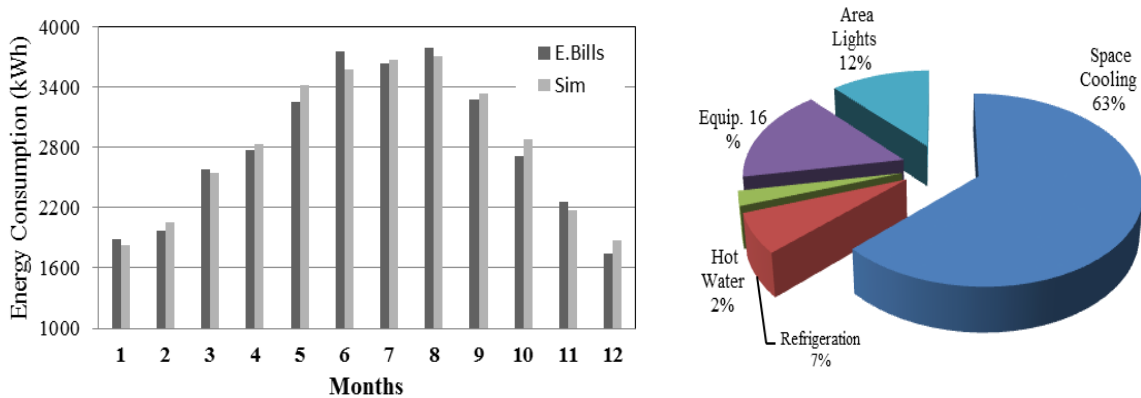
Figure 2.4 Comparison between electricity bills and energy simulation results in traditional house base model in *Al-Majaridah, Asir* with the distribution of yearly energy consumption of end-use equipment
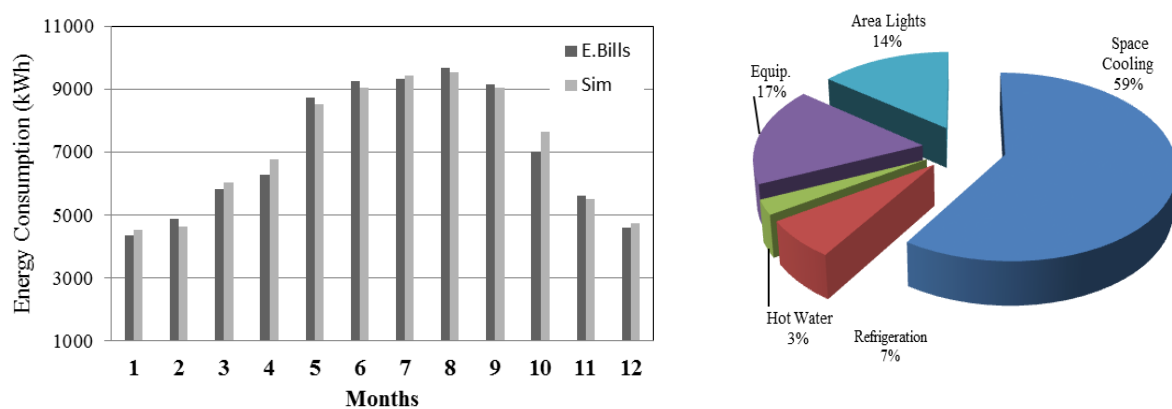
Figure 2.5 Comparison between electricity bills and energy simulation results in villa base model in *Madinah* with the distribution of yearly energy consumption of end-use equipment

2.5.2. *Alternative energy efficiency measures*

As described in the test matrix, each representative building type and, eight alternative energy efficiency measures were selected and run with each of the 15 weather climate files. For discussion purposes, the results for the traditional house (considered typical) located in the Jazan

region, (a hot-and-humid climate), are given below and shown in Figure 2.6. In addition, the impacts of applying the alternative energy efficiency measures are discussed below.

2.5.3. Air conditioning system efficiency

The base case window air conditioning units were considered to have an EER of 8.5. Upgrading to higher EER, of 11, resulted in annual reduction in energy consumption by 18%. On the other hand, using the current available minimum EER (7.5) caused an increase of 11% compared to the base case.

2.5.4. Wall and roof insulation

Currently 70% of Saudi houses have walls and roofs without insulation. Insulation with an R-9.19 (h-ft^2-F/Btu) was added to both the walls and the roof. As a result, 27% of the consumed annual energy was saved and a 37% saving was achieved on cooling capacity.

2.5.5. Window type and area

Double-glazed clear glass "1/8 in" windows were used in the base cases residences. The using of highly efficient window glazing, "double-glazed with low emissivity glass" saved only 1%, and 2% in annual total electricity use and cooling electricity use, respectively. However, compared with a single pane window, 6% of annual energy consumption can be reduced. Similarly, saving percentages with different window areas of 10%, 20% and 30% were investigated and shown in Figure 2.6.

20

2.5.6. Combination of an efficient air conditioning system and added wall and roof insulation

An implementation of both an efficient window air conditioner (11 EER) and insulated walls/roof (R-9.19 (h-ft2-F/Btu)) resulted in a total annual energy saving of 38% and cooling energy use reduction of 52%. Finally, the combination of the insulation and AC-EER 11 compared to the rest of building configurations represents 94% and 96% of the total potential on annual reduction and cooling reduction.
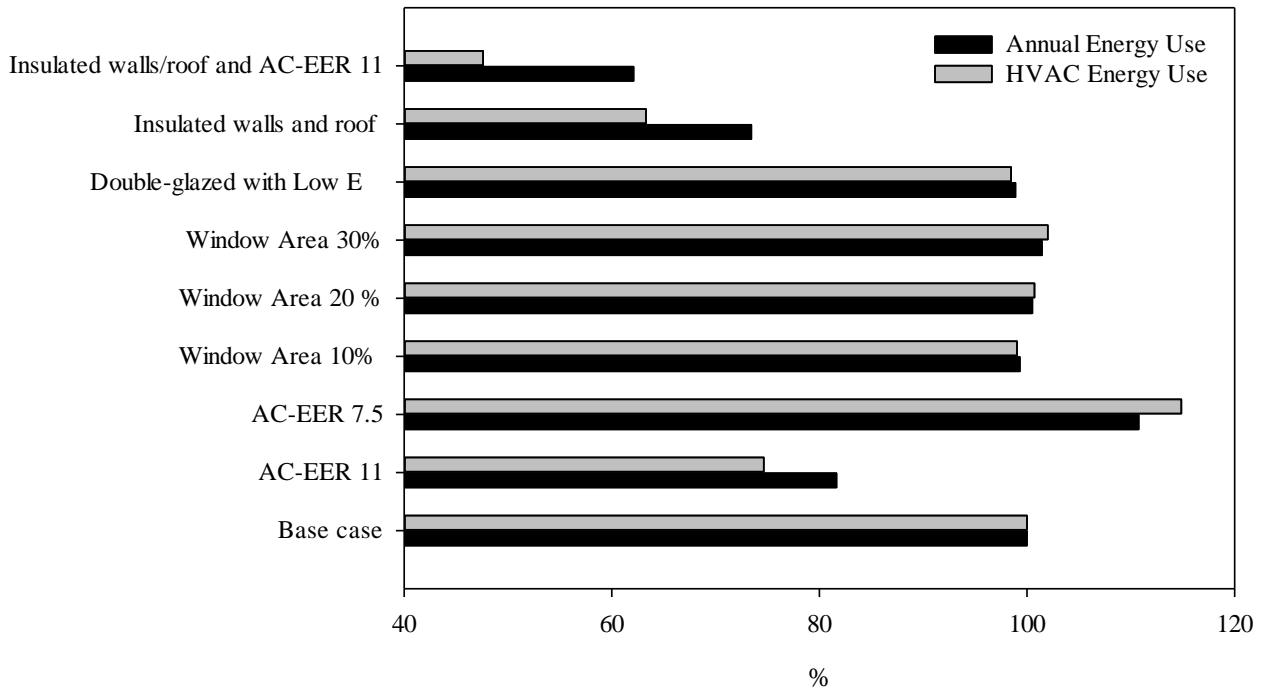
Figure 2.6 Percentage comparison of annual total electrical energy use and cooling electrical energy use for a traditional house in Jazan region, as compared to each energy efficiency measure. Note that the base case is set at 100%

2.5.7. GIS representation of country energy consumption

GIS was used to represent the residential areas and to characterize the energy intensities and consumptions by regions. Since the spatial residential data was not available for all Saudi cities, theses data was created by digitizing the current residential area for the country. Figure 2.7 shows the current residential area in all Saudi regions. After creating the necessary spatial data, the residential building energy use intensities (EUI) and consumption data were geospatially mapped for the country, as shown in Figures 2.8 and 2.9.
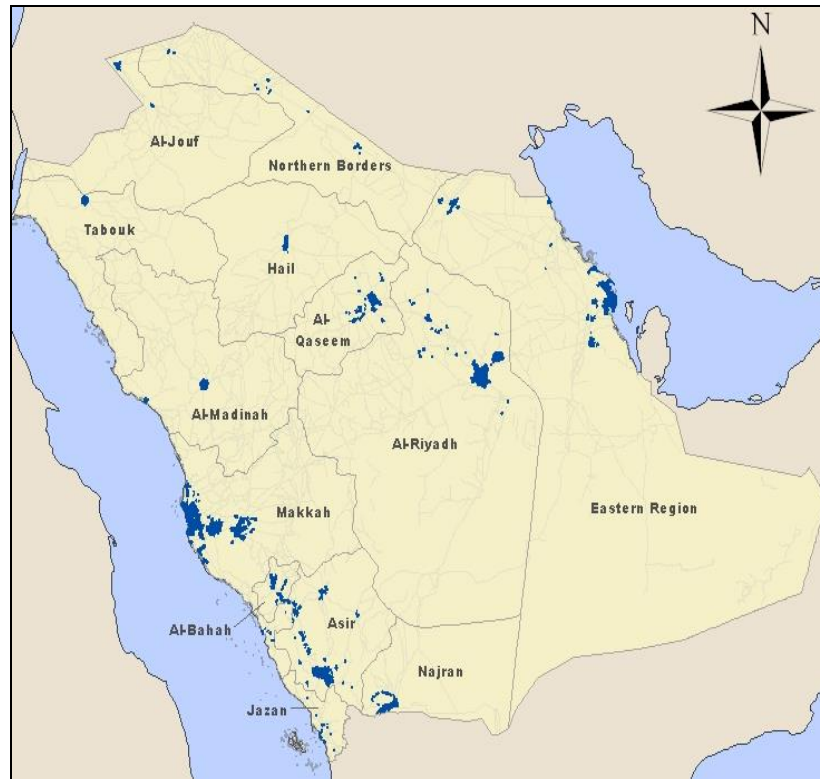
Figure 2.7 The map of Saudi Arabia showing the 13 administrative regions and the shaded area represents the most populated current residential areas

EUI average for housing units

EUI (kBtu/hr-ft²)
- 25-30
- 31-40
- 41-45
- 46-50
- 51-55
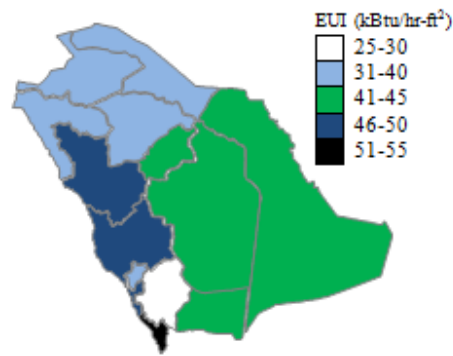
EUI average for apartments

EUI (kBtu/hr-ft²)
- 25-30
- 31-35
- 36-40
- 41-45
- 46-50
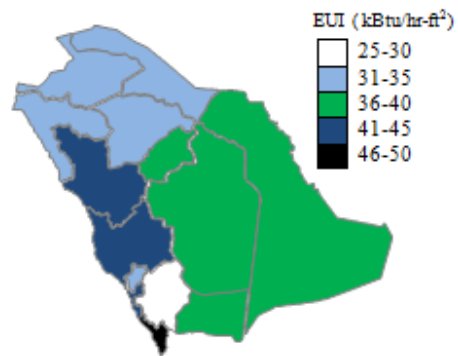
EUI average for traditional houses

EUI (kBtu/hr-ft²)
- 25-30
- 35-40
- 41-45
- 46-50

EUI average for villas

EUI (kBtu/hr-ft²)
- 35-40
- 41-45
- 46-50
- 51-55
- 56-60
- 61-65
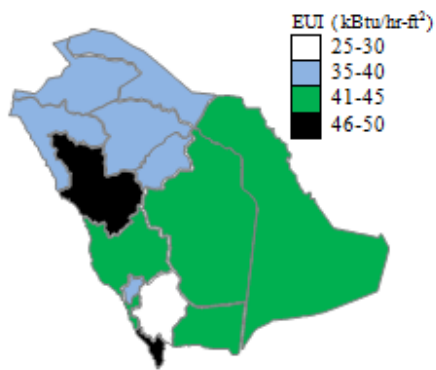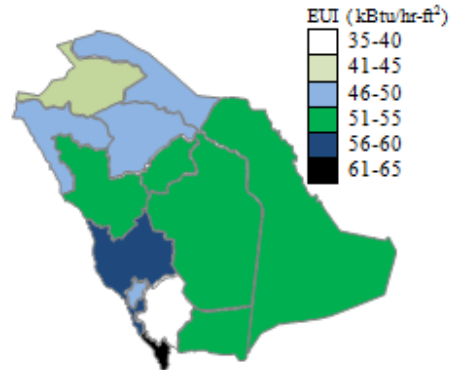
Figure 2.8 Energy use intensities (EUI) of Saudi residence buildings by regions
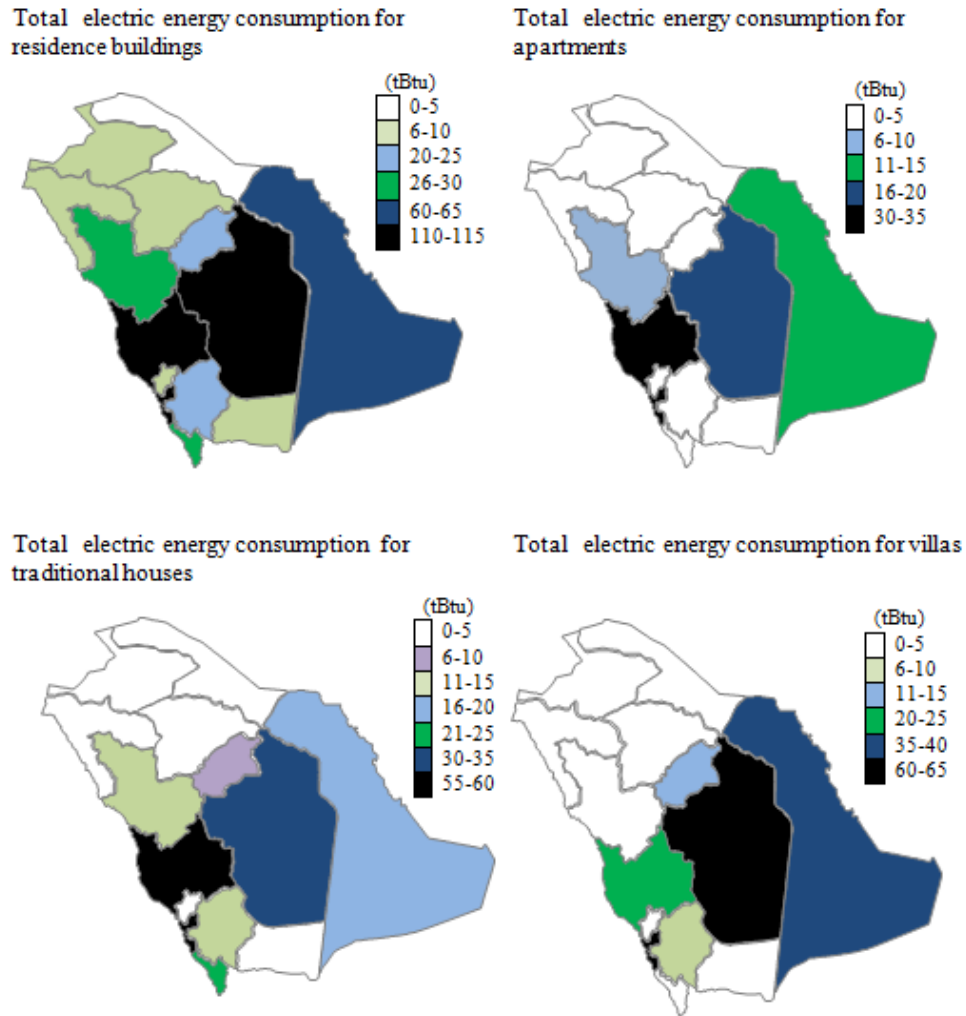
Figure 2.9 Total energy consumption of Saudi residence buildings by regions

In general, Saudi Arabia climate can be described as hot-and-dry in the middle parts of the country, hot-and-humid along the two coasts (i.e., Red Sea and Arabian Gulf), cold-and-dry in the north regions. Finally, the mountainous south-west of the country is cold in the winter and moderate in the summer [12]. As shown in Figure 2.8, the energy intensity for the hot-and-humid region has the highest, followed by hot-and-dry, cold-and-dry, and the mountainous region. Consequently, housing units in higher energy intensity required more annual energy compared

with other housing units in less energy intensity areas. Moreover, more potential annual electric

energy saving was predicted by the simulations results in hot-and-humid traditional house,

apartments and villa units. Energy consumption of Saudi housing units by regions was shown in

Figure 2.9. Al-Riyadh and Makkah regions shared the largest portion of the total energy

consumptions since they account for half of the total housing units in the Kingdom of Saudi

Arabia. Finally, Table 2.6 summarizes the potential energy saving for each residence type under

the major Saudi climates.

Table 2.6 Summary of the maximum potential energy saving in housing units (as compared to
base case) under the major Saudi climates

Climate zone	City, Region	Annual energy reduction (%)			Annual cooling energy reduction (%)		
		Apartment	Traditional house	Villa	Apartment	Traditional house	Villa
Hot-dry	Riyadh, Al-Riyadh	28.4	31.9	20.8	46.2	46.8	37.7
	Madinah, Al-Madinah	30.4	33.6	23.1	47.7	48.1	40.2
Hot-humid	Jazan, Jazan	34.3	38.0	25.7	51.2	52.4	42.3
	Jeddah,Makkah	31.3	34.7	22.3	49.9	50.6	39.7
	Dammam, Eastern	27.1	30.2	19.5	45.0	45.0	36.0
Cold-dry	Skaka, Al-Jouf	25.0	28.8	18.0	48.1	49.0	39.9
	Hail, Hail	26.2	29.6	17.7	47.6	47.9	36.1
	Arar, Northern Boorder	25.5	29.0	17.4	47.0	47.0	36.4
	Buraydah, Al-Qaseem	27.2	30.7	18.9	46.5	47.1	36.5
	Hafr Al-Batin, Eastern	24.6	29.1	19.4	42.4	44.5	37.1
	Tabuk, Tabuk	27.6	31.3	18.2	51.0	51.5	38.3
Mountainous	Abha, Asir	15.2	22.3	11.1	37.0	45.7	28.9
	Al-Aqiq, Al-Bahah	19.8	25.7	14.2	39.0	46.6	31.7
	Al-Majaridah, Asir	25.5	29.7	18.1	43.4	46.1	34.6
	Najran, Najran	27.2	31.0	18.9	45.7	47.2	35.5

2.6. Summary and conclusions

In 2011, residential buildings in Saudi consumed approximately 50% of the country's total electricity. So, the study described in this paper was undertaken to gain a better understanding of residential energy use in Saudi Arabia and the influence of various building and system energy efficiency measures. The base design residential models were carefully constructed and compared to eight building envelope/system configurations. As a result of the study, the following conclusions were drawn:

1. A high potential savings were predicted in Saudi residence buildings. This illustrates that the current residence building envelops are poorly designed to minimize energy use.

2. The majority of annual energy and cooling reduction was identified to be in housing units located in hot-and-humid and hot-and dry climate zones. A focus toward improvement in these two areas would yield the greatest energy efficiency impact.

3. GIS representation showed that more that 85% of the current Saudi residence buildings are located in very harsh climates.

4. Reducing heat gain by adding thermal insulation and use of high efficient air conditioning units have the greatest potential on annual energy (94%) and cooling reduction (96%) compared to the rest of building configurations.

5. Spatial data for residence buildings in all Saudi cities was produced and available for future studies.

2.7. References

[1]   Saudi Electric Company, 2001-2011, Annual Reports.

[2]   U.S. Energy Information Administration, 2012, Annual energy review.

[3]   Saudi Aramco, 2011, "Kingdom Energy Efficiency", Report.

[4]   Elhadidy, M.A., Ul-Haq, M., and Ahmad, A., 2001, "Electric energy consumption in selected residential buildings at KFUMP, Dhahran, Saudi Arabia", Proc. Mediterranean Conference for Environment and Solar, Beirut- Lebanon, pp.23-26.

[5]   Central Department Of Statistics & Information in Saudi Arabia, 2012, http://www.cdsi.gov.sa/english/.

[6]   Banque Saudi Fransi, 2011, "Saudi Arabia Economics", Report.

[7]   EIA, Residential Energy Consumption Survey, 2009, U.S. Department of energy, Washington, DC.

[8]   Arab Union of Producers, Transporters and Distributors of Electricity, 2008, Annual Report.

[9]   Said, S.A.M, and Kadry, H.M., "Generation of representative weather-year data for Saudi Arabia", Applied Energy, 48, pp. 131-136.

[10] Said, S.A.M., Kadry, H.M., and Ismail, B.I., 1996, "Climatic conditions for Saudi Arabia", ASHREA Transactions, 102(1), pp. 37-44.

[11] Ahmed, A. 2004, "Energy simulation for a typical house built with different types of masonry building materials", The Arabian Journal for Science and Engineering, 29(2B).

[12] AL-Homoud, M.S., 2004, "The effectiveness of thermal insulation in different types of buildings in hot climates", Thermal Envelope and building Sciences, 27(3), pp. 227-235.

[13] Taleb, H.M., and Sharples, S., 2011, "Developing sustainable residential buildings in Saudi Arabia: A case study", Applied Energy, 88, pp. 383-391.

[14] eQuest Description, http://www.doe2.com/equest/.

[15] GIS Description, http://www.esri.com/.

[16] Central Department of Statistics and Information of Saudi Arabia, 2004 and 2007 housing census.

[17] Ammar Almutairi, 2012, Personal contact.

[18] Saleh Algarni, 2012, Personal contact.

[19] Mued Alharthi, 2012, Personal contact.

[20] Saudi Electric Company, http://www.se.com.sa.

[21] Al-Riyadh Development Authority, 2010, "The reality and the future of housing in the city of Riyadh, Saudi Arabia", Report in Arabic.

[22] Heiple, S., and Sailor, D., 2008, "Using building energy simulation and geospatial modeling techniques to determine high resolution building sector energy consumption profiles", Energy and Buildings, 40(8), pp. 1426–1436.

[23] Ministry of Municipal and Rural Affairs (MOMRA) of Saudi Arabia, http://www.momra.gov.sa/.

3. Survey of Sky Effective Temperature Models Applicable to Building Envelope Radiant Heat Transfer

3.1. Abstract

Radiative sky cooling is a result of heat loss by long wave emission towards the sky. For the use in heat transfer applications and calculations, researchers have studied and proposed different sky effective temperature models and correlations since the early 1900s. One such use is for calculating a building's cooling loads, where the sky long wave exchange is an effective building energy balance element. Several factors influence the effective sky temperature, including location, ambient temperature, dew point temperature, and cloud cover. As a result, knowledge of current sky temperature models is important to better understand and characterize building heat transfer interactions; i.e. sky long wave radiative exchange. Therefore, the objective of the work described in this paper is to provide a comprehensive survey of existing sky temperature models from the available literature. The role of sky radiative exchange within building energy calculation is demonstrated. Moreover, the models are categorized by data input requirements and wide-ranging results are shown under various climate conditions. Finally, for selected models, a comparison of hourly sky radiation exchange from a horizontal surface is provided.

3.2. Introduction

During summertime conditions, heat gain through a building's exterior surface includes various forms of absorbed incident solar radiation, long wavelength radiation exchange, and absorbed heat via convection. For many years, the conventional method to account these

three energy interactions has been to incorporate an effective outdoor air temperature known as the 'sol-air' temperature (Kuehn et al. 1998; ASHRAE 1989). Under this method, the radiative exchange between a building's external surfaces and the sky, also known as the sky long wave radiation exchange, is simplified through the use of linearized radiation coefficients and a constant effective sky temperature correction factor. Similarly, current building energy simulation software programs use simple empirical models to predict the sky effective temperature and radiation exchange. Of singular interest in this paper is the current knowledge of modeling the sky effective temperature.

The sky long wave radiation exchange is mainly a function of the sky effective temperature. In particular, radiative cooling is a result of heat loss by long wave radiation emission towards the sky, where the sky can be used as a heat sink for exterior surfaces of buildings. Radiative cooling is largest (i.e., the effective sky temperature is the lowest) at night when the sky is clear and humidity is low. Clouds trap heat and increase the sky temperature (Saitoh and Fujino 2001). On a clear night, a building's external surface temperatures typically drop below the ambient temperature due to heat loss to the sky. In fact, recently the night sky cooling phenomenon has motivated applications such as thermal collectors, movable insulations, and air-water roof radiators through experiments and theoretical investigations. Eicker and Dalibard (2011) developed a new thermal collector for the night cooling of buildings in central Spain that provides a cooling power of 42.5 W/m^2 (12.7 Btu/hr-ft^2). Cavelius et al. (2005) claimed that the night sky can provide cooling power in the range of 20-80 W/m^2 (6.3-25.4 Btu/hr-ft^2). For predictions, accurate estimations of the sky temperature are critical. For example, at mid-latitude sites, it has been reported that a 5% error of estimating the sky long wave radiation may

represent 20 W/m^2 (6.3 Btu/hr-ft^2) (Berdahl and Fromberg 1982). As a result, predictions of sky temperature have been an interest for many investigators.

Researchers have studied and proposed numerous sky effective temperatures models since the early 1900s. Most of these sky temperature models are proposed in an approximated manner due to the lack of accurate measured data (Martin and Berdahl 1984). Poor agreements are expected because these sky models are related to local weather conditions and specific sites, as well as difficulty in finding reliable measured data. Therefore, variations between the sky temperature models have been a motivation for developing new sky models for different locations over the years (Tang et al. 2004). Furthermore, success of several radiant systems in residential buildings has attracted researchers for generating an accurate database of atmospheric radiation (Clark and Allen 1978). In general, the current sky models are developed based on local weather and site locations and, unfortunately, do not cover much of the world.

Although the use of the 'sol-air model' is defined to give approximated results (Spitler 2010), the model does not account for variations with time, the effect of cloudiness, dust or different locations. In fact, cloud cover has a strong influence on sky radiation (Mills 1995). Since individual models are limited to certain weather conditions and specific sites, each model may not apply for different sites and climate conditions. Furthermore, several studies have been performed on thermal buildings' performances without careful consideration of sky radiation effect. Very simple approximations for the long wave radiation between the sky and the buildings' surfaces have been used. For example, the sky temperature was assumed to be 12°C (21.6°F) or 6°C (10.8°F) below ambient temperature, (AL-Sanea 2000) and (Praëne et al. 2005), for daily calculation. Other studies limited the radiation cooling on buildings to the temperature difference between the buildings' surface and ambient temperature (Khedari et al. 2000; Chesné

et al. 2011). However, in a recent a study, the difference between the ambient and the sky temperature in desert areas can reach 25°C (45°F) (Twidell and Weir 2005).

To better quantify the influence of sky long wave radiation exchange on a building's external surface, an accurate sky effective temperature should be considered. Therefore, this paper provides a comprehensive review of existing sky temperature models, both clear and cloudy, from the available literature. The models were categorized by data input requirements and computational approaches. The model results were demonstrated under various climate conditions. Finally, for selected models, a comparison of hourly sky radiation exchange from a horizontal surface is provided.

3.3. *Heat transfer mechanisms within building horizontal surfaces*

A composite horizontal surface (roof) of multiple layers M is shown Figure 3.1. The roof's outside surface is exposed to outside convection heat flux (q_{conv}), solar absorbed (q_{abs}), and sky long wave radiation exchange (q_{sky}). The inside surface of the composite roof is subjected to combined internal convection and radiation heat transfer (q_i). All these parameters are varying with time of day, month of year, and location. Therefore, the heat transfer characteristic across the roof is considered a transient heat transfer phenomenon. During a clear sky night, the net heat transfer balance is negative (cooling) due to the long wave radiation between the roof and the sky. In other words, for this case the roof is losing heat to the sky. However, during the daytime, the net heat transfer balance is positive (heating) because of the dominance of incident radiation on the solar radiation exchange. Note that for a non-horizontal surface, calculating the effective sky temperature requires a path length (McQuiston et al. 2005).
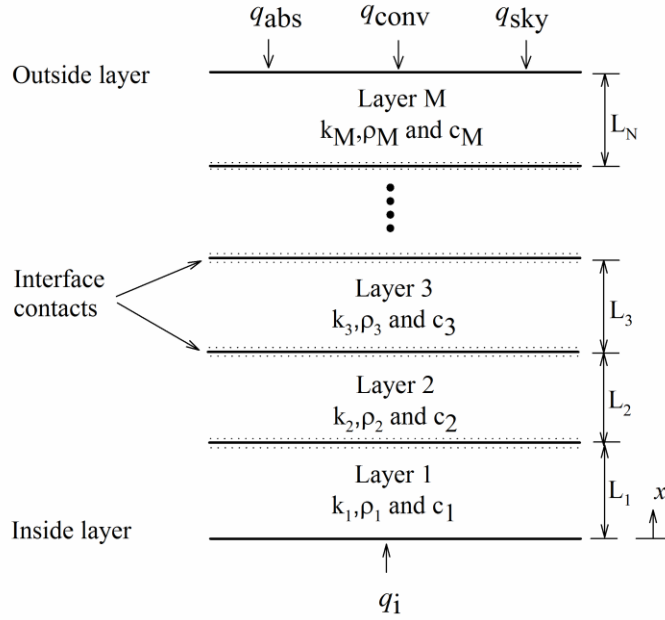
Figure 3.1 A composite roof with multiple layers M

The long wave radiation exchange between the sky and a building roof surface can be estimated as (Al-Sanea 2002):

$$q_{sky} = \varepsilon\sigma F_{SS}(T_{sky}^4 - T_{x=L}^4) \tag{1}$$

where the sky view factor with respect to flat roof equals 1.

As an example, Figure 3.2 shows results from modeling a horizontal roof's heat transfer components and variation during the 21st of July for the hot-dry climate and clear sky conditions of Phoenix, Arizona, U.S. The heat transfer components were calculated numerically by using the implicit finite difference method (Al-Sanea 2002). In the model, the ambient air temperatures

are sinusoidal averaged for the day (McQuiston et al. 2005). The ambient air temperature used was 40.15°C (maximum) and 27.32°C (minimum) (104.3°F and81.2°F, respectively), respectively (NOAA 2014). The incident total solar radiation on the horizontal roof was calculated by using ASHRAE clear sky model (ASHRAE 2013) for the latitude and longitude of Phoenix, Arizona. Garg's (1982) model was used to predict the sky temperature. In the simulation, roof consists of 150 mm (5.9 in.) of reinforced concrete and a layer of plaster attached to the inside of the roof was selected. Thermo-physical properties of the roof materials were given by Al-Sanea (2000).

During daylight hours, the solar absorbed (q_{solar}) is the dominant heat gain onto the surface. On the other hand, the sky long wave radiation (q_{sky}) contributes as a cooling source for buildings, as long as the sky temperature is lower than the ambient temperature. The outside roof convection (q_{conv}) heat transfer is the result of the difference between the outside roof and ambient temperature difference.

As shown in Figure 3.2, q_{sky} represents a big portion of the roof cooling load which helps reduce the total heat gain over the course of the day. This example demonstrates the potential importance of accounting for sky cooling, a strong function of the sky temperature. Analysis of heat transfer components for different climatic locations result in similar profiles with varying amplitude. As would be expected in cooler climates, the long wave sky cooling may be minimized.
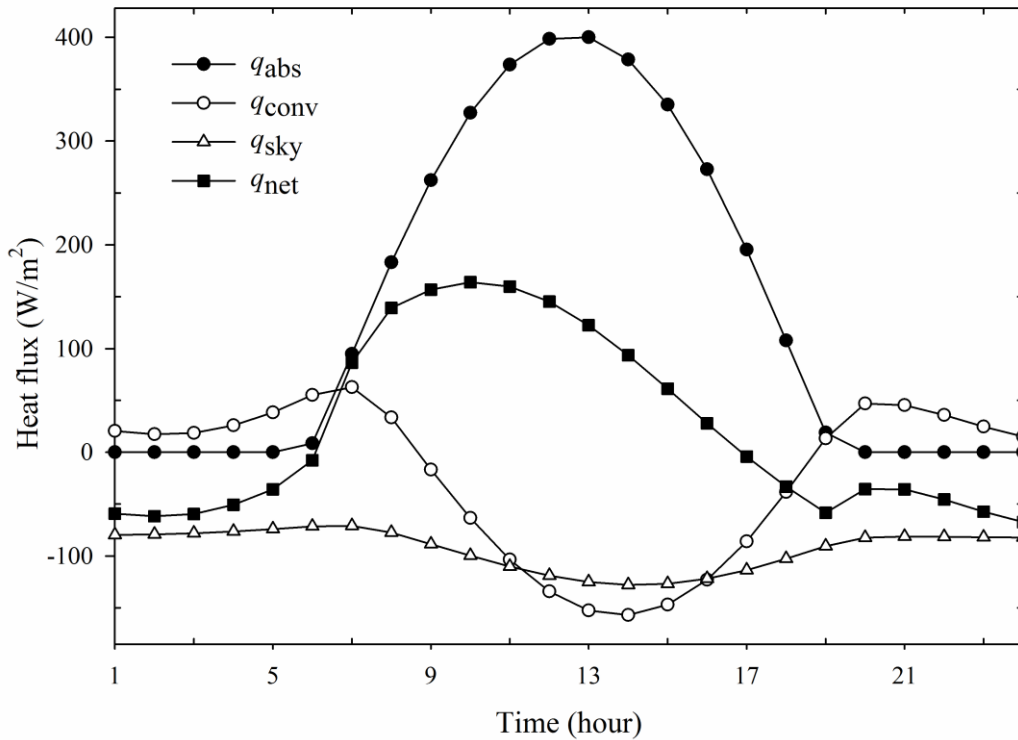
Figure 3.2 Roof's heat transfer components at various time of a day on July 21st for the hot-dry climate and clear sky conditions of Phoenix, Arizona, U.S

3.4. Sky temperature models classifications

The sky temperature is unlike the ambient air temperature. In general, the effective sky temperature is always lower than the ambient air temperature due to a decrease in elevation (Mills 1995). In addition, the difference between ambient air temperature and sky temperature is higher in the summer months, especially under clear sky conditions. Because of the water vapor and carbon dioxide heat absorption in cloudy sky conditions (Berdahl and Fromberg 1982), clouds usually increase the effective sky temperature causing it to approach the ambient air temperature. Moreover, the effective sky temperature depends on many factors such as ambient

temperature, dew point, amount of clouds, and the site conditions. Therefore, these factors have to be considered when developing sky temperature models.

Within the literature, there are several sky temperature models and emissivity correlations that have been proposed to estimate the effective sky temperature. Most of these models apply to clear sky conditions. Other models use correction factors to account for average cloud cover. The effective sky or atmospheric temperature can be related to ambient air temperature by using the following equation (Centeno 1982):

$$T_{sky} = (\varepsilon_{sky})^{0.25} T_{amb} \qquad\qquad (2)$$

Estimating the sky temperature can be classified within three main methods: empirical methods, radiation charts and detailed methods. Empirical methods are based on measurements and collected atmospheric data. Radiation charts are based on theoretical or empirical radiation calculations to generate a minimum, mean and maximum monthly sky temperature in chart formats (Cole 1976). Detailed methods, on the other side, are computer program models that utilize very detailed atmospheric constituents (Berdahl and Fromberg 1982). These kinds of computer programs require very detailed inputs and are considered time consuming similarly radiation charts methods. Therefore, the focus in this study is on the empirical methods.

In empirical methods, sky models can be divided into two groups: clear and cloudy sky models. Each of these models can be classified into direct sky temperature models and atmospheric emissivity correlations. Associated with atmospheric emissivity correlations, equation (2) should be used to calculate the effective sky temperature as a function of local

ambient air temperature. Figure 3.3 represents a classification of effective sky temperature models and their dependent parameters.
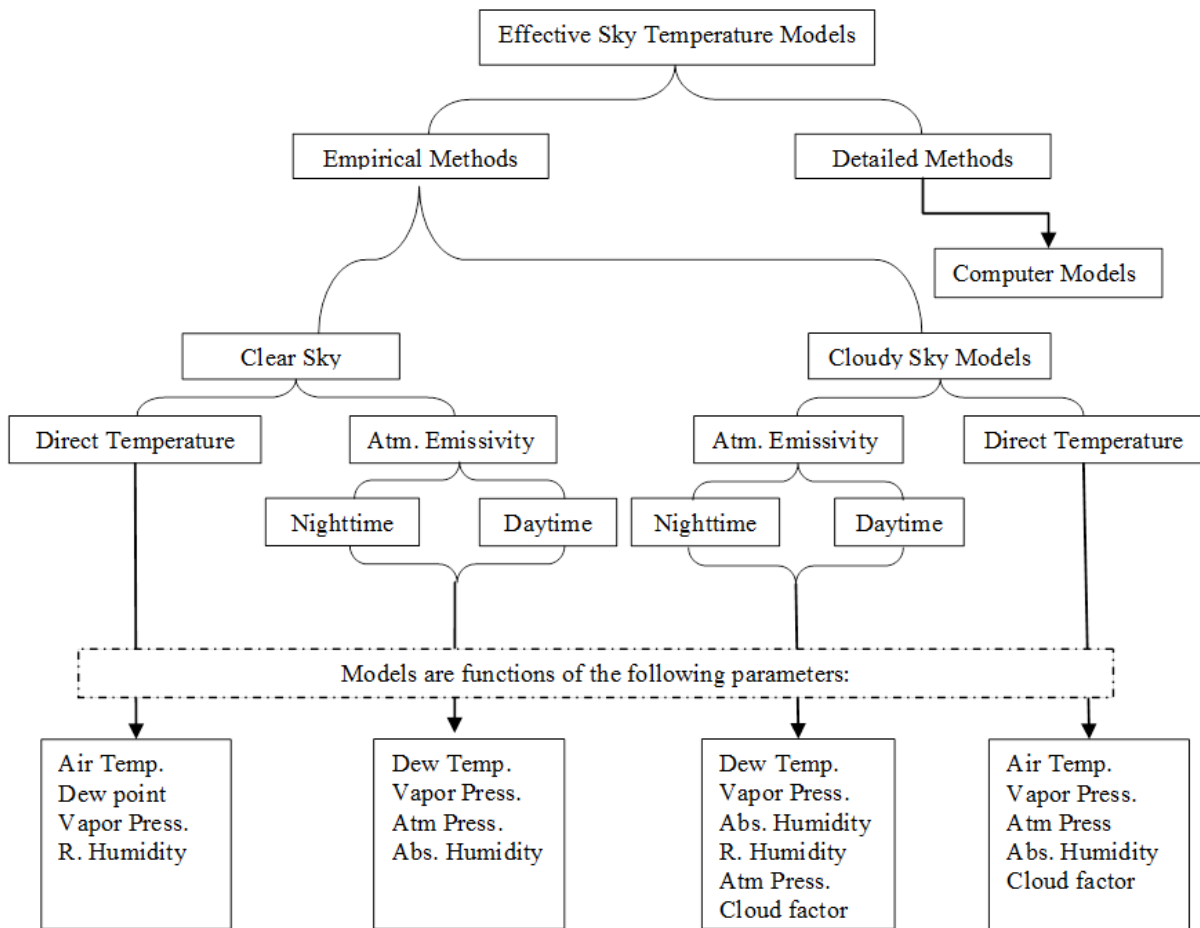
Figure 3.3 Sky temperature models classifications

For clear sky models, Table 3.1 lists the available atmospheric emissivity correlations. In general, these atmospheric emissivity algorithms are essentially functions of the dew point temperature [Models 1-11] and a few of water vapor partial pressure [Models 12-18]. Moreover, some investigators have provided specific emissivity sky models for nighttime and others for

daytime sky temperature [Models 1-2 and 4-5]. Emissivity correlations models from Table 3.1 are discussed below.

3.4.1. Berger et al. (1984) Model

Berger et al. (1984) developed two separate models [1 and 2] to predict daytime and nighttime sky emissivity. The two models were based on five years' measurements and analysis at Carpentras, France through January 1976 to December 1980. In Berger et al.'s model, measurements of sky radiation fluxes were taken for every three hours and then integrated hourly for 859 daytime and 750 nighttime measured data points. The root mean square error over T_{sky} is 2.7°C (4.9°F).

3.4.2. Tang et al. (2004) Model

Tang et al. (2004) developed another nighttime emissivity correlation based on a short period of time (August 10 - October 25, 2002) for the climate of Negev Highlands, Israel. The model is valid for a narrow range of ambient temperatures, between 19°C (66.2°F) to 33.5°C (92.3°F) and average relative humidity of 26% to 90%. The method of open pond temperature variation and radiation exchange with sky, at nighttime, is used in the model to develop the correlation. The method is considered simple in comparison to other models' methods, where direct hourly measurements of sky long wave radiation fluxes are used. Furthermore, the model is not recommended for very hot, dry climates. The standard deviation of sky emissivity for a linear regression that was reported in Tang et al.'s emissivity model is 0.051.

3.4.3. Clark and Allen (1978) Model

Clark and Allen (1978) collected 800 measurements of nocturnal net radiosity of the sky from October of 1976 till September 1977 at Trinity University, San Antonio Texas. As a result of the observations, the night sky emissivity correlation was developed with an error of 10 W/m^2 (3.2 Btu/hr-ft^2). The absence of accurate long term related atmospheric data, at that time, could be the result of the error. The model can be used for dew point temperatures in the range of -20.2°C (-4.4°F) to 24.5°C (76.1°F). Based on the instrument's measurement accuracy at the time, the reported error was stated as "small".

3.4.4. Berdahl and Fromberg (1982) Model

Berdahl and Fromberg (1982) presented two models for day and nighttime clear sky emissivity. The measurements of long wave radiation were collected during 11 summer months in 1979 for three different U.S. locations: Tucson, Arizona, Gaithersburg, Maryland, and St. Louis, Missouri. The reported standard error was 0.031. Berdahl and Fromberg (1982) noticed that the average daytime sky emissivity is lower than the average nighttime sky emissivity by 0.016. In general, since the model is based on summer collected data, it may not be applicable for other weather conditions. Later, a set of 57 months of sky long wave radiation data was collected by Berdahl and Martin (1984) for six U.S. sites to develop a new model with better accuracy. These sites were Tucson, Arizona (AZ); San Antonio, Texas (TX); Gaithersburg, Maryland (MD); St. Louis, Missouri (MO); West Palm Beach, Florida (FL); and Boulder City, Nevada (NV). Compared to the old model, the effect of the site on the sky emissivity was notable. The new model showed that Gaithersburg, Maryland has a higher sky emissivity than the rest of the other sites by an average of 0.019. The new model was recommended to be used for the range of -13 ≤ Tdp ≤ 24°C (8.6 ≤ Tdp ≤ 75.2°F).

3.4.5. Bliss (1961) Model

Bliss (1961) presented analytical procedures for calculating the clear sky emissivity. In addition, Bliss used water vapor emissivity measured data by (Hottel 1942) and (Kondratyev 1969) to develop Bliss (1961) sky model. The range of the dew point in the model is $-20 < Tdp < 30°C$ ($-4 < Tdp < 86°F$). However, the calculated sky emissivity is always higher than the measured emissivity.

3.4.6. Chen et al. (1991) Model

Chen et al. (1991) measured 150 nights of data in order to develop the dew point sky emissivity model. The model based on data collected in Omaha, Nebraska and Big Bend, Texas. The variation between the results of Clark and Allen (1978) and Berdahl and Fromberg (1982) were the motivation of Chen et al.'s (1991) work. The results of the model agree with Berdahl and Fromberg (1982) model. The model's root square error is 0.588. In 1995, Chen et al., (1995) collected a larger set of data over 1400 points to develop a better fit model. The result of the new model is within 2% difference with Berdahl and Fromberg (1982) and 7% difference with Clark and Allen (1978). The range of dew point in the new model is $0 < Tdp < 30°C$ ($32 < Tdp < 86°F$). Therefore, Chen et al.'s model (1991) is not recommended to apply in such a site where the dew point is below $0°C$ ($32°F$).

3.4.7. Melchora's (1982a) Model

Measurements were carried out in Venezuela. The model is applicable for ambient temperatures between $-10.2°C$ ($13.6°F$) and $29.9°C$ ($85.8°F$) and relative humidity range of 40-100 %. The valid elevation that can be used in this model is from 0 to 3000 m (9842.5 ft).

3.4.8. Angstrom's (1918) Model

Angstrom's (1918) model is considered one of the earliest works that attempted to predict the sky emissivity. The model was developed by a long series of observations and is only a function of the actual atmospheric vapor pressure, in millibars. Angstrom (1918) developed the model using measurements at Bassour, Algeria at an elevation of 1160 m (3805.8 ft) and later at Mt. Whitney, California at an elevation of 2860 m (9383.2 ft). Many investigators developed their models using Angstrom formula structure with only modified coefficients, such as Robitzsch (1926), Raman (1935), and Melchor (1982a).

3.4.9. Sloan et al. (1956) Model

Sloan et al. (1956) developed a model as a function of absolute humidity only. The measurements were taken for the two years of 1954-1956 in Columbus, Ohio.

3.4.10. Idso (1981) Model

Idso (1981) used one year's worth of measurements to evaluate this sky emissivity model. The model is valid for ambient temperatures of $-5.2 \leq Tamb \leq 40.9°C$ ($22.7 \leq Tdp \leq 105.6°F$) and vapor pressures within $30 \leq Pv \leq 3000$ Pa ($0.4 \leq Pv \leq 435.1$ psi).

Table 3.1 Clear sky atmospheric emissivity models

Model		Site	Author/Reference
1	$\varepsilon_{sky} = 0.77 + 0.0038T_{dp}$	Carpentras, France	Berger et al. (1984)
2	$\varepsilon_{sky} = 0.752 + 0.0048T_{dp}$		
3	$\varepsilon_{sky} = 0.754 + 0.0044T_{dp}$	Negev Highlands, Israel	Tang et al. (2004)
4	$\varepsilon_{sky} = 0.741 + 0.0062T_{dp}$	AZ/MD, and MO	Berdahl and Fromberg

5	$\varepsilon_{sky} = 0.727 + 0.0061 T_{dp}$		(1982)
6	$\varepsilon_{sky} = 0.711 + 0.56(T_{dp}/100) + 0.73(T_{dp}/100)^2$	AZ, TX, MD, MO, FL, NV	Berdahl and Martin (1984)
7	$\varepsilon_{sky} = 0.8004 + 0.00396 T_{dp}$	AZ	Bliss (1961)
8	$\varepsilon_{sky} = 0.8 + T_{dp}/250$		
9	$\varepsilon_{sky} = 0.736 + 0.00577 T_{dp}$	Omaha, Nebraska Big Bend, TX	Chen et al. (1995)
10	$\varepsilon_{sky} = 0.732 + 0.00635 T_{dp}$		Chen et al. (1991)
11	a. $\varepsilon_{sky} = 0.787 + 0.764 Ln(T_{dp}/273)$ b. $\varepsilon_{sky} = 0.787 + 0.0028 T_{dp}$	San Antonio, TX	Clark and Allen (1978) Clark et al. (1985)
12	$\varepsilon_{sky} = 0.56 + 0.08 P_v^{0.5}$	Los Chorros, Macuto, Caracalleda, Maracaibo, and Mérida, Venezuela	Melchor (1982a)
13	$\varepsilon_{sky} = 0.48 + 0.058 P_v^{0.5}$	Bassour, Algeria	Angstrom (1918)
14	$\varepsilon_{sky} = 0.50 + 0.032 P_v^{0.5}$	Whitney, CA	
15	$\varepsilon_{sky} = 0.62 + 0.029 P_v^{0.5}$	Poona, India	Raman (1935)
16	$\varepsilon_{sky} = 0.34 + 0.110 P_v^{0.5}$	Lindenberg, Germany	Robitzsch (1926)
17	$\varepsilon_{sky} = (0.135 \times P_{atm} + 6 P_v)/T_{amb}$		
18	$\varepsilon_{sky} = 0.7 + 5.95 \times 10^{-5} \times P_v e^{(1500/T_{amb})}$	Phoenix, AZ	Idso (1981)
19	$\varepsilon_{sky} = 0.3714 + 0.01923 \times AH$	Columbus, OH	Sloan et al. (1956)

On the other hand, two clear sky direct temperature models are summarized in Table 3.2. Swinbank (1963) averaged the elevation and the humidity values and proposed a direct sky model as a function of ambient air temperature. Garg (1982) evaluated the sky temperature as 20 °C (36°F) below the ambient temperature based on measured data in Australia. Though these models are fairly simple, associated errors are expected.

Table 3.2 Clear sky direct temperature models

Model		Site	Author/Reference
20	$T_{sky} = T_{amb} - 20$	Australia	Garg (1982)
21	$T_{sky} = 0.0552T_{amb}^{1.5}$	Australia	Swinbank (1963)

Finally, the impact of cloudiness on sky temperature is difficult to evaluate, and only a few researchers have attempted to predict it. Recently, a complete set of weather files covering 3012 international locations outside U.S. and Canada has been released as typical meteorological year (IWEC2) format (Huang et al. 2014). The new set of weather data includes values for hourly opaque and total cloud cover. The cloud cover data are necessary for building simulation programs to better predict the sky temperature under cloudy sky conditions. In Table 3.3, the cloud atmospheric emissivity correlations were introduced by the following authors:

3.4.11. Kasten and Czeplak (1980) Model

Kasten and Czeplak (1980) introduced a cloudiness factor (C_{cover}) that can take values between 0 (for clear sky) and 1 (for totally cloudy sky). The model was based on hourly sky heat flux measurements that were taken for 10 years (1964-1973) during the daytime. Kasten and Czeplak's study is based on long term collected hourly data of solar and terrestrial radiation to calculate the effect of cloudiness.

3.4.12. Melchor (1982b) Model

Melchor (1982b) developed another model from the exploration of several measurements that have been taken by other investigators in the US, France, India, England, Germany, and Sweden. The model is valid for the same range of weather conditions as stated in Melchor's

(1982a) clear sky emissivity model. In addition, Melchor's (1982b) model is a detailed model that accounts for several factors; the ambient temperature, site elevation, the relative humidity, and degree of cloudiness are considered. In the model, the degree of cloudiness ranges between 1 for very cloudy and 0 for clear sky conditions. Due to the large number of variables incorporated by Melchor's (1982b) model, it is considered more comprehensive than others.

3.4.13. Berdahl and Martin (1984) Model

Berdahl and Martin (1984) introduced a cloud sky fraction (fcloud) to account for the cloudiness effect. In case of clear sky conditions, the cloud sky fraction is zero and one for overcast sky. Berdahl and Martin used the same data as in Berdahl and Fromberg (1982) model to explore the effect of cloudiness. In the model, cloudiness emissivity was assumed to be 0.9. In general, Berdahl and Martin's (1984) model is similar to Kasten and Czeplak's (1980) model.

3.4.14. Aubinet's (1994) Model

Aubinet's (1994) measurements were carried out at Gembloux, Belgium. The model is a result of measurements that were taken for 274 days (1992-1993). The mean square error between calculated and measured data of daily mean infrared sky radiation (as defined by sky emissivity model (26)) is 92 W/m^2 (29.2 Btu/hr-ft^2). In the model, the clearness index (K_0) was used as an indicator for the effect of average cloud cover.

3.4.15. Clark and Allen (1978) Model

Clark and Allen (1978) estimated the effect of cloud cover through developing a cloud correction factor (Ca). The cloud correction factor is defined as the ratio of measured cloud sky atmospheric radiation to estimated clear sky atmospheric radiation. The formula of the correction

factor is a function of opaque sky cover (*N*) where *N* equals 0 for clear sky and 10 for overcast

sky. The model is valid for the same range of weather conditions as Clark and Allen's (1978)

clear sky emissivity model.

Table 3.3 Cloudy sky atmospheric emissivity models

Model		Site	Author/Reference
22	$\varepsilon_{sky} = \varepsilon_{sky-clear} + 0.8(1 - \varepsilon_{sky-clear})C_{cover}$	Hamburg, German	Kasten and Czeplak (1980)
23	$\varepsilon_{sky} = (1-N) \times [57.723 + 0.9555(0.6017)^Z] \times 10^{-4} \times T_{amb}^{1.1893} \times$ $H^{0.0665} + N[1 - (3000 + 1751 \times Z^{0.652}) \times H^{-3/2} \times T_{amb}^{-1}]^4$	Venezuela	Melchor (1982b)
24	$\varepsilon_{sky} = \varepsilon_{sky-clear} + \varepsilon_{cloud}(1 - \varepsilon_{sky-clear})f_{cloud}$	AZ, TX, MD, MO, FL, NV	Berdahl and Martin (1984)
25	$\varepsilon_{sky} = 0.682 + 0.0352 \times \ln(P_v) + 0.133 \times \ln(1 - K_0)$	Gembloux, Belgium	Aubinet (1994)
26	$\varepsilon_{sky} = C_a \varepsilon_{sky};$ $C_a = 1 + 0.0224N - 0.0035N^2 + 0.00028N^3$	San Antonio, TX	Clark and Allen (1978)
27	$\varepsilon_{sky} = (0.53 + 0.065.P_v^{0.5})(1 - 0.1N) + 0.1N$	Benson, England	Daguenet (1985)
28	$\varepsilon_{sky} = (0.43 + 0.082.P_v^{0.5})(1 - 0.1N) + 0.1N$	Upasala, Sweden	
29	$\varepsilon_{sky} = (0.44 + 0.061.P_v^{0.5})(1 - 0.1N) + 0.1N$	Washington, DC	
30	$\varepsilon_{sky} = (0.62 + 0.029.P_v^{0.5})(1 - 0.1N) + 0.1N$	Poona, India	

Other investigators studied the effect of cloud cover on long wave radiation between building

surfaces and the sky. Cloudy sky direct temperature models are summarized in Table 3.4. These

models are also briefly discussed below:

3.4.16. Dreyfus (1960) Model

Dreyfus (1960) introduced the simplest model of the direct sky temperature models. Dreyfus assumed that the sky effective temperature is equal to the ambient temperature in case of extreme cloudy sky conditions.

3.4.17. Whillier (1967) Model

Whillier (1967) proposed a similar model where the temperature of sky was assumed to be 6°C (10.8°F) below the ambient. In both models, neither cloudiness effect nor site conditions were considered.

3.4.18. Fuentes (1987) Model

Fuentes (1987) modified Swinbank's (1963) model of clear sky to account for the average cloudy sky by using a clearness index of 68 cities in US. Fuentes used the overall clearness index of 0.61. In addition, Fuentes assumed that cloudiness and sky insolation causes the sky temperature to be 32% closer to the ambient than Swinbank's (1963) model.

3.4.19. Aubinet (1994) Model

Aubinet (1994) introduced a cloudy sky direct model based on the same data as in Aubinet's (1994) model of cloudy sky atmosphere emissivity. However, the mean square error between calculated and measured data of daily mean infrared sky radiation (as defined by sky temperature model (35)) is 71 W/m^2 (22.5 Btu/hr-ft^2). Therefore, Aubinet (1994) model for cloudy direct sky temperature is more accurate than Aubinet's (1994) model of cloud-sky atmospheric emissivity. In the model, the sky clearness index (K_t) was introduced and defined as the ratio between global solar horizontal radiation and extraterrestrial solar radiation.

3.4.20. Daguenet (1985) Model

Daguenet (1985) developed complicated formulas where the effect of ambient temperature, vapor pressure and the emissivity of the sky were considered, in addition to cloudiness degree (N). A value of 8 represents clear sky and 0 for cloudy sky. Note that the model is not very sensitive to the degree of cloudiness.

Table 3.4 Cloudy sky direct models

Model		Site	Author/Reference
31	$T_{sky} = T_{amb}$	—	Dreyfus(1960)
32	$T_{sky} = T_{amb} - 6$	U.S.	Whillier (1967)
33	$T_{sky} = 0.037536T_{amb}^{1.5} + 0.32T_{amb}$	68 U.S. sites	Fuentes (1987)
34	$T_{sky} = 94 + 12.6\ln(P_v) - 13K_t + 0.341T_{amb}$	Gembloux-Belgium	Aubinet (1994)
35	$a.\ T_{sky} = (\dfrac{L}{\sigma})^{0.25}$ $b.\ L = L_0(1+0.01A) + \dfrac{BC(8-N)}{8}$ $c.\ L_0 = 3.6(T_{amb} - 273) + 231$ $d.\ A = 10.1\ln(P_v) - 12.3$ $e.\ B = 1.7(T_{amb} - 273) + 107$ $f.\ C = -0.22\ln(P_v) + 1.25$	Various international sites	Daguenet (1985)

3.5. Sky Temperature models variations

In order to explore the variation between the sky temperature models, both the direct sky temperature and atmospheric emissivity models were analyzed and compared to ambient air temperature. Weather conditions, such as ambient air temperature and dew point temperature for a 24 hour period of Al-Madinah, Saudi Arabia, were used as inputs for the sky models. The

47

ambient air temperatures were sinusoidal averaged for the day (McQuiston et al. 2005). A

43.33°C (110°F) and 30.50°C (87°F) were used as a maximum and minimum air ambient

temperature, respectively (Meteorological and Environmental Protection Administration of Saudi

Arabia 2013). The variations between the models can be a result of model limitations and

accuracy of collected data. A comparison of the four set of sky temperature models are

classified and presented in the following sections:

3.5.1. *Clear sky atmospheric emissivity models*

Figure 3.4 illustrates a comparison between clear sky atmospheric emissivity models and the

ambient temperature for a 24 hour period. In general, the comparison shows that the sky

temperature can be cooler than the air temperature by 40°C(72°F), as estimated by Angstrom's

(1918) United States model. On the other hand, Clark and Allen's (1978) model predicts a

highest sky temperature to be 18°C (32.4°F) below the air temperature. Although both models of

Angstrom and Clark were based on measurements in the U.S., they represent the two most

extreme models. The rest of the clear sky emissivity models fall between the models of

Angstrom: U.S. (1918) and Clark and Allen (1978). Robitzsch (1926) predicted a similar sky

temperature in Germany compared to Angstrom: Algeria's (1918) model results. The two models

of Berger et al. (1984)   for day and nighttime were combined and the results presented in one

curve. The nighttime emissivity of Berger et al. (1984) in the combined model led to lower sky

temperatures during the night. Finally, for the rest of the models, the average sky simulated

results were predicted to be around 20°C (36°F) below ambient air temperature.

Figure 3.4 Computed sky temperatures and comparison of hourly variations between clear sky emissivity models and measured ambient air temperature over a 24 hour period
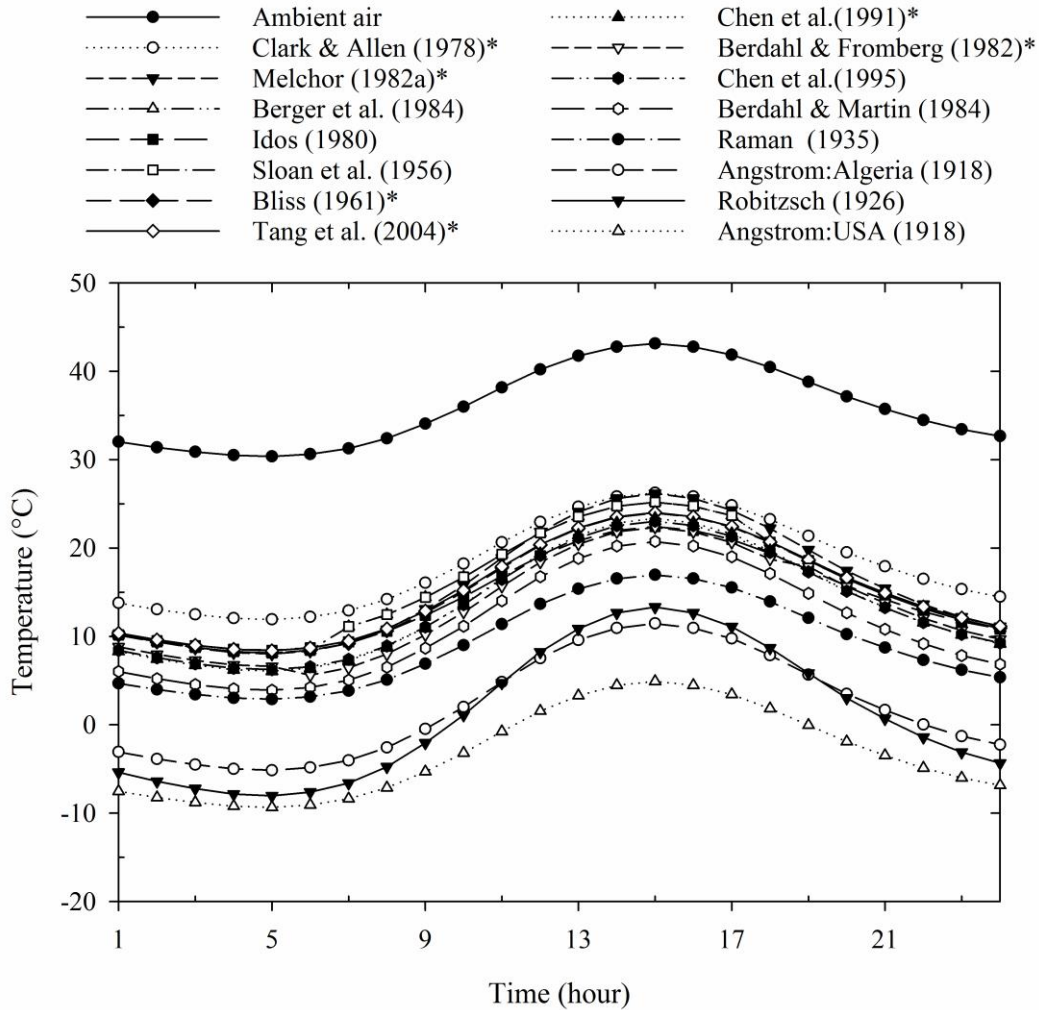
*Note, portions of the temperature range shown may exceed the published limits of model.

3.5.2. Clear sky direct temperature models

Garg's (1982) and Swinbank's (1963) simulation results are presented in Figure 3.5. The sky temperature is estimated to be lower by Garg (1982), who simply assumed that the sky temperature is 20°C (36°F) below the air temperature. Swinbank's model shows that the sky

temperature drops by 5°C (9°F) at midday and 10°C (18°F) at midnight below the air

temperature.
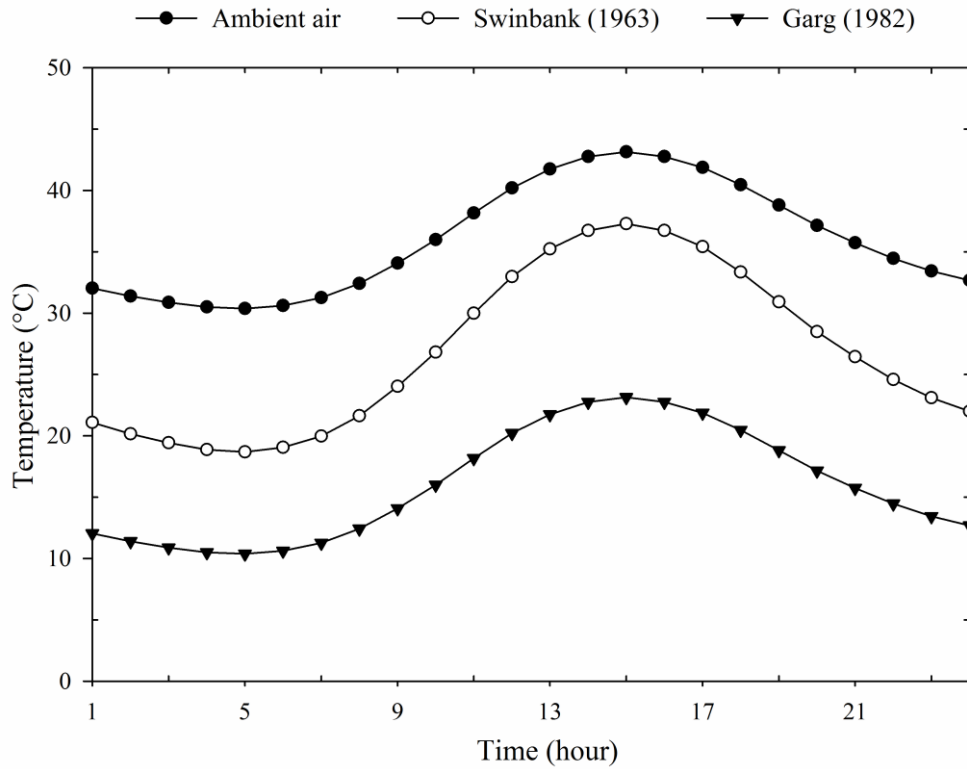
Figure 3.5 Comparison of hourly variations between clear sky direct temperature models and measured ambient air temperature over a 24 hour period

3.5.3. Cloud sky emissivity models

Variation between cloudy sky emissivity models is shown in Figure 3.6. For average cloudy

sky conditions, the estimated sky temperatures can fall between 20°C (36°F) below the air

temperature, as estimated by Daguenet (1985) United State model, and 10°C (18°F) below the

air temperature, as predicted by Berdahl and Martin's (1984) model.
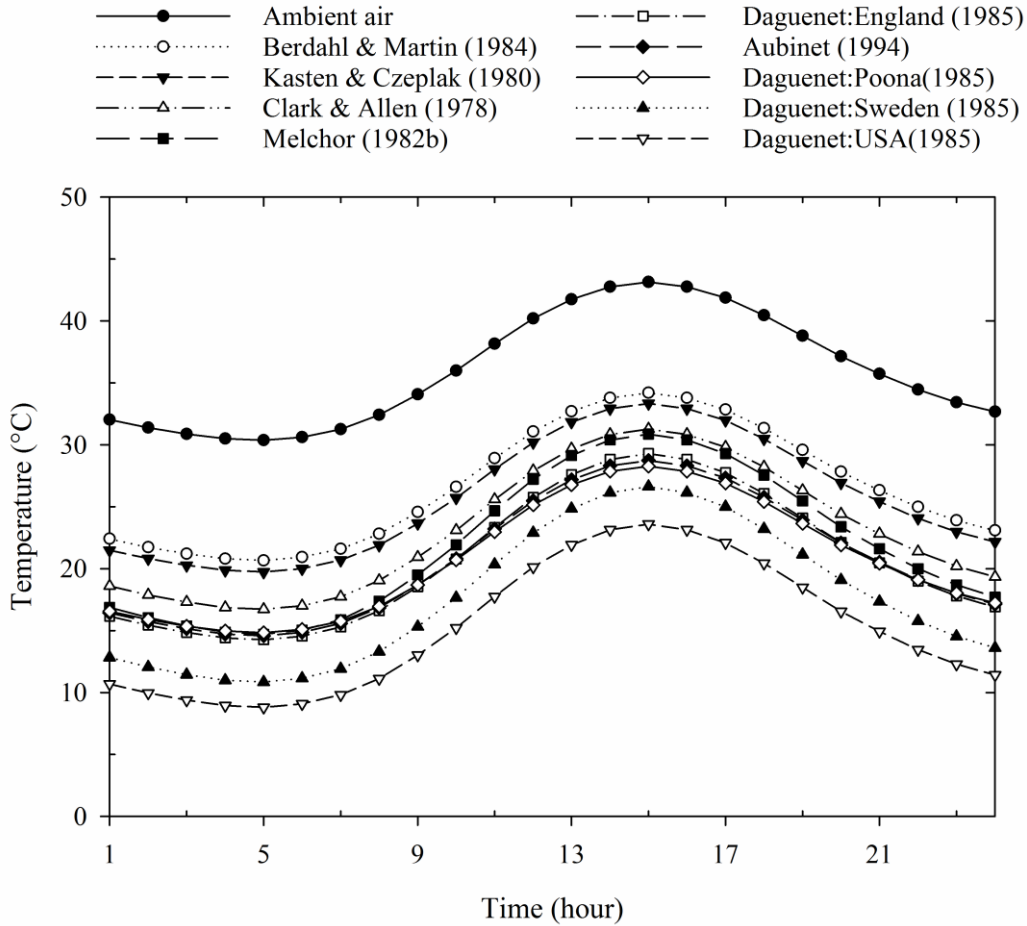
Figure 3.6 Comparison of hourly variations between cloudy sky emissivity models and measured ambient air temperature over a 24 hour period

3.5.4. Cloud sky direct models

Figure 3.7 shows variations of cloudy sky direct models compared to the ambient air

temperature. Aubinet's (1994) model gave the lowest estimate for sky temperature, around 29 °C

(52.2°F) below the ambient temperature. As stated earlier, Dreyfus (1960) assumed that cloudy

sky temperature is the same as air temperature. As a result, Dreyfus's model is considered to be the highest approximation for the sky temperature in the literature. Whillier (1967) and Fuentes (1987) predicted similar sky temperature for several cities in the U.S.; however, Fuentes predicted larger differences between sky and ambient temperatures early in the day and smaller during the afternoon hours. Daguenet's (1985) detailed model estimated the average cloudy sky to be slightly higher than Aubinet's (1994) prediction.
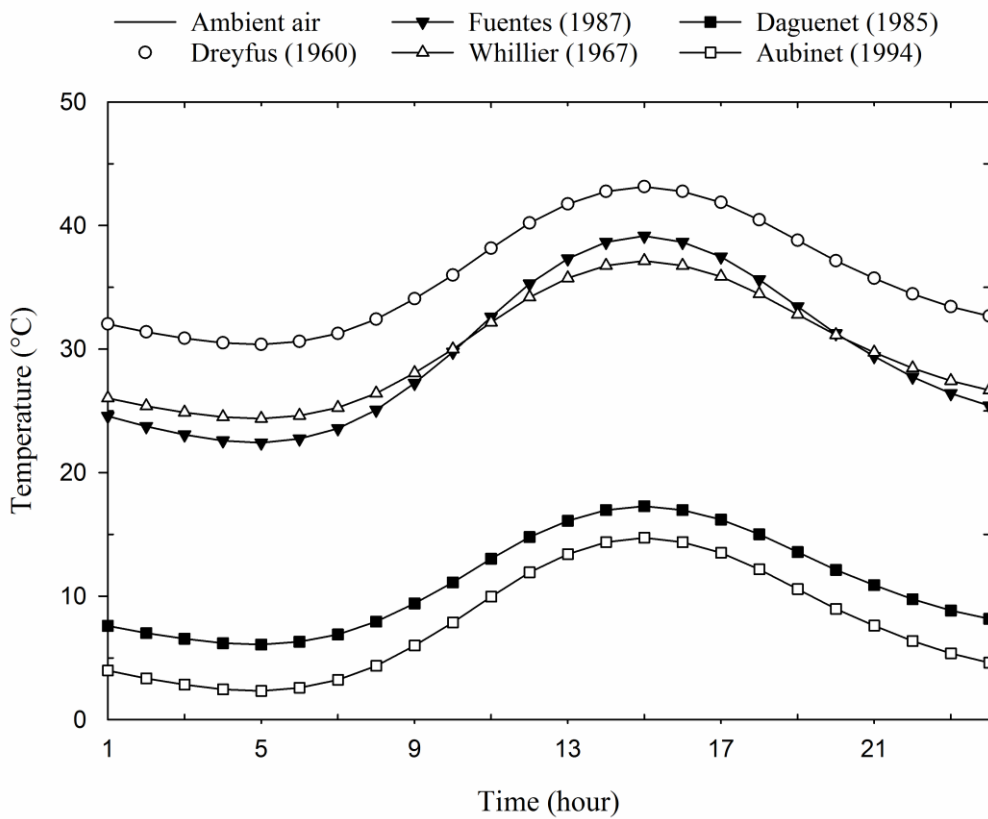
Figure 3.7 Comparison of hourly variations between cloudy sky direct models and measured ambient air temperature over a 24 hour period

3.6. Climate's effect on sky models prediction

Because there are few locations with a representative sky temperature model, the literature leads to varying results. To demonstrate the effect of climates on available sky temperature models outside their assigned uses, four general climate conditions were chosen. These climates are: extreme hot-dry, hot-dry, hot-humid, and moderate. Corresponding sites with July maximum and minimum ambient air and dew point temperatures are listed in Table 3.5.

Table 3.5 Weather Data for Climate Sites

Climate type	Site	Max. air temp. °C(°F)	Min. air temp. °C(°F)	Max. dew point temp. °C (°F)	Min. dew point temp. °C(°F)
Extreme hot-dry	Al-Madinah, Saudi Arabia	43.33 (110)	30.50 (87)	5.00 (41)	-5.55 (22)
Hot-dry	Phoenix, AZ	40.00 (104)	27.22 (81)	17.77 (64)	9.44 (49)
Hot-humid	Houston, TX	32.77 (91)	23.38 (74)	23.89 (75)	21.11 (70)
Moderate	Chicago, IL	27.77 (82)	18.33 (65)	18.88 (66)	13.33 (56)

Three sky temperature models, Melchor (1982a), Melchor (1982b) and Aubinet (1994), were selected and tested under each climate. Results of the tests are discussed below and shown in Figures 3.8, 3.9, 3.10 and 3.11 for extreme hot-dry, hot-dry, hot-humid, and moderate climates respectively.

3.6.1. The Melchor (1982a)

Model for clear sky is a solo function of vapor pressure. For hot-humid climates, the model predicted a higher sky temperature where it reaches the ambient temperature at midday. The

result was not expected. In the literature, the sky temperature only reaches ambient air temperature in cases of very cloudy conditions. Therefore, the model over predicted results can be expected in very humid climates. In hot-dry and moderate climates, the model gave higher readings compared with the other two models. Under a hot-dry climate, the differences between the Melchor (1982a) model and ambient temperatures are twice the value in morning than that during late hours due to low dew point temperatures.

3.6.2.   The Melchor (1982b)

Model expected minimum sky temperature in both hot-humid and moderate climates. On the other hand, in a very hot-dry climate, the model fails to predict similar results in both climates as shown in Figures 3.8 and 3.9. However, the model expected very low sky temperature at hours 5 and 6 AM due to low dew point temperatures. Because of the model limitations, the model is not recommended for climates where ambient temperature is higher than 30°C (86°F) and very dry climates.

3.6.3.   The Aubinet (1994)

Model depends on measuring vapor pressure and ambient air temperature. In higher air temperature and lower vapor pressure, as in the cases in Figures 3.8 and 3.9, the model predicts lower sky temperature compared to the other two models. In the case of moderate air dry bulb and dew point temperatures, the model predicted a larger difference between sky and ambient temperatures during morning and late hours over the course of the day.
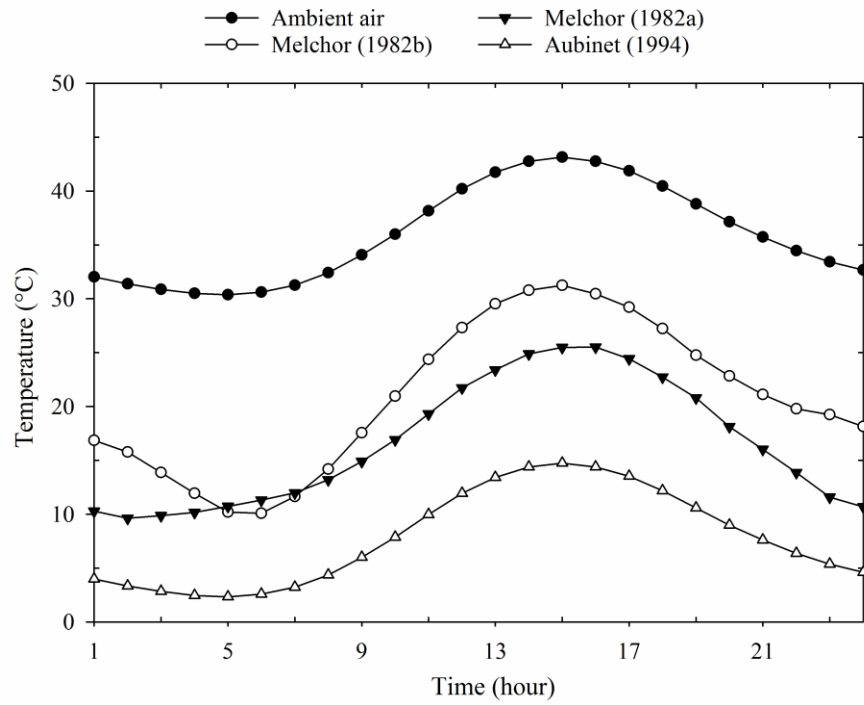
Figure 3.8 Sky temperature variations using three sky models from literature under extreme hot-dry climate conditions
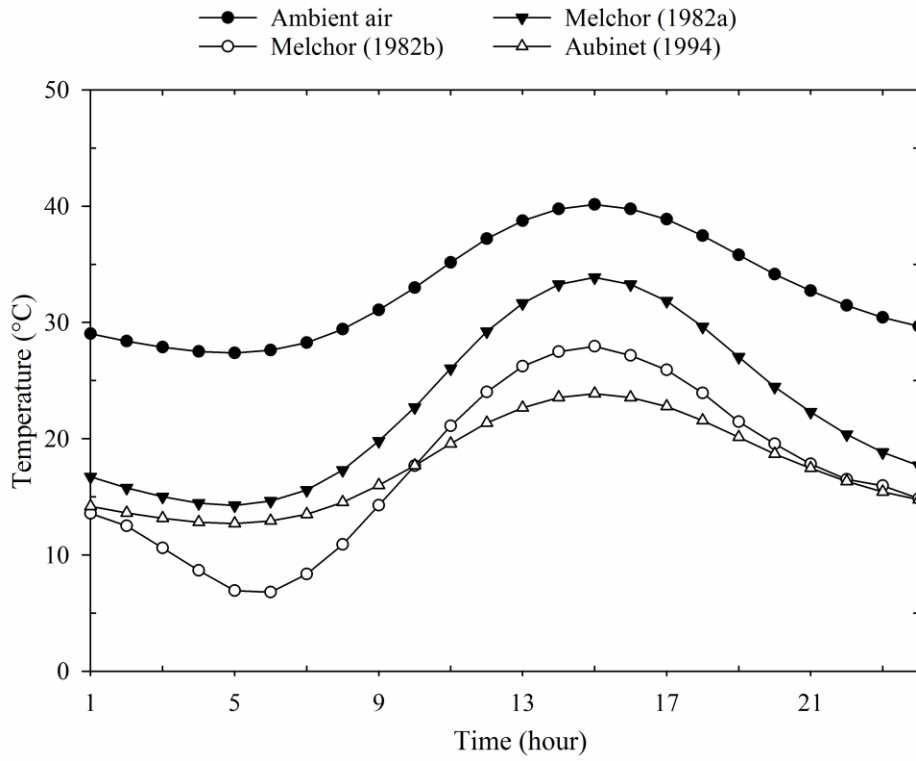
Figure 3.9 Sky temperature variations using three sky models from literature under hot-dry
climate conditions
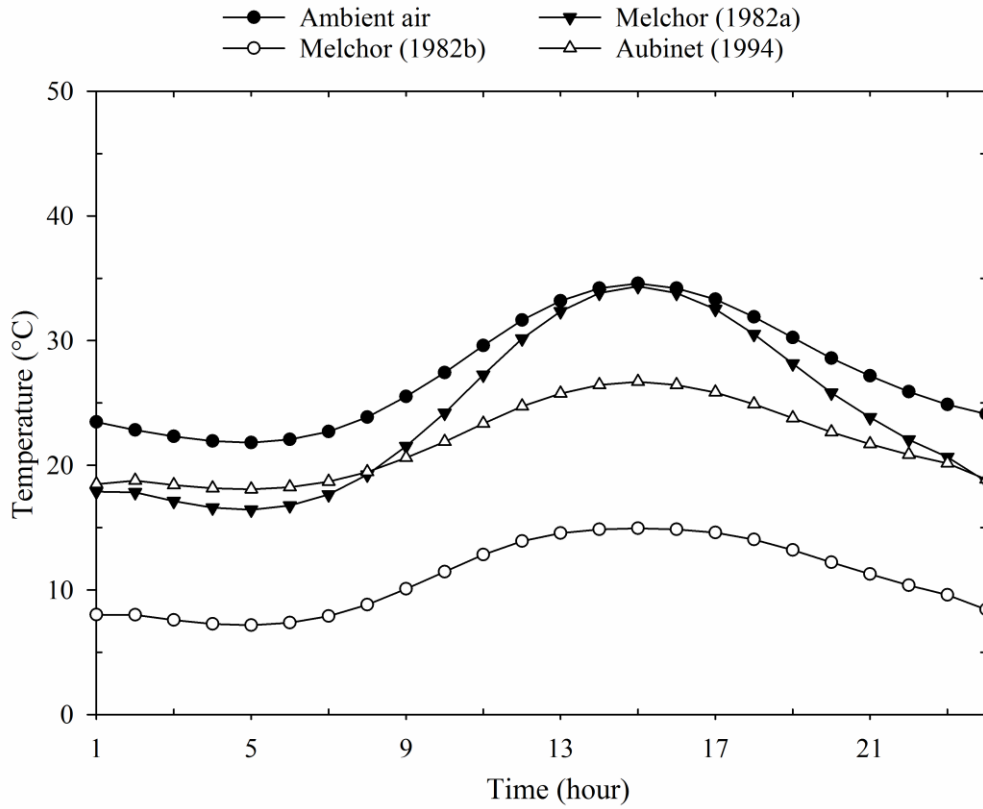
Figure 3.10 Sky temperature variations using three sky models from literature under hot-humid climate conditions
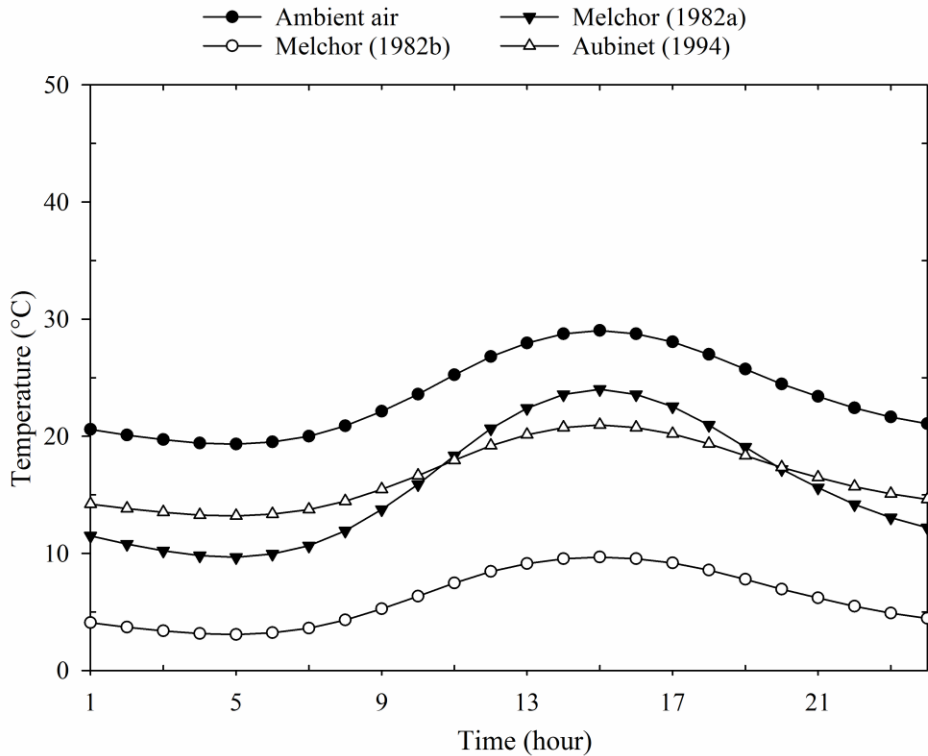
Figure 3.11 Sky temperature variations using three models from literature under moderate climate conditions

3.7. Sky cooling load variations

To demonstrate the influence of the effective sky temperature on the radiative heat exchange, selected sky temperature models over a 24 hour period were tested in the extreme hot-dry climates of Al-Madinah, Saudi Arabia. A typical horizontal surface consists of 150 mm (5.9 in.) of reinforced concrete and a layer of plaster attached to the inside of the surface was selected. Three different sky temperature models were selected to cover the area of the existing sky temperature models prediction. The models by Dreyfus, Angstrom, and Daguenet were used. Dreyfus's (1960) and Angstrom's (1918) models are two extreme sky temperature models, while the Daguenet (1985) Sweden model is considered to be an average estimate of the sky

temperature. Results are presented in Figure 3.12. The daily average sky cooling loads were found to be 293.9, -3828.5, and -1849.9 W-hr /m^2 (93.2, - 1213.6, -586.4 Btu/ft^2) respectively. It is interesting that to see the peak sky cooling effect occurs at midday; however, since the peak solar radiation absorbed happens at midday as well, the cooling sky effect is not as apparent. This example demonstrates how significantly different the sky cooling load can be, and thus the impact on cooling load calculations, with different sky effective temperatures.

It should be noted that for cloudy sky conditions, the sky cooling effectiveness is reduced since the sky temperature more closely approaches the ambient temperature. Although roof thermal insulation is essential to proper building performance, it may hinder the singular benefit of sky cooling. Furthermore, sky radiation exchange during totally cloudy conditions could, in some select cases, result in a heat gain to the building. And, in the winter months, the sky cooling effect becomes unfavorable. All of these factors emphasize the importance of accurate predictions of sky long wave radiation heat exchange.
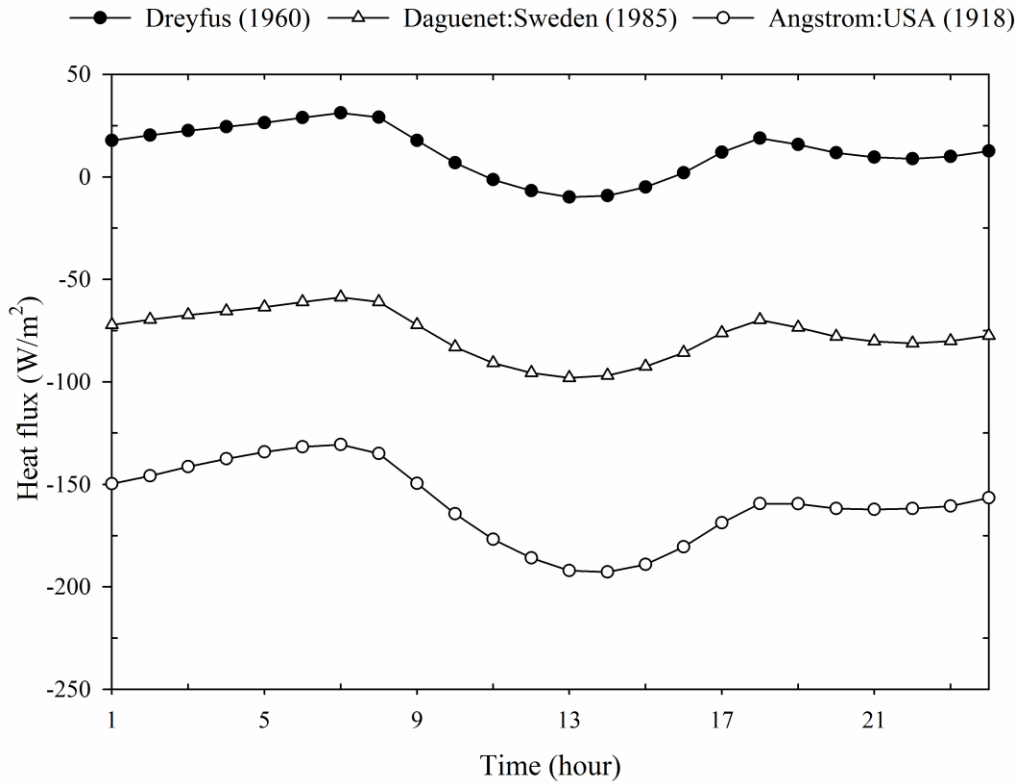
Figure 3.12 Hourly sky radiation exchange over a 24 hour period

3.8. Conclusions

Several sky temperature models, including clear and cloudy sky models, have been reviewed. Selected sky temperature models were also investigated with different climate condition types. The effect of sky cooling on a horizontal surface was shown, including hourly sky cooling variations with selected sky temperatures models over a 24 hour period.

Although the sky temperature models were based on site-specific collected data for a variety of factors, each was presented as a simple algebraic correlation. Among all the sky temperature models, Garg (1982), Swinbank (1963), Dreyfus (1960) and Whillier (1967) are considered the

60

simplest since they are a function of only the ambient air temperature. By using these models, the effective sky temperature can be easily calculated. However, using simple sky models may cause unnecessary errors in estimating the sky temperature. Models such as Melchor (1982b) and Daguenet (1985) account for many factors that strongly affect the sky temperature.

Generally, current sky effective temperature models vary greatly in both form and complexity. It was found that the simplest models were the ones most often utilized. Because there are few locations with a representative sky temperature model, the literature leads to varying results. Therefore, knowledge of current clear and cloudy sky temperature models including their assigned uses (such as a data range, period of collections, proper model location and climate condition) helps in finding a suitable model for a selected site. Furthermore, there is a need for additional data and research that captures additional variables and lead to better sky temperature predictions: for example, improved models including factors that capture daily cycles or hourly changes that are independent of location, and that account for dust storms or smog beyond cloudiness factors.

3.9. References

[1] Al-Sanea, S.A., 2000. Evaluation of Heat Transfer Characteristics of Building Wall Elements. Journal of King Saud University 12(2), 285-313.

[2] Angstrom, A., 1918. A study of the radiation of the atmosphere. Smith. Misc. Coll., 65(3), Washington, D.C.

[3] ASHRAE., 1985. ASHRAE Handbook- Fundamentals. American society of heating, Refrigeration and Air-Conditioning Engineers, Inc., Atlanta.

[4] ASHRAE., 1989. ASHRAE Handbook- Fundamentals. American society of heating, Refrigeration and Air-Conditioning Engineers, Inc., Atlanta.

[5] Aubinet, M., 1994. Longwave sky radiation parameterizations. Solar Energy 53 (2), 147-154.

[6] Berdahl, P., Fromberg, R., 1982. The thermal radiance of clear skies. Solar Energy 29(4), 299-314.

[7] Berdahl, P., Martin, M., 1984. Emissivity of clear skies. Solar Energy 32(5), 663-664.

[8] Berger, X., Buriot D., Garnier, F., 1984. About the equivalent radiative temperature for clear skies. Solar Energy 32(6), 725-733.

[9] Bliss, R., 1961. Atmospheric radiation near the surface of the ground: a summary for engineers. Solar Energy 32(5), 103-120.

[10] Cavelius, R., Isaksson, C., Perednis, E., Read, G. 2005. Passive cooling technologies. Austrian Energy Agency.

[11] Centeno, M., 1982. New formulae for the equivalent night sky emissivity. Solar Energy 28(6), 489-498.

[12] Chen, B., Clark, D., Maloney, J., Mei, W., Kasher, J., 1995. Measurement of night sky emissivity in determining radiant cooling from cool storage roofs and roof ponds. In proceedings of the National Passive Solar Conference, vol. 20, 310-313.

[13] Chen, B., Kasher, J., Maloney, J., Girgis, G., Clark, D., 1991. Determination of the clear sky emissivity for use in cool storage roof and roof pond applications. In proceedings of the American Solar Energy Society, Denver, CO.

[14] Chesné, L., Duforestel, T., Roux, J. J., Rusaouën, G., CETHIL, I. L., 2011. Exploitation of the environmental energy resources: indicators and design strategies. In proceeding of the 12th Conference of the International Building Performance Simulation Association, pp., 2672-2679.

[15] Clark, G., Allen, C., 1978. The estimation of atmospheric radiation for clear and cloudy skies. In proceedings of 2nd National Passive Solar Conference (AS/ISES), pp., 675–678.

[16] Clark, G., Loxsom, F., Allen, C., Treat, C., 1985. Assessment of Passive Cooling Rates and Application in the U.S., DOE Contract DE- AC03-77CS31600.

[17] Cole, R.J., 1976. The longwave radiative environment around buildings. Building and Environment 11(1), 3-13.

[18] Daguenet, M., 1985. Les séchoirs solaires: théorie et pratique.

[19] Eicker, U., Dalibard, A., 2011. Photovoltaic–thermal collectors for night radiative cooling of buildings. Solar Energy 85(7), 1322-1335.

[20] Fuentes, M.K., 1987. A simplified thermal model for flat plate photovoltaic arrays. Sandia Report SAND85-0330-UC-63, Albuquerque, N.M.

[21] Garg, H.P., 1982. Treatise on solar Energy, vo1: Fundamental of solar energy. Chichester: John Wiley & Sons.

[22] Hottel, H. C., Egbert, R. B., 1942. Radiant heat transmission from water vapor. Trans. American Institute of Chemical Engineers, 531-568.

[23] Huang, Y., Su, F., Seo, D., Karati, M., 2014. Development of 3012 IWEC2 weather files for international locations (RP-1477). ASHRAE Transactions 120(1), New York City, NY, Jan. 18-22.

[24] Idso, S. B., 1981. On the systematic nature of diurnal patterns of differences between calculations and measurements of clear sky atmospheric thermal radiation. Quarterly Journal of the Royal Meteorological Society 107(453), 737-741.

[25] Kasten, F., Czeplak, G., 1980. Solar and terrestrial dependent on the amount of the type of cloud. Solar Energy 24(2), 177-188.

[26] Khedari, J., Waewsak, J., Thepa, S., Hirunlabh, J., 2000. Field investigation of night radiation cooling under tropical climate. Renewable energy 20(2), 183-193.

[27] Kondratyev, K.Y., 1969. Radiation in the Atmosphere. Academic Press, New York.

[28] Kuehn, T.H., Ramsey, J.W., Threlkeld, J.L., 1998. Thermal Environmental Engineering. Third ed., Prentice Hall.

[29] Martin, M., Berdahl, P., 1984. Characteristics of infrared sky radiation in the United States. Solar Energy, 33(3), 321-336.

[30] McQuiston, F.C., Parker, J.D., Spitler, J.D., 2005. Heating, Ventilating, and Air Conditioning: Analysis and Design. Sixth ed., John Wiley& Sons, New York.

[31] Melchor, C.V., 1982. New formula for the equivalent night sky emissivity. Solar Energy 28(6), 489-498.

[32] Meteorological and Environmental Protection Administration of Saudi Arabia, 2013, http://www.pme.gov.sa.

[33] Mills, A.F., 1995. Heat and Mass Transfer. Second ed. McGraw-Hill Higher Education.

[34] National Oceanic and Atmospheric Administration (NOAA), 2013, http://www.nws.noaa.gov/climate/.

[35] Praëne, J. P., Garde, F., Lucas, F. 2005. Dynamic modelling and elements of validation of a solar evacuated tube collector. *Ninth International IBPSA Conference*, Montreal, Canada, 953–960.

[36] Raman, P.K., 1935. Heat radiation from the atmosphere at night. Proc. Ind. Acad. Sci. 1:815

[37] Robitzsch, M. 1926. Arbeiten Observatorium. Lindenberg, Germany, vol. 15 pp. 194.

[38] Saitoh, T. S., Fujino, T., 2001. Advanced energy-efficient house (HARBEMAN house) with solar thermal, photovoltaic, and sky radiation energies (experimental results). Solar energy 70(1), 63-77.

[39] Sloan, R., Shaw, J. H., Williams, D., 1956. Thermal radiation from the atmosphere. Journal of the Optical Society of America, 46(7), 543-547.

[40] Spitler, J. D., 2010. Load Calculation Applications Manual. American society of heating, Refrigeration and Air-Conditioning Engineers, Inc., Atlanta.

[41] Swinbank, W., 1963. Long-wave radiation from clear skies. Quarterly Journal of Royal Meteorological Society 89, 339-348.

[42] Tang, R., Etzion, Y., Meir, I. A., 2004. Estimates of clear night sky emissivity in the Negev Highlands, Israel. Energy conversion and management 45(11), 1831-1843.

[43] Twidell, J.W., Weir, T.D., 2005. Renewable Energy Resources. Second ed., Taylor & Francis.

[44] Whillier, A., 1967. Design factors influencing solar collectors in low temperature engineering applications of solar energy. ASHRAE, New York.

Appendix 1: Nomenclature of Chapter 3

AH	= absolute humidity, (%)
C, f	= sky cloudiness
F_{ss}	= view factor with respect to sky
H	= relative humidity, (%)
M	= roof multiple layers
N	= opaque sky cover
K_0	= clearness index
P_v	= vapor pressure, (mbar) except models: *25, 34*, and *35.f* in (Pa)
P_{atm}	= Atmospheric pressure, (mbar)
q_{conv}	= outside roof heat convection, (W/m^2)
q_i	= combined internal heat transfer, (W/m^2)
q_{sky}	= sky long wave radiation, (W/m^2)
q_{solar}	= absorbed solar radiation, (W/m^2)
T_{amb}	= ambient air temperature, (K) except models *20 and 32* in (°C)
T_{dp}	= dew point temperature, (°C) except model *11.a* in (K)
T_{sky}	= sky effective temperature, (K) except models *20 and 32* in (°C)
$T_{x=L}$	= outside roof surface temperature, (K)
Z	= site elevation, (m)
$k_{1,..,M}$	= roof layers thermal conductivities, (W/m K)
$L_{1,..,M}$	= roof layers thickness, (mm)
$c_{1,..,M}$	= roof layers thermal capacities, (J/kg K)
Greek	
$\rho_{1,..,M}$	= roof layers densities, (kg/m^3)
ε	= roof outside surface emissivity
ε_{sky}	= sky effective emissivity
σ	= Stefan–Boltzmann constant, (W/m^2 K^4)

4. Effect of Clouds and Dust Storms on the Sky Radiation Exchange for Buildings Located in Hot-Dry Climates

4.1. Abstract

This paper evaluates the impact of effective sky temperatures on building radiation exchange under clear, cloudy, and dusty conditions for extreme hot and dry climates. In part, a dusty sky temperature model has been introduced as a function of atmospheric aerosol optical depth. The sky radiative exchange was evaluated using a one-dimensional transient heat transfer model with numerical calculations performed using the fully implicit finite difference method. The newly available ASHRAE 2013 clear sky model was evaluated and implemented to calculate the hourly incident solar radiation for a horizontal roof under the extreme hot-dry climate conditions of Riyadh, Saudi Arabia. Results showed that in clear sky conditions, sky long wave radiation contributes to a reduction of the total heat gain. A daily mean clear sky cooling around 2645 W-hr/m^2 and 2385 W-hr/m^2 was estimated for July and January, respectively. In contrast, cloud and dust covers increase effective sky temperature and diminish the role of sky radiative cooling. Depending on severity, the mean contributed sky cooling heat exchange was found to range between 436 W-hr/m^2 and 1636 W-hr/m^2 for dust storm and scattered cloudy sky conditions, respectively. Similarly, the ASHRAE 2013 clear sky model and the sky temperature models were shown for four other extreme hot-dry global sites.

4.2. Introduction

In extreme hot and dry climates, excessive heat causes an occupant thermal discomfort. Therefore, buildings consume a substantial portion of energy due to the high demand on cooling (Ben Cheikh and Bouchair 2004). For example, in Saudi Arabia, about 76% of generated electric energy is used for operating residential, governmental and commercial buildings. About half of the total consumption is used for the residential sector (Saudi Electric Company 2012). The residential sector high consumption is due to the inefficient buildings and harsh climate of Saudi Arabia. Moreover, the energy required to cool buildings account for a big portion, up to 73% of the total electric energy (Elhadidy et al. 2001, Algarni and Nutter 2013). Therefore, an optimum design of building elements is very essential.

Several studies have evaluated the thermal performance of building elements, analytically, experimentally, and with numerical modeling. Various methods of solving heat conduction in building composite roofs, such as Green functions and Laplace transforms, were described by Ozisik (1993). A comprehensive review on experimental studies and several building design tools was prepared by Balaras (1996). The study presented the concept of thermal mass and summarized parameters that affect the performance of thermal mass on building cooling load. A one-dimensional transient model to evaluate the thermal behavior of building walls was described by Al-Sanea (2000). The model was solved by using the finite difference method. The interface resistances between wall layers were ignored and constant thermal properties assumed. McQuiston et al. (2005) described several methods of calculating transient conduction heat through building walls and roofs. Such methods include Lumped parameter, numerical (finite difference and finite element), frequency response, and Z-transform methods.

Specific studies such as the optimum location of the insulation layer and its optimum thickness were investigated. Al-Sanea and Zedan (2001) investigated the effect of insulation layer location in the building wall on daily mean heat transfer and peak loads on local hot-dry of Riyadh, Saudi Arabia. They recommended locating the insulation single layer near the outer wall surface. A similar study was done by Ozel and Pihtili (2007a). They investigated the most suitable location of multi insulation layers on building roofs. Using three layers of insulation on the outer, middle, and inner surfaces of the roof were recommended while the total wall thickness was kept constant. In addition, it has been shown that a similar configuration can be applied on the wall elements (Ozel and Pihtili 2007b). Al-Sanea et al. (2012) introduced and numerically developed the concept of optimum thermal mass thickness and location on dynamic heat transfer behavior of insulated walls. Adjustments were made to the wall insulation layer and varying thermal mass thickness to keep the total composite wall thermal resistance constant. In addition, the importance of light roof color on building heat gain in hot climates has been discussed (Suehrcke et al. 2008).

In many extremely hot and dry climate areas, such as the Middle East, a horizontal roof is the most common building roof type. Regardless of building orientation, the outside roof surfaces are exposed to external environmental conditions. Solar radiation, outdoor air temperature, sky long wave radiation, and other factors strongly affect inside comfort of the building and the cooling equipment capacity. Therefore, properly estimating the cooling and heating loads depends on an accurate consideration of these influential factors.

As the major contributor, incident radiation predictions are necessary for building load calculations (Maxwell 1998, Rigollier et al. 2000, Yang and Koike 2002). The ASHRAE 1967 clear sky model has been used in most previous building energy studies to calculate the solar

68

radiation during daytime (Gueymard and Thevenard 2009). The model can be applied at any selected site as a function of location, the standard meridian and knowledge of clearness factor. The model was recently upgraded twice, in 2009 and 2013, providing better accuracy and versatility (ASHRAE 2009, ASHRAE 2013).

Sky radiative exchange is a parameter that generally contributes in reducing building cooling loads, and is mainly a function of the effective sky temperature. Several sky temperature models have been proposed to account for the effect of sky long wave radiation. A detailed review has been performed by (Algarni and Nutter 2015). Generally, evaluation of sky temperature is a strong function of site location and climate conditions. Therefore, a local sky temperature model is required for sky cooling predictions. Nevertheless, for many hot and dry climate areas, the lack of local sky temperature models is problematic. For example, even though Tang et al. (2004) developed a sky temperature model for the climate of the Negev Highlands in Israel, the model is not recommended for extreme hot-dry Saudi conditions; the model is limited to the ambient air temperature in the range of 19°C to 33.5°C. In most building energy studies, the impact of sky long wave radiation is not fully predicted, especially for dusty climates. It was found that the simplest models were the ones most often utilized. Some parameters, which may impact the sky temperature models, are neglected, such as atmospheric aerosols (i.e. dust and smog). Moreover, the literature reveals the application of sky radiative cooling is not currently commercially available (Eicker and Dalibard 2011). Therefore, there is a need for additional data and research that captures additional variables leading to better sky temperature predictions. As a result, the current study aims to numerically quantify the influence of sky radiative cooling effects on building roof thermal behavior under the conditions of extreme hot-dry climates.

In this study, the ASHRAE 2013 clear sky model (ASHRAE 2013) has been implemented

for accurate estimation of the hourly solar radiation. Moreover, newly available measured sky

temperatures of Saudi Arabia have been compared with published sky models to assess the best

fit model under Saudi sky conditions. Furthermore, a dusty sky temperature model has been

proposed using the Aerosol Optical Depth (AOD). The impacts of sky temperature on the

cooling load gained though non-insulated and insulated roofs are studied. Finally, the impact of

sky radiative exchange has been also evaluated in four other extreme hot-dry global sites

including Alice Springs, Australia; Jaisalmer, India; Khartoum, Sudan; and Phoenix, AZ, United

States.

4.3. *Problem formulation and computational procedures*

A composite horizontal surface (roof) of multiple layers as denoted by (N) is shown in Figure

4.1. The roof's outside surface is exposed to convection heat flux (q_{conv}), solar absorbed (q_{solar}),

and sky long wave radiation exchange (q_{sky}). The inside surface of the composite roof is

subjected to combined internal convection and radiation heat transfer, (q_i), (Spitler 2010). During

a clear sky night, the net heat transfer balance is negative (cooling) due to long wave radiation

between the roof and sky. In other words, the roof is losing heat to the sky. Generally, long wave

radiation exchange between the sky and the roof surface can be calculated by the following

equation:

$$q_{sky} = \varepsilon \sigma F_{SS} (T_{sky}^4 - T_{x=N}^4) \qquad (1)$$

where the sky view factor with respect to flat roof equals 1 assuming that there are not tall buildings in the surrounding area.

Note that for a non-horizontal surface, calculating the effective sky temperature requires a path length (McQuiston et al. 2005).
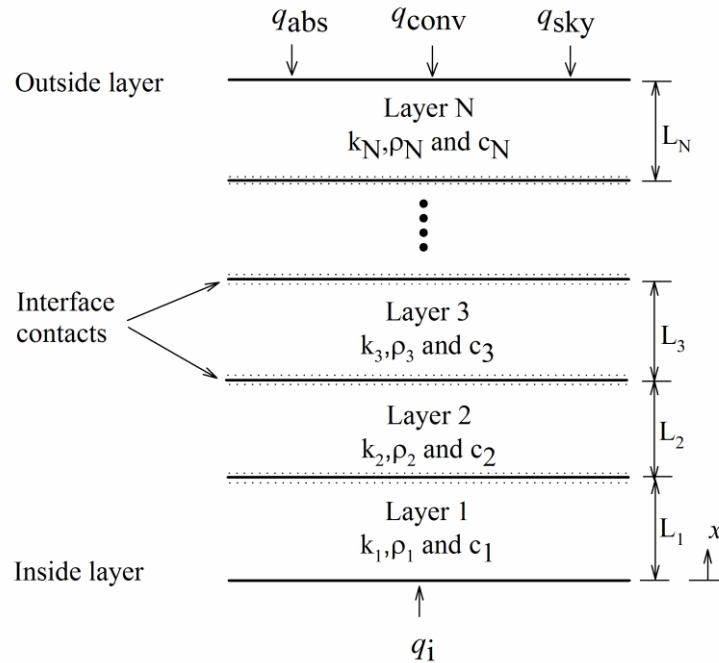
Figure 4.1 A composite roof with multi layers N

The finite-difference solutions for solving the one-dimensional heat transfer equations are used to calculate absorbed solar flux, outside convention flux, sky long wave radiation, and combination of internal convection and radiation heat transfer (Al-Sanea 2002).

The numerical calculations have been performed using the fully implicit finite difference method under the climate conditions of Riyadh, Saudi Arabia. Table 4.1 summarizes input parameters used in the model calculations.

71

Table 4.1 Input parameters used in the model calculations

Parameter	Description
Location	Riyadh, Saudi Arabia
Latitude	24.70 N
Longitude	46.73 E
Elevation	620 m
Indoor set point temperature	25°C
Roof solar absorptivity	0.4

4.4. Roof description and thermal properties

Two roof configurations are considered in this study: a non-insulated roof and an insulated roof. The non-insulated roof represents 70% of the current residential roof type in Saudi Arabia (Saudi Aramco 2011), and consists of 150 mm of reinforced concrete and a layer of plaster attached to the inside of the roof. Additional insulation near the inside roof layer is added to represent the second case, the insulated roof. Thermo-physical properties of the roof materials tested in the study are listed in Table 4.2.

Table 4.2 Roof materials thermo-physical properties (Croy and Dougherty 1983)

Material	k (W/m K)	ρ (kg/m³)	c (J/kg K)	Thickness (mm)
Cement plaster	0.72	1858	837	20
Reinforced concrete	1.73	2243	920	150
Extruded polystyrene	0.029	35	1213	60

4.5. ASHRAE clear sky models

Several ASHRAE clear sky models have been introduced in literature to calculate the total solar incident during a day (ASHRAE 1985, 2009). To minimize the variation with measured

solar radiation, ASHRAE 2013 clear sky model (ASHRAE2013, Gueymard and Thevenard 2013) was introduced to calculate the solar radiation components using beam and diffuse optical depths. The optical depths accounts for the effect of dust and smoke particles. ASHRAE 2013 model calculates beam normal and diffuse horizontal radiation as functions of site specific data. Moreover, the model does not require knowledge of the clearness number in calculation. ASHRAE 2013 clear sky model can be summarized in the following equations:

The beam normal radiation is calculated as:

$$E_b = E_0 \exp\left(-\tau_b . m^{a_b}\right) \qquad (2)$$

And the diffuse horizontal radiation can be calculated as:

$$E_d = E_0 \exp\left(-\tau_d . m^{a_d}\right) \qquad (3)$$

Air mass (m) is defined as (Kasten and young, 1989):

$$m = 1/\left[\sin\beta + 0.50572(6.07995 + \beta)^{-1.6364}\right] \qquad (4)$$

The air mass exponents can be calculated as:

$$a_b = 1.454 - 0.406.\tau_b - 0.268.\tau_d + 0.021.\tau_b.\tau_d \qquad (5)$$

$$a_d = 0.507 + 0.205.\tau_b - 0.080.\tau_d - 0.190.\tau_b.\tau_d \qquad (6)$$

Generally, ASHRAE 2013 clear sky model was introduced for better estimation of solar radiation. The model was validated with clear solar irradiation data collected in several stations such as Golden Colorado, USA; Darwin, Australia; and Xianghe, China.

In the current study, ASHRAE 2013 clear sky model has been implemented to calculate the daily hourly solar radiation of Riyadh, Saudi Arabia. The site specific data: beam and diffuse optical depths are given in ASHRAE (2013) as shown in Table 4.3. In fact, ASHRAE (2013) provides measured solar data such as clear sky beam normal and diffuse horizontal radiations along with corresponding optical depths for 28 stations in Saudi Arabia.

Table 4.3 Beam and diffuse pseudo-optical depths data for Riyadh, Saudi Arabia (ASHRAE 2013)

	Jan	Feb	Mar	Apr	May	Jun	Jul	Aug	Sep	Oct	Nov	Dec
τ_b	0.425	0.483	0.549	0.603	0.646	0.565	0.538	0.517	0.451	0.421	0.413	0.402
τ_d	2.147	1.936	1.755	1.620	1.504	1.603	1.683	1.747	1.930	2.090	2.162	2.224

The results of ASHRAE 2013 model for calculating the average monthly incident solar radiation for 12 months compared with the measured data (ASHRAE 2013) are presented in Figure 4.2. Good agreement between the calculated and measured global horizontal solar radiation was obtained. Therefore, ASHRAE 2013 model was implemented in this study without modification to predict the hourly incident solar radiation for a horizontal roof.
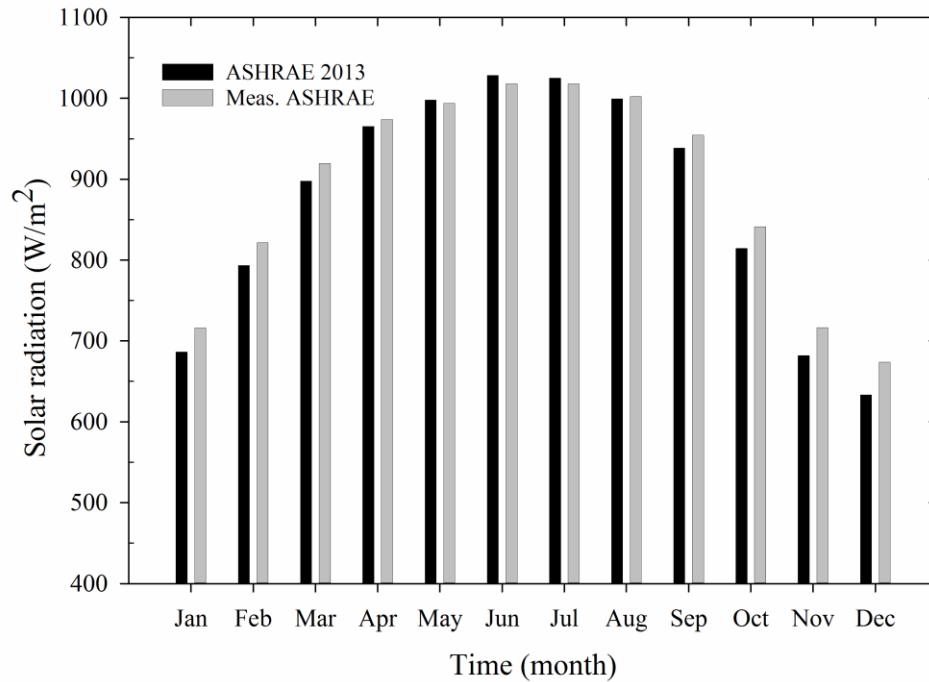
Figure 4.2 Monthly variation of calculated and measured (Meas.) global horizontal radiation at noon for the 12 months of Riyadh, Saudi Arabia

4.6. Sky temperature models

Current sky and emissivity models are mainly focused on two sky conditions; clear and cloudy sky (Algarni and Nutter 2015). Moreover, within the literature, the effect of dust on sky temperature conditions has not yet been numerically modeled. In Saudi Arabia, the desert represents a big part of the country, where dust storms are very common during spring and summer (Notaro et al. 2013).

The sky of Saudi Arabia can be described as clear, cloudy, or dusty. Unfortunately, a model that predicts effective sky temperatures has not been developed for Saudi Arabia conditions. Therefore, the first step was to choose the most appropriate sky temperature model compared to

local measured data. Then use the best fit sky temperature model in the numerical transient model.

Recently, extensive measurements on the sky of Riyadh, Saudi Arabia for all sky conditions have been measured (Maghrabi 2012). The data was collected by using a single channel infrared detector from June 2008 to May 2011, where the collected data was taken every 15 minutes. The accuracy of the detector sensor is ± 0.15°C and ± 2% humidity at ambient temperature of 25°C (Maghrabi et al. 2011).

Maghrabi (2012) classified cloudy sky into three types; scattered, partly, and overcast. Similarly, dusty sky was divided into blowing dust, dust storm and severe storm as a function of visibility (Furman 2003). Mean, minimum, and maximum relative sky temperatures along with collected data amount and visibility were summarized in Table 4.4.

Table 4.4 Relative sky temperatures of Riyadh, Saudi Arabia (Maghrabi 2012)*

Sky condition		Data amount (hours)	Mean	Min	Max	Visibility (km)
			Relative Sky Temperature (°C)			
Clear		6511	-28.16	-48.00	-2.12	9.81
Cloudy	Overcast	546	-10.18	-26.54	5.31	6.06
	Partly	239	-14.02	-29.54	2.44	6.08
	Scatter	370	-17.48	-37.69	5.23	5.77
Dust	Blowing dust	1160	-11.51	-20.83	-0.02	2.90
	Dust storm	109	-6.13	-18.20	4.00	0.78
	Severe storm	46	2.90	-3.10	8.50	0.14

*Sky temperature equals to the relative sky temperatures added to the ambient temperature.

In clear sky conditions, measured data showed that the relative sky temperature ranges between -48.00°C to -2.12°C with a mean of -28.16°C as shown in Table 4.4. Similar reading for cloudy and dusty skies can be applied. Both cloud and dust conditions participate in changing the

sky radiation conditions and then increasing effective sky temperature. In the literature, the lowest relative sky temperature was reported as -40°C in Atacama Desert of Chile (Eriksson and Granqvist 1982). Therefore, the minimum clear sky temperature of Saudi is considered to be the lowest measured temperature based on Maghrabi (2012) measurements. On the other hand, the sky temperature is higher than the ambient temperature by 8.5°C in case of severe storm. However, the sky temperature usually does not pass the ambient temperature as proposed in the most sky temperature models in literature (Berger et al. 1984, Berdahl and Fromberg 1982, Melchor 1982).

In comparison with sky temperature models, very good agreement between the measured mean clear sky temperature and clear sky model is obtained by using Aubinet's (1994) correlation:

$$T_{Sky} = 94 + 12.6\ln(P_v) - 13K_t + 0.341T_{amb} \qquad (7)$$

The Aubinet (1994) correlation accounts for the effect of water vapor pressure in millibars and the ambient air temperature in K. The model also accounts for the sky clearness index (K_t) and is defined as the ratio between global solar horizontal radiation and extraterrestrial solar radiation. An hourly variation between measured clear sky and predicted sky temperatures by Aubinet (1994) is shown in Figure 4.3.
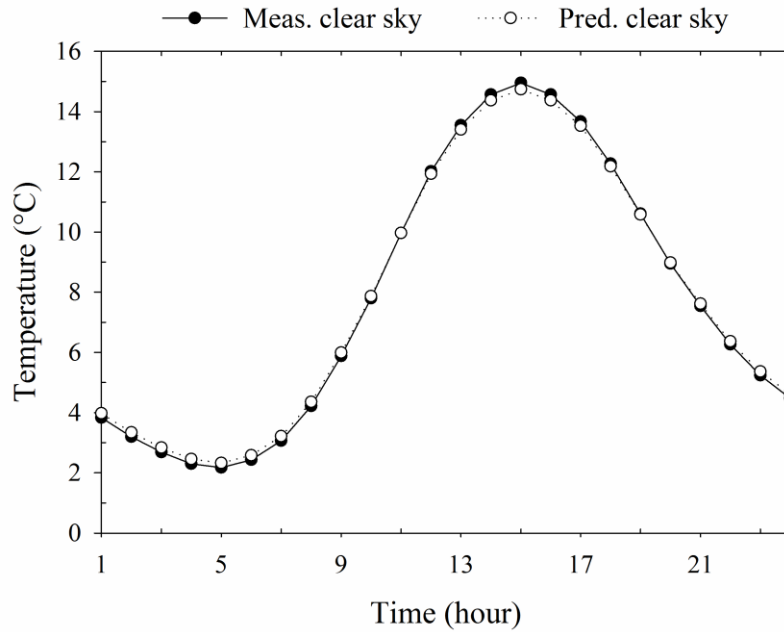
Figure 4.3 Comparison of hourly variations between measured (Meas.) and predicted (Pred.)
clear sky temperatures

The agreement between mean measurements of cloudy sky conditions and predicted sky
models are estimated by using Berdahl and Martin's (1984) model. The model accounts for the
effect of water vapor content and cloud cover degree. In addition, the model's cloudiness
emissivity of the sky was assumed to be 0.9.

Berdahl and Martin (1984) predicted the sky temperature using the following equation:

$$T_{Sky} = (\varepsilon_{Sky-clear} + \varepsilon_{cloud}(1 - \varepsilon_{Sky-clear})f_{cloud})^{0.25} \times T_{amb} \qquad (8)$$

where

$$\varepsilon_{Sky-clear} = 0.787 + 0.764Ln(T_{dp} / 273) \qquad (9)$$

78

In the Berdahl and Martin (1984) model, the cloud sky fraction (f_{cloud}) was assumed to be zero in the case of clear sky conditions, and one for overcast sky. However, compared to the measured data, the model agreed with the measured sky temperatures for fraction factors of 0.1, 0.2, and 0.4 for scattered, partly, and overcast skies respectively. Therefore, it is concluded that the Berdahl and Martin (1984) sky fraction for Saudi clear sky is ranged between 0 and 0.5 as shown in Figure 4.4.
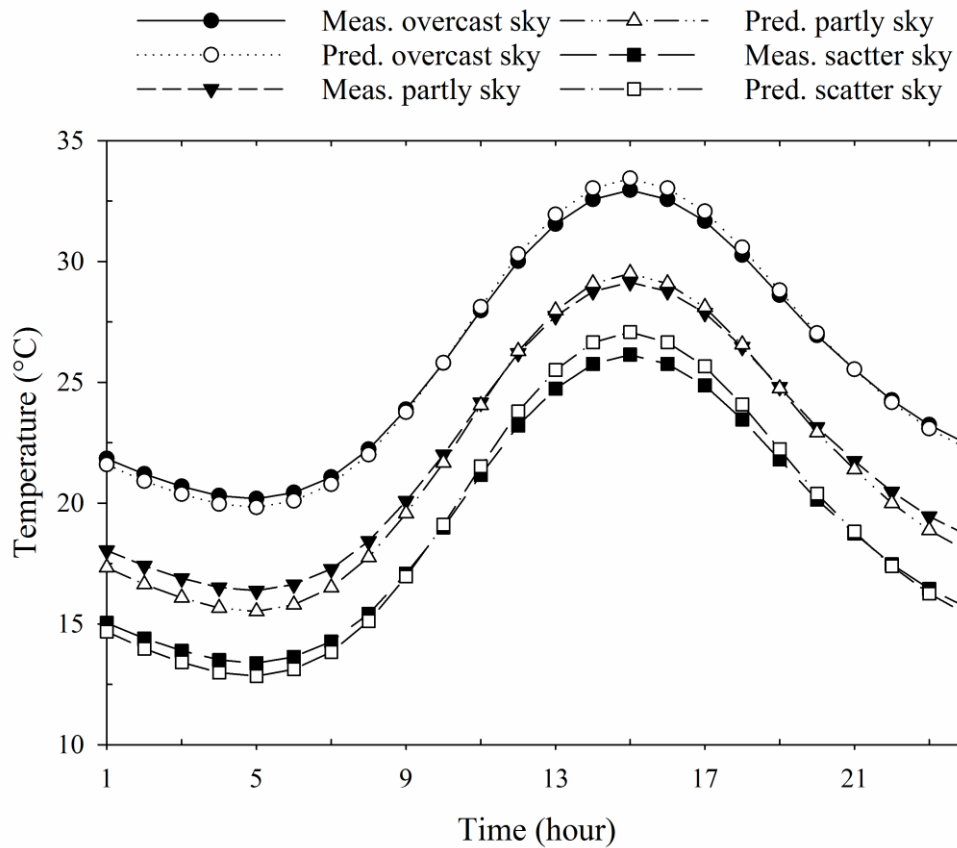
Figure 4.4 Comparison of hourly variations between measured (Meas.) and predicted (Pred.) cloudy sky temperatures

Similar to the Berdahl and Martin model, the following general model is proposed to account for dusty sky conditions:

$$T_{Sky} = (\varepsilon_{Sky-clear} + \varepsilon_{dust}(1 - \varepsilon_{Sky-clear})AOD)^{0.25} \times T_{amb} \qquad (10)$$

In the new dusty sky model, the dusty sky emissivity is assumed to be 0.8 due to dust high emissivity (Maghrabi et al. 2011). Generally, Aerosol Optical Depth (AOD) varies between 0 corresponds to an extremely clean sky and 1 for very dusty sky. The dusty sky model approximated the measured Saudi sky temperatures for AOD of 0.4, 0.7, and 0.9 for blowing dust, dust storm, and severe dust storm respectively as shown in Figure 4.5

AOD worldwide hourly- monthly ground-based measurements are available at AERONET web site (http://aeronet.gsfc.nasa.gov/new_web/data.html). The AERONET data are cloud cleared; therefore, the dusty sky model is recommended for annual building simulation models for dusty and non-cloudy climates. Figure 4.6 shows NASA map of world average AOD from June 2000 through May 2010, (http://earthobservatory.nasa.gov/Features/Aerosols/). It shows West Africa, the Middle East, India, and China share a big portion of desert dust and smoke concentration.
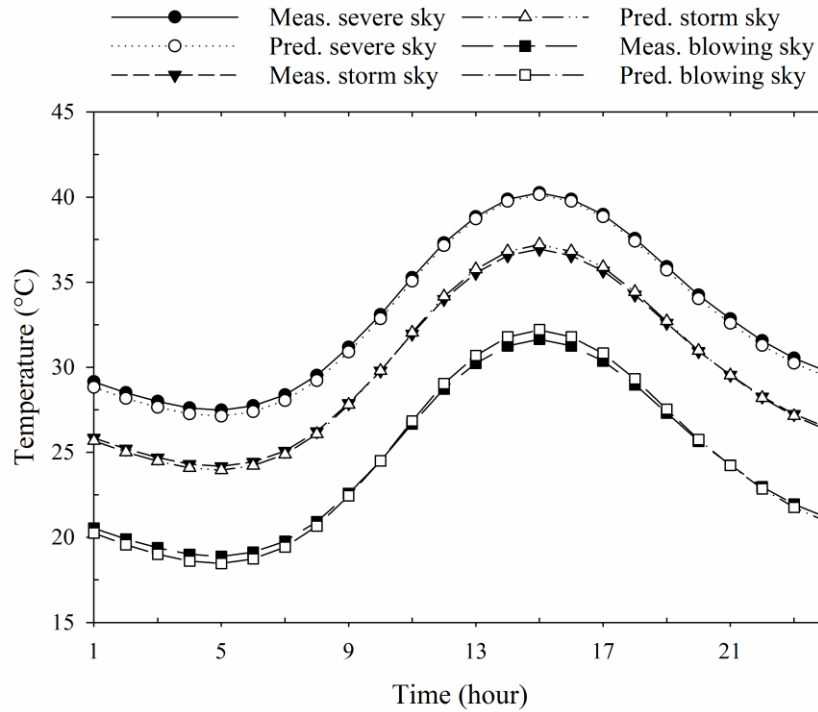
Figure 4.5 Comparison of hourly variations between measured (Meas.) and predicted (Pred.) dust sky temperatures
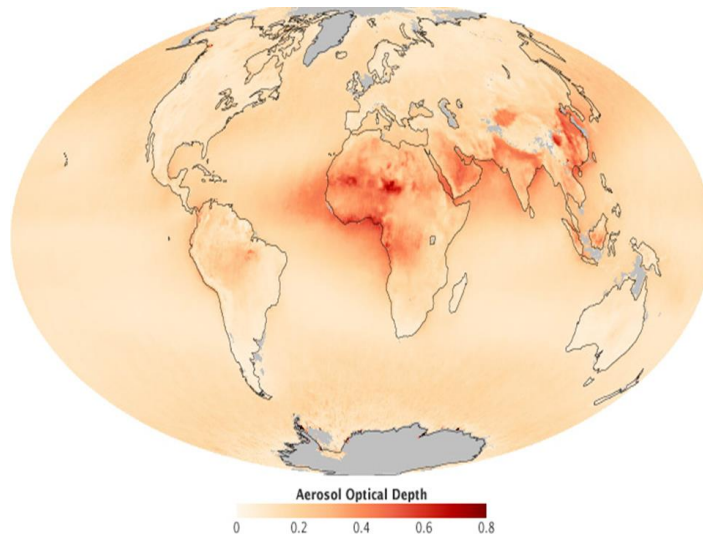
Figure 4.6 NASA world AOD distribution where dark red indicates sky high aerosol concentration and light beige represents a clean sky

81

For this study, the recommended sky temperature models with their sky factors for Riyadh, Saudi Arabia are summarized in Table 4.5. These models can be used for sites which have similar sky and climatic conditions.

Table 4.5 Recommended sky temperature models for Riyadh, Saudi Arabia

Sky condition		Model	Sky Factor/AOD
Clear		Aubinet (1994)- Equation 7	0
Cloudy	Overcast	Berdahl and Martin (1984)- Equation 8	0.1
	Partly		0.2
	Scatter		0.4
Dust	Blowing dust	Dusty sky model-Equation 10	0.4
	Dust storm		0.7
	Severe storm		0.9

4.7. Results and Discussion

The results of heat transfer through the non-insulated and insulated roofs are presented. In both cases, clear sky conditions are assumed. Then the sky long wave radiation exchange is presented for clear, cloudy and dusty Saudi sky conditions and four other extreme hot-dry global sites including Alice Springs, Australia; Jaisalmer, India; Khartoum, Sudan; and Phoenix, AZ, United States.

4.7.1. Non-insulated roof heat transfer components

Figure 4.7 shows the inner and outer temperature distribution of a non-insulated roof along with the ambient temperature of July. Results were considered after several cycles to represent the steady periodic situation over a complete cycle. In addition, the inside room temperature was

set as 25°C. Results showed fluctuations in the inside roof surface temperature due to the ambient temperatures and absorbed solar radiation variations. It should be noted that the outer roof surface temperatures are higher after midday due to the solar radiation peak and below the ambient temperature in night and morning hours because of night sky cooling.
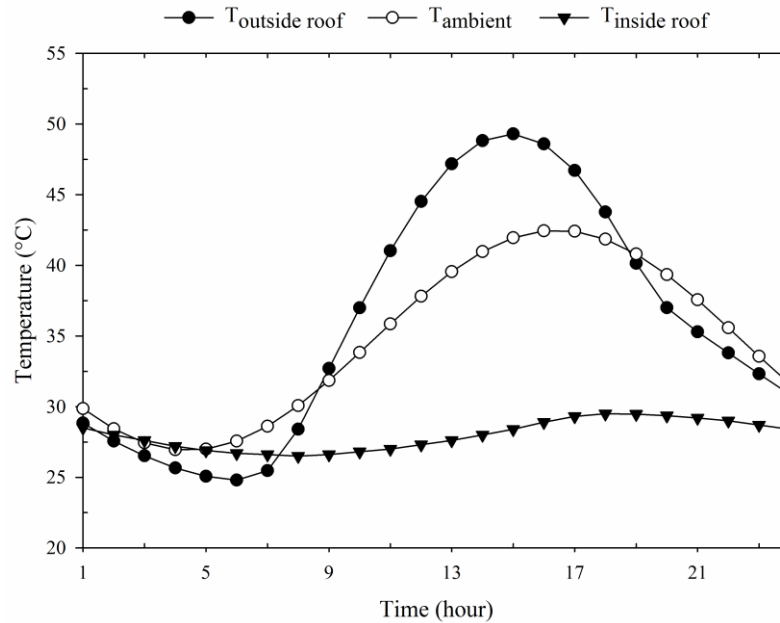
Figure 4.7 Non-insulated roof temperature distributions during a day of July Riyadh, Saudi Arabia

Typically, during daylight hours, the solar absorbed (q_{solar}) is the dominant heat gain onto the surface. On the other hand, the sky long wave radiation (q_{sky}) contributes as a cooling source for buildings as long as the effective sky temperature is lower than the ambient air temperature. The outside roof convection (q_{conv}) heat transfer is the result of the difference between the outside roof and ambient temperature difference. Similarly, the combined internal convection and

83

radiation heat transfer (q_i) is the result of the difference between the inside roof and room design temperature difference.

As shown in Figure 4.8, q_{sky} represents a major heat loss factor (i.e. off-setting heat gains); greatest at midday, which helps reduce the total heat gain over the course of the day. In general, q_{sky} help to reduce heat all day long and shows clearly at night in the absence of solar radiation. In addition, q_{conv} losses are negative whenever the outside roof temperature is higher than the ambient air temperature. Finally, the total net heat transfer (q_{net}) is positive during daytime and negative at nights because of the sky night cooling effect. The total daily q_{net} should be equal to the q_i.
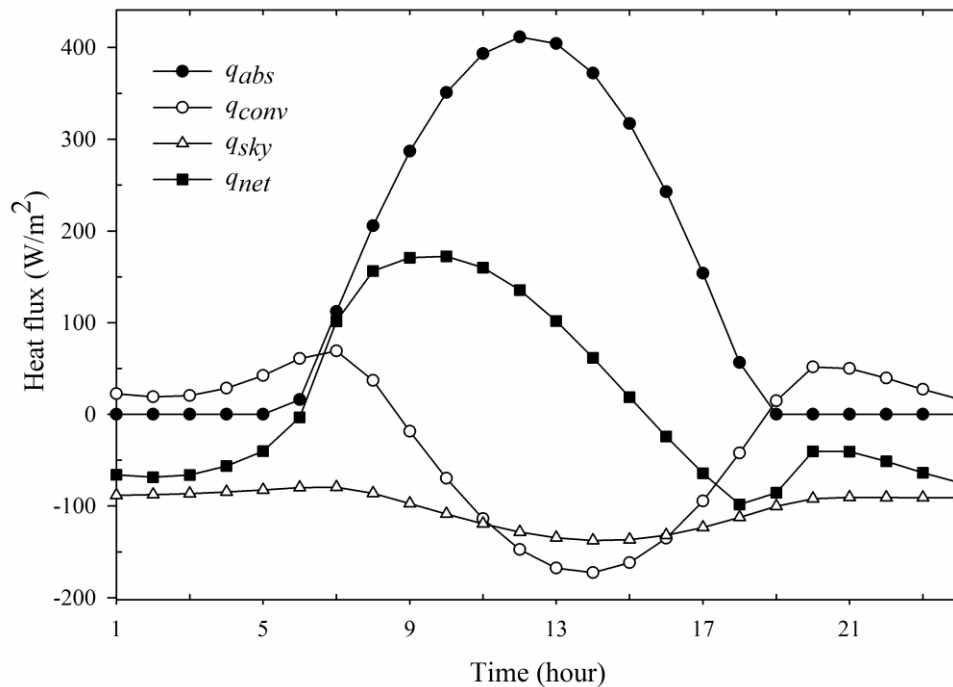
Figure 4.8 Non-insulated roof heat transfer components variations during a typical summer day of July Riyadh, Saudi Arabia

4.7.2. Insulated roof heat transfer components

The insulated roof represents a typical residential roof with an inner single insulation layer. Figure 4.9 shows the variation of inner and outer roof surface temperatures with the ambient temperature during the 21st of July. The insulation improves roof thermal behavior compared to non-insulated results; the inner surface fluctuations are reduced and as a result, better thermal comfort and a lower amount of cooling is required. The inner roof temperature is closer to the setting temperature during the early hours of the day and higher in the late afternoon.
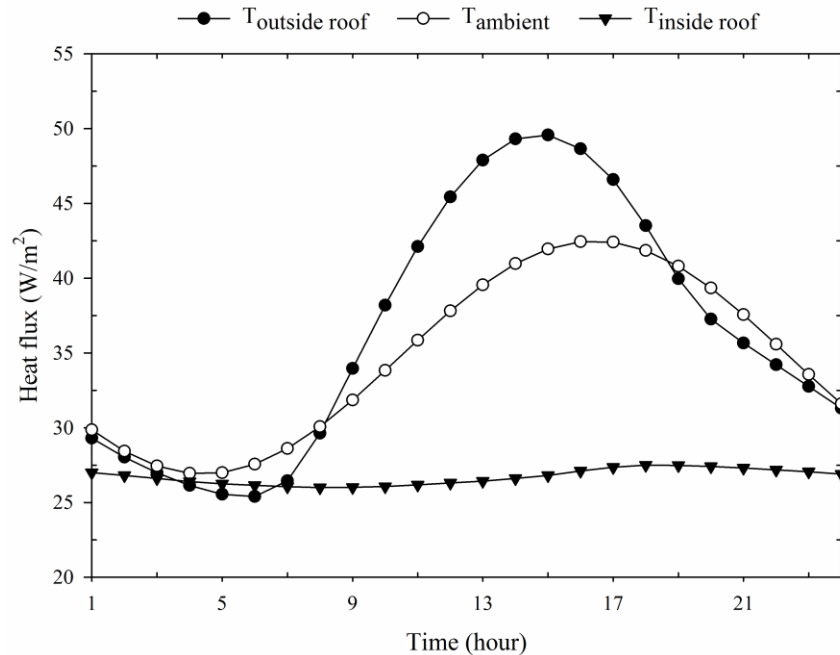
Figure 4.9 Insulated roof temperature distributions during a day of July Riyadh, Saudi Arabia

Figure 4.10 shows similar profiles for roof heat components as shown in the case of the non-insulated roof. However, the combined internal heat transfer rate is reduced because the inner surface fluctuations are less. As a result, the total net heat transfer is lower compared to the non-insulated roof case. Insulation helps reducing surface temperature fluctuations by around $2^{\circ}C$

85

during peak hours and 57% less inside surface combined heat transfer rate or "required cooling load".
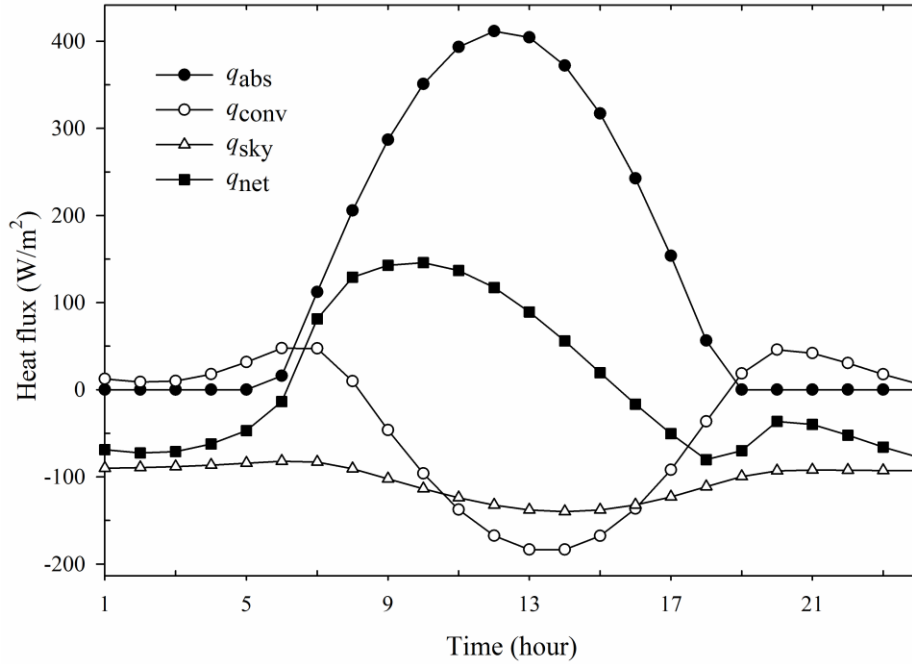
Figure 4.10 Insulated roof heat transfer components variations during a typical summer day of July Riyadh, Saudi Arabia

4.7.3. *Sky long wave radiative exchange*

The sky long wave radiative exchange varies with effective sky temperature and the roof's exterior surface temperature. A daily absorbed solar radiation of 3322.51 W-hr/m^2 and 2028.67 W-hr/m^2 were estimated in July and January respectively. The steady 24 hour exterior surface temperature distribution of the non-insulated roof for July and January was selected. Then the sky radiative exchange using the mean, minimum and maximum effective sky temperature models are calculated for the seven sky conditions and results are shown in Figure 4.11.

Results show that clear sky and severe storm dusty sky conditions are the two most extreme cases. In clear sky conditions (Figure 4.11a), the sky cooling exchange is the most beneficial for building in all sky models for both July and January. A daily mean clear sky cooling around 2645 W-hr/m^2 and 2385 W-hr/m^2 is estimated in July and January respectively. On the other hand, sky cooling diminishes during severe storm conditions where the sky releases heat to the building.   Generally the sky long wave radiation contributes to a cooling exchange with buildings under all sky conditions except severe storm dusty sky. The estimated cooling exchange can be in a mean range between 436 W-hr/m^2, in dust storm conditions, and 1636 W-hr/m^2, in scattered cloudy sky conditions. Furthermore, a similar daily profile of sky long wave exchange for July and January can be observed. However, in case of using the maximum sky temperature model, better sky long exchange is always expected for January. Finally, the sky radiative exchange is estimated for four other extreme hot-dry global sites. The ASHRAE 2013 clear sky model and the sky temperature models (as recommended in Table 4.5) were implemented to evaluate the impact of different sky conditions. The ASHRAE IWEC2 weather data was used to estimate Alice Spring sky factors. Similarly, National Weather Service Forecast Office was used to estimate phoenix sky factors. Khartoum and Jaisalmer sky's factors were equaled to Saudi sky factors due to the lack of their sky data and their similar sky conditions. As shown in Table 4.6, very similar results were found compared to the Saudi Sky impact with a maximum variation of + 4% as in Khartoum site. Under all sites conditions, sky radiative exchange generally participates in reducing roof exterior surface temperatures, resulting in lowering heat transfer into buildings.
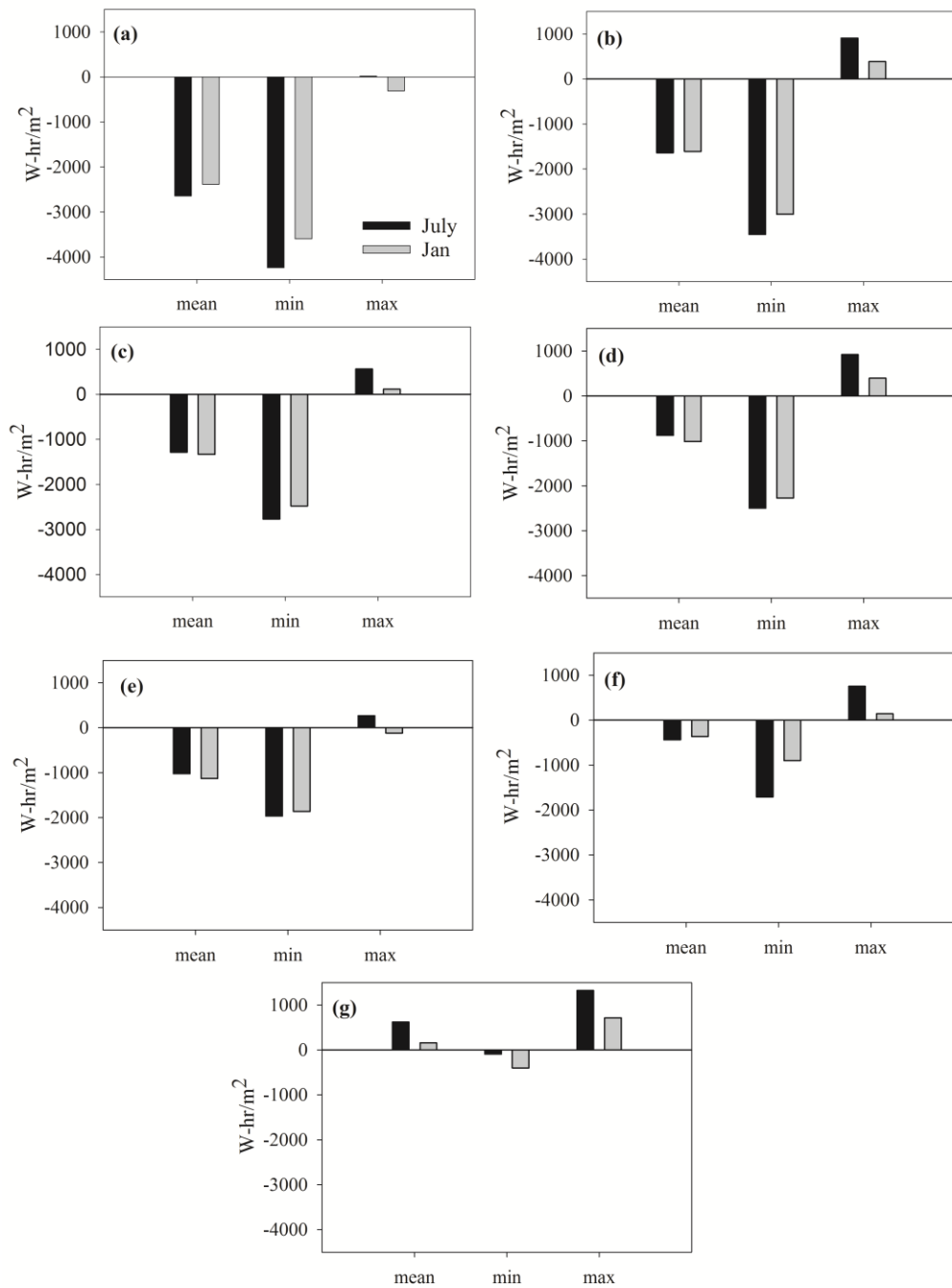
Figure 4.11 Daily heating and cooling sky long wave radiative exchange over a horizontal surface using the mean, minimum, and maximum effective sky temperatures under: (a) clear sky, (b) scattered cloudy sky, (c) partly cloudy sky, (d) overcast cloudy sky, (e) blowing dusty sky, (f) storm dusty sky, and (g) severe storm dusty sky. Not shown is a daily absorbed solar radiation of 3322.51 W-hr/m^2 and 2028.67 W-hr/m^2 were estimated in July and January of Riyadh, Saudi Arabia respectivel

Table 4.6 Daily mean sky long wave radiative exchange over a horizontal surface in extreme hot-dry global sites

Sky Condition		Alice Springs, Australia*±		Jaisalmer, India		Khartoum, Sudan		Phoenix, AZ, United States*+		Riyadh, Saudi Arabia	
		Daily sky-roof long wave exchange load, (W-hr/m²)									
		Summer	Winter	Summer	Winter	Summer	Winter	Summer	Winter	Summer	Winter
Clear		-2595	-2328	-2618	-2344	-2725	-2481	-2592	-2326	-2645	-2385
Cloudy	Scatter	-1599	-1570	-1620	-1579	-1685	-1671	-1610	-1575	-1636	-1607
	Partly	-1260	-1301	-1271	-1310	-1323	-1387	-1265	-1307	-1285	-1334
	Overcast	-863	-994	-871	-1001	-906	-1059	-859	-987	-880	-1018
Dust	Blowing dust	-1002	-1098	-1012	-1110	-1052	-1174	-998	-1095	-1022	-1129
	Dust storm	-	-	-431	-659	-448	-697	-	-	-435	-671
	Severe storm	-	-	615	158	640	167	-	-	621	160

*AOD of 0.2 was used for the blowing dust case
+Sky factors of 0.2, 0.4, and 0.5 were used for the cloudy sky conditions (source: http://www.nws.noaa.gov/)
± Sky factors of 0.2, 0.3, and 0.4 were used for the cloudy sky conditions (source: ASHRAE IWEC2 weather data)

4.8. Summary and Recommendations

4.8.1. Summary

The effect of sky radiative cooling on building roofs was investigated in this study. The study was performed by considering the following three steps. First, the newly ASHRAE 2013 clear sky model was implemented for better estimation of solar radiation during daytime. Second, the measured sky temperatures were compared with sky models in literature and then appropriate sky temperature models selected and dusty sky model proposed. Third, as a result of the previous steps, the one-dimensional transient model was developed to investigate the effect of sky radiative exchange on building roofs. Two kinds of horizontal roofs were considered in the study under the extreme hot-dry climate of Riyadh, Saudi Arabia.

Based on the local extensive measurements of Saudi sky, clear sky temperatures were predicted by using the Aubinet (1994) model. It was found that the Berdahl and Martin (1984) model agreed with the measured scattered, partly, and overcast cloudy sky temperatures using fraction factor of 0.1, 0.2, and 0.4 respectively. Furthermore, the dusty sky model agreed with the measured blowing dust, dust storm, and severe storm dusty sky temperatures with AOD of 0.4, 0.7, and 0.9 respectively. In the numerical model results, sky long wave radiation generally contributes in reducing the total roof heat gain. Finally, the effects of sky long wave radiation on a horizontal surface were shown, including sky radiative exchange under all Saudi skies conditions over a 24 hour period for winter and summer and similar extreme hot-dry global sites.

4.8.2. Recommendations

This work has shown that sky long wave radiative exchange is generally a benefit for building cooling loads; therefore, the effective sky temperatures should be carefully predicted and included in building load calculations. For all Saudi skies and similar hot and dry climate site conditions (i.e., Alice Springs, Australia; Jaisalmer, India; Khartoum, Sudan; and Phoenix, AZ, United States.), the presented sky models should be used instead of approximation. In a dusty climate, using hourly-monthly AOD as a dusty cover in annual simulation is also recommended. Careful consideration for calculating horizontal and non-horizontal surfaces incident solar radiation is required. ASHRAE 2013 clear sky model shows better results and accuracy than the previous ASHRAE clear sky models. Therefore, ASHRAE 2013 clear sky model is recommended for solar radiation calculations. Future research efforts should include the effect of dust and aging with time on the roof solar properties. Finally, improving current residential roof insulation helps in reducing cooling load and improves thermal comfort.

4.9. References

[1] Al-Sanea, S.A. 2000. Evaluation of Heat Transfer Characteristics of Building Wall Elements. *Journal of King Saud University* 12(1):285–313.

[2] Al-Sanea, S. A. 2002. Thermal performance of building roof elements. *Building and Environment* 37(7): 665–675.

[3] Al-Sanea, S.A., and M.F., Zedan. 2001. Effect of insulation location on thermal performance of building walls under steady periodic conditions. *International Journal of Ambient Energy* 22(2):59–72.

[4] Al-Sanea, S.A., M.F., Zedan, and S.N., Al-Hussain. 2012. Effect of thermal mass on performance of insulated building walls and the concept of energy savings potential. *Applied Energy* 89(1):430–442.

[5]   Algarni, S., and D., Nutter. 2013. Geospatial Representation of the Residential Energy Use in Saudi Arabia. Proceedings of the 2013 ASME Early Career Technical Conference (ECTC), April 4–6, Tulsa, Oklahoma, USA.

[6]   Algarni, S., and D., Nutter. 2015. Survey of Sky Effective Temperature Models Applicable to Building Radiant Heat Transfer. ASHRAE *Transactions*, vol. 121, part 2-in press.

[7]   ASHRAE. 1985. *1985 ASHRAE Handbook—Fundamentals*. Chapter 27, Fenestration. Atlanta: ASHRAE.

[8]   ASHRAE. 2009. *2009 ASHRAE Handbook—Fundamentals*. Chapter 14, Climatic design information. Atlanta: ASHRAE.

[9]   ASHRAE. 2013. *2013 ASHRAE Handbook—Fundamentals*. Chapter 14, Climatic design information. Atlanta: ASHRAE.

[10]   Aubinet, M. 1994. Longwave sky radiation parameterizations. *Solar Energy* 53 (2):147–154.

[11]   Balaras, C.A. 1996. The role of thermal mass on the cooling load of buildings. An overview of computational methods. *Energy and Buildings* 24(1):1–10.

[12]   Berdahl, P., and R., Fromberg. 1982. The thermal radiance of clear skies. *Solar Energy* 29(4):299–314.

[13]   Berdahl, P., and M., Martin. 1984. Emissivity of clear skies. *Solar Energy* 32(5):663–664.

[14]   Berger, X., D., Buriot, and F., Garnier. 1984. About the equivalent radiative temperature for clear skies. *Solar Energy* 32(6):725–733.

[15]   Ben Cheikh, H., and A., Bouchair. 2004. Passive cooling by evapo-reflective roof for hot dry climates. *Renewable Energy* 29(11):1877–1886.

[16]   Croy, D. E., and D. A., Dougherty. 1983. *Handbook of thermal insulation applications*. NASA STI/Recon Technical Report N, 83, 27158, Denver, Colorado

[17]   Eicker, U., and A., Dalibard. 2011. Photovoltaic–thermal collectors for night radiative cooling of buildings. *Solar Energy* 85(7):1322–1335.

[18]   Eriksson, T.S., and C.G., Granqvist. 1982. Radiative cooling computed for model atmospheres. *Applied Optics* 21(23):4381–4388.

[19] Elhadidy, M.A., Ul-Haq, M., and Ahmad, A., 2001, "Electric energy consumption in selected residential buildings at KFUMP, Dhahran, Saudi Arabia", *Proceedings of the Mediterranean Conference for Environment and Solar, Beirut- Lebanon*, 23–26.

[20] Furman, H. K. H. 2003. Dust storms in the Middle East: Sources of origin and their temporal characteristics. *Indoor and Built Environment* 12(6):419–426.

[21] Gueymard, C. A., and D., Thevenard. 2009. Monthly average clear-sky broadband irradiance database for worldwide solar heat gain and building cooling load calculations. *Solar Energy* 83(11):1998–2018.

[22] Gueymard, C.A. and D., Thevenard. 2013. Revising ASHRAE Climatic Data for Design and Standards – Part II, Clear-Sky Solar Radiation Model (1613-RP). *ASHRAE Transactions,* 119(2):194–209.

[23] Kasten, F., and A. T., Young. 1989. Revised optical air mass tables and approximation formula. *Applied optics* 28(22):4735–4738.

[24] Maghrabi, A. H. 2012. Modification of the IR sky temperature under different atmospheric conditions in an arid region in central Saudi Arabia: Experimental and theoretical justification. *Journal of Geophysical Research: Atmospheres* 117(D19):1984–2012.

[25] Maghrabi, A., B., Alharbi, and N., Tapper. 2011. Impact of the March 2009 dust event in Saudi Arabia on aerosol optical properties, meteorological parameters, sky temperature and emissivity. *Atmospheric Environment* 45(13):2164–2173.

[26] Maxwell, E. L. 1998. METSTAT—The solar radiation model used in the production of the National Solar Radiation Data Base (NSRDB). *Solar Energy* 62(4):263–279.

[27] McQuiston, F.C., J.D., Parker, and J.D., Spitler. 2005. *Heating, Ventilating, and Air Conditioning: Analysis and Design,* 6th Ed. Chapter 8, The cooling load. New York: John Wiley& Sons.

[28] Melchor, C.V. 1982. New formula for the equivalent night sky emissivity. *Solar Energy* 28(6):489–498.

[29] Notaro, M., F., Alkolibi, E., Fadda, and F., Bakhrjy. 2013. Trajectory analysis of Saudi Arabian dust storms. *Journal of Geophysical Research: Atmospheres* 118(12):6028–6043.

[30] Ozel, M., and K., Pihtili. 2007a. Investigation of the most suitable location of insulation applying on building roof from maximum load levelling point of view. *Building and Environment* 42(6):2360–2368.

[31] Ozel, M., and K., Pihtili. 2007b. Optimum location and distribution of insulation layers on building walls with various orientations. *Building and Environment* 42(8):3051–3059.

[32] Ozisik, M.N.. 1993. *Heat conduction*, 2nd Ed. New York: John Wiley& Sons.

[33] Rigollier, C., O., Bauer, and L., Wald. 2000. On the clear sky model of the ESRA-European Solar Radiation Atlas-with respect to the Heliosat method. *Solar energy* 68(1):33–48.

[34] Saudi Aramco. 2011. Kingdom Energy Efficiency. Riyadh, Saudi Arabia.

[35] Saudi Electric Company. 2012. Annual Report. Riyadh, Saudi Arabia.

[36] Spitler, J.D. 2010. *Load Calculation Applications Manual*, SI Ed. Chapter 2, Fundamentals of heat transfer and thermodynamics. Atlanta: ASHRAE.

[37] Suehrcke, H., E. L., Peterson, and N., Selby. 2008. Effect of roof solar reflectance on the building heat gain in a hot climate. *Energy and Buildings* 40(12):2224–2235.

[38] Tang, R., Y., Etzion, and I. A., Meir. 2004. Estimates of clear night sky emissivity in the Negev Highlands, Israel. *Energy conversion and management* 45(11):1831–1843.

[39] Yang, K., and T., Koike. 2002. Estimating surface solar radiation from upper-air humidity. *Solar Energy* 72(2):177–186.

Appendix 2: Nomenclature of Chapter 4

AOD	= Aerosol optical depth
a_b	= beam air mass exponents
a_d	= diffuse air mass exponents
$c_{1,..,N}$	= roof layers thermal capacities, (J/kgK)
E_b	= beam normal irradiance, (W/m^2)
E_d	= diffuse horizontal irradiance, (W/m^2)
E_0	= solar constant, (W/m^2)
F_{ss}	= view factor with respect to sky
f_{cloud}	= cloud sky fraction
K_t	= clearness index
$k_{1,..,N}$	= roof layers thermal conductivities, (W/mK)
$L_{1,..,N}$	= roof layers thickness, (m)
m	= air mass
N	= roof multiple layers
P_v	= vapor pressure, (millibars)
q_{conv}	= outside roof heat convection, (W/m^2)
q_i	= combined internal heat transfer, (W/m^2)
q_{sky}	= sky long wave radiation, (W/m^2)
q_{solar}	= absorbed solar radiation, (W/m^2)
T_{amb}	= ambient air temperature, (°C)
T_{dp}	= dew point temperature, (K)
T_{sky}	= effective sky temperature , (°C)
$T_{x=L}$	= exterior surface temperature , (°C)
Greek	
τ_b	= beam pseudo-optical depth
τ_d	= diffuse pseudo-optical depth
$\rho_{1,..,N}$	= roof layers densities, (kg/m^3)
ε	= exterior surface emissivity
ε_{cloud}	= cloudy sky emissivity
ε_{dust}	= dusty sky emissivity
ε_{sky}	= sky emissivity
$\varepsilon_{sky\text{-}clear}$	= clear sky emissivity
β	= solar altitude angle
σ	= Stefan–Boltzmann constant, (W /m^{2}K^4)

5. Influence of Dust Accumulation on Building Roof Thermal Performance and Radiant Heat Gain in Hot-Dry Climates

5.1. Abstract

This paper presents an effort to estimate the impact of dust accumulation on exterior building roof absorptivity and total radiative heat gain. A new model is introduced to calculate a building solar absorptivity as a function of dust accumulation rate. Hourly dust deposition is modeled using the Non-hydrostatic Multi-scale Model (NMMB) to predict monthly averaged dust accumulation over time. The correlation sensitivities to its input parameters and the impact of dust accumulation on building annual loads are also studied. Results show that dust accumulation increases the roof solar absorptivity from its initial value up to dust absorptivity based on the site climatic condition and roof characteristics. The predicted monthly averaged accumulated dust for all studied sites varies between 1.3 and 73.8 g/m^2/month. The new model has resulted in an annual cooling space increase of 44.7 to 181.1 kWh/m^2/year, for the selected hot-dry sites with moderate to extreme dust storm conditions. Heating reductions were found to be 0.5-13.1 kWh/m^2/year which are not significant in comparison to the increase in annual cooling load. The results of this work were attempted to improve the predictive capability of current building simulation models.

5.2. Introduction

In buildings, roofs are exposed to a big portion of incident solar radiation, which affects the required cooling load by increasing the roof surface temperature. A roof's exterior surface is, in

fact, exposed to several environmental factors specific to the local climate such as dust, rain, sunlight, snow, and wind, all of which contribute to variations in the roof's thermal properties.

Several studies and field test measurements have been conducted to investigate changes in roof thermal properties due to weathering factors and dirt over a large time interval. For example, Berdahl et al. [1] provided an overview of weathering factors that influence roof solar absorptivity of different roof material. The study also explained that roof weathering can increase the solar absorptivity value except in the case of very low-reflective roof materials. Suehrcke et al. [2] investigated the effect of weathering on building solar absorptance over a long period of time. After eight years, weathered white paint with a low initial absorptivity of 0.2 demonstrated an increase of 15%. The Cool Roof Rating Council (CRRC) [3] published a set of extensive roof solar absorptivity and emissivity data in Arizona, Florida, and Ohio in the US. Sleiman et al. [4] analyzed around 1357 CRRC roof samples and found that the mean solar reflectance loss was -6 % to 17% of product type after three years of natural exposure. Weather and age effect are the driving factors in the study. However, these analyses may be refined since CRRC recently released over 2480 samples of roof products [3]. Similarly, the California Energy Commission estimated a reduction in solar reflectance to be 0% to 30% for a typical white membrane and white applied coating within the first three years [5].

Several studies have concluded that improving roof thermal performance results in a major reduction in building energy consumption. For example, high reflective roof (cool roof) has been widely introduced to improve roof thermal performance by reducing cooling energy demand [6-9]. Field tests in Florida and California showed that a 15% and 50% reduction of cooling load can be reached using high reflective building roof coatings [10]. Although installing cool roof has been recommended to reduce heat gain and to improve thermal comfort [11-14], dust

accumulation on building roof may diminishes the benefit of cool roof systems in hot-dry dusty climates.

Dust accumulation on a building roof is a common environmental factor that widely impacts roof thermal performance in hot-dry climates. Within the United States, the high plains area has moderate aerosol (dust) concentration levels. Deserts in North Africa, the Middle East and Asia are the main sources of such storms, and North African and Middle Eastern deserts are considered the two biggest natural dust sources, 50% and 25% respectively [15]. Consequently, dust accumulation on a building's roof can be expected to occur in and around these extremely hot and dry locations.

Dust flux has been measured and modeled for different applications such as human health impact, air quality, soil formation, and transportation visibility. Several experimental studies have measured dust deposition rates as an average over fairly short time periods in areas such as North Africa, America, the Middle East, and Asia [16–23]. Additionally, dust atmospheric models have been designed to predict dust emission, concentration and deposition [24–26]. Dust accumulation can be then be calculated as the sum of hourly dust deposition over a selected time period.

Because dust has a relatively high absorptivity, accumulated dust on a roof's surface will increase the overall roof absorptivity, resulting in higher absorbed solar radiation into the building. As a result, the absorbed solar radiation increases the demand for air conditioning, which may further increase greenhouse gas emissions. Moreover, in hot and dry climates in particular, where air conditioning usage is extremely high, dusty roofs lead to very high peak energy consumption, creating a need for more power plants. It would seem that ultimately, accumulated dust on rooftops in fact renders cool roofs inefficient. To the authors' best

98

knowledge, the impact of dust accumulation is generally overlooked, whereas estimating it would significantly improve roof thermal performance.

The purpose of this study is to provide a physical understanding of the impact of accumulated dust specifically on horizontal building roof thermal performance. Also, the study is attempted to improve the capability of existing building energy simulation models for an accurate estimation of the building's' required cooling load, especially in hot-dry dusty climates.

In this paper, the influence of dust accumulation on the absorptivity of a horizontal surface (e.g., a building roof) and heat gain are studied. A correlation between roof solar absorptivity and dust accumulation is introduced. In addition, dust deposition is modeled to predict the monthly and annual dust accumulation on a building roof using a more accurate calculated solar absorptivity. Finally, the study covers parameter sensitivity and overall impact of roof dust accumulation with annual building loads.

5.3. Heat transfer mechanisms within dust particles and settling roof surface

A horizontal surface (roof) with settling idealized dust particles is shown in Figure 5.1. Roof surface to dust particles heat transfer mechanisms can be defined as Packed Beds heat transfer and summarized as follows: (1) conduction heat transfer between dust particle to another particle and dust particle to roof surface, (2) convection heat transfer between ambient air, roof surface, and dust particle, and (3) radiation heat transfer between dust particle to another particle, and particle to roof surface.
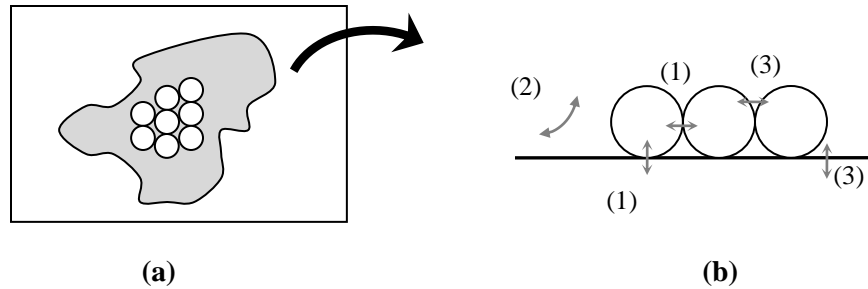
Figure 5.1 **(a)** Roof top view settling dust particles and **(b)** heat transfer modes within dusty surface-side view including: (1) conduction, (2) convection, and (3) radiation heat transfer

However, combined conduction and radiation heat transfer from particle to particle and particle to surface can be ignored due to dust particle and roof surface thermal equilibrium [27, 28]. In addition, because the dust particles are tiny compared to roof surface, particles can be considered as planes. That is, view factors between particles as well as between particles and roof surface are approximated as zeros; hence, radiant heat transfer does not take place. As a result, for building energy calculation, accumulated dust over a building roof can be approximated as a coating layer. Due to its high absorptivity, accumulated dust strongly affects total roof surface solar absorptivity, λ. As shown in Figure 5.2, a fully dusty roof ($\lambda=0.8$) is subjected to double the amount of absorbed solar radiation as compared to a non-dusty concrete roof ($\lambda=0.4$).
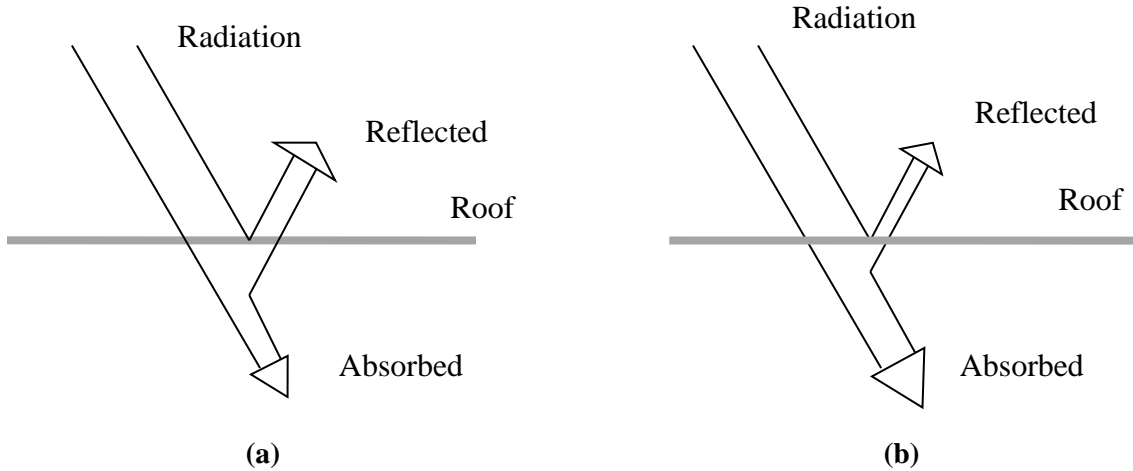
Figure 5.2 Variation of absorbed solar radiation under two roof conditions; **(a)** clean roof and **(b)** dusty roof

5.4.   Role of solar absorptivity and thermal emissivity in building heat gain

Roof solar absorptivity is a key factor in determining exterior roof surface temperature. Generally, lower solar absorptivity maintains a lower roof surface temperature and vice versa. An energy balance on a building's horizontal roof under steady state conditions can be written as:

$$\lambda I_{solar} = h_{out}(T_S - T_a) + F\varepsilon\sigma(T_S^4 - T_{sky}^4) + h_{in}(T_{in} - T_{set}) \qquad (1)$$

Equation (1) shows solar absorptivity, thermal emissivity, and other environmental factors affecting the roof's outside surface temperature. In general, low solar roof absorptivity and high thermal emissivity (cool roof) are usually recommended to reduce roof surface temperature, thereby reducing the cooling load.

Usually a roof has high thermal emissivity (about 0.9 for most nonmetal materials), which offsets the dust impact. In the very different case of materials with low emissivity, such as aluminum coating and unpainted metal, the dust actually serves to increase roof emissivity, thus lowering roof surface temperature. However, on the other hand, due to its high absorptivity, the net effect of accumulated dust is an increase in total roof absorptivity, resulting in a greater total expected absorbed solar radiation into the building. And although a high solar absorptivity slightly reduces winter heating load, in hot and dry climates, any such benefit is greatly outweighed by an overall greater increase in annual cooling load. Despite their critical significance, transient solar absorptivity and thermal emissivity are often not included building energy calculations. To conclude, solar absorptivity and thermal emissivity are both key parameters that affect the roof surface temperature, and each is influenced by accumulated dust.

5.5. *Mathematical model of roof solar absorptivity in dusty conditions*

The literature indicates a linear relationship between roof solar absorptivity and the weather-age effect as a function of exposure time, and can be written as:

$$\lambda = \lambda_{new-roof} + \beta(\lambda_{dust} - \lambda_{new-roof}) \qquad (2)$$

Based on more than three years of field experiments, β was approximated as constant values such as 0.3 by California Energy Commission [5] and 0.17 as proposed by Sleiman et al. [4]. In dusty climates, a roof is exposed to dust deposition which affects total roof solar absorptivity. Therefore, total roof solar absorptivity may be written as a function of dust accumulation $f(M)$ as follows:

$$\lambda = \lambda_{new-roof} + \frac{A_{dust}}{A_{roof}}(\lambda_{dust} - \lambda_{new-roof}) \qquad (3)$$

or

$$\lambda = \lambda_{new-roof} + f(M)(\lambda_{dust} - \lambda_{new-roof}) \qquad (4)$$

The accumulated dust particles, including sand, clay and other particles, are analyzed by considering several assumptions. Homogenous dust particle distribution as well as a spherical dust particle with a fixed mean diameter and density is assumed. And the rate of dust deposition on a building's horizontal rooftop and at ground level are assumed to be identical. In addition, a gray, diffuse, and opaque roof surface is assumed. Therefore, settled dust particles per unit area that may cover a roof area of $N\pi r^2$.

In an analysis similar to Al-Hasan's [29] dusty photovoltaic panel, accumulated dust mass flux on a roof is defined as the product of total number of dust particles, a dust particle's volume, and dust density. The total number of dust particles can be calculated as:

$$N = \frac{M}{V_p \times \rho_p} = \frac{M}{\left(\frac{3}{4}\pi r_p^3\right) \times \rho_p} \qquad (5)$$

As a result, a ratio of unit area covered by dust (A) is defined as:

$$A = \frac{1.5M}{\rho_p \times d_p} \qquad (6)$$

Clearly, it is improbable that a single layer of equally distributed and non-overlapping dust particles would completely cover an entire roof area, since small gaps between settling dust particles usually exist. For example, dust particle arrangement in square and hexagon packing covers 78% and 91% of the underlying area, respectively [30] as shown in Figure 5.3.
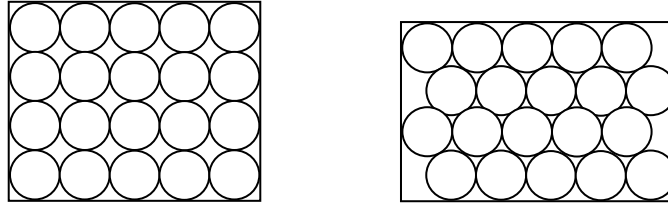
Figure 5.3 Square and hexagon particles packing

Therefore, equation (6) may be written as a function of a packing factor (*f*) as follows:

$$A = \frac{1.5M}{\rho_p \times d_p} f \qquad (7)$$

Finally, by substituting equation (7) in equation (4), the roof solar absorptivity can be expressed as a function of dust accumulation, dust size, density, and packing factor as follows:

$$\lambda = \lambda_{new-roof} + \frac{1.5M}{\rho_p \times d_p} f(\lambda_{dust} - \lambda_{new-roof}) \qquad (8)$$

Therefore, Roof total roof solar absorptivity can be calculated using equation (8) which is constrained by the following three main conditions; clean, partly dusty, or fully dusty as shown in equation (9).

$$if \ A \left(= \frac{1.5M}{\rho_p \times d_p} f \right) = \begin{cases} 0 \\ (0,1) \\ \geq 1 \end{cases} \Rightarrow \begin{cases} \lambda = \lambda_{new-roof} \\ Calc. \ \lambda \\ \lambda = \lambda_{dust} \end{cases} \qquad (9)$$

In equation (9), when there is no dust covering the roof ($A=0$), the solar absorptivity of the roof is equal to the absorptivity of new roof material, and when the roof is completely covered ($A \geq 1$), the solar absorptivity of the roof is equal to dust absorptivity. Otherwise, solar absorptivity of the roof is calculated using equation (8) which is applicable to any location where dust accumulation may exist.

5.6. Dust accumulation prediction

Accumulated dust is a result of dust deposition over a selected time range. The dust deposition rate is defined as the process of dust removal from the atmosphere as dry or wet depositions. Dry dust deposition is a result of gravitational, turbulent and molecular diffusions [31]. In general, wet deposition is similar to dry deposition but associated with rain droplets. Usually the particle diameter of atmospheric dry dust deposition is greater than 5 µm, whereas that of wet dust deposition is less than 5 µm diameters [32].

Dust flux deposition can be calculated as the product of deposition velocity and the dust concentration at a selected reference elevation. Several factors govern the process of deposition including the physical and chemical properties of the particles, metrological factors, and

underneath surface characteristics [33]. The physical properties are dust type, size, shape, and density, in addition to dust particle concentrations in the air. In addition, the dust settling surface itself has an impact on the deposition process. An accurate calculation of dust accumulation must take into consideration all of these factors.

The accumulated dust flux can be predicted to evaluate the impact of accumulated dust through field measurements or numerical models. In the field, dust accumulation can be measured by various methods. In West Niger, Goossens and Rajot [34] used and tested seven different theoretical and experimental techniques. El-Desoky et al. [16] and Modaihsh and Mahjou [17] collected the dust by using a marble dust collector. Malakootian et al. [18] used the British standard method for collecting dust samples. McTainsh et al. [21] recommended avoiding dry traps since they missed collecting 36% of the total dust fallout.

Dry and wet dust depositions have been comparatively modeled and simulated in the literature. In this study, the Non-hydrostatic Multi-scale Model (NMMB) is used to predict dust accumulation for the selected sites. The NMMB model has been developed by Barcelona Supercomputing Center (BSC) in Barcelona, Catalonia, Spain. In the NMMB, modeling dry dust deposition due to gravitational, diffusion, impaction, and interception mechanisms is based on the mathematical model of Zhang et al. [35], which is a widely accepted model for dust deposition prediction. The model predicts hourly dry-wet dust emission, concentrations, transport, depositions and other dust aspects for an hourly time scale. The NMMB model can predict dust deposition at any selected location for a certain time interval. Then, the hourly dry-wet dust deposition can be summed to obtain the measure of accumulated dust. The NMMB model outputs are given in different numerical file formats including NetCDF, csv, and xml, that could potentially be coupled with building energy simulation programs such as EnergyPlus [35].

106

Finally, a detailed description of NMMB model, annual simulations, evaluation and experimental validation are given by Pérez et al. [15] and Haustein et al. [36].

5.7. Sensitivity Analysis

Since roof solar absorptivity correlation is mainly a function of dust particle mean diameter and density, the correlation is tested to evaluate its sensitivity to these two parameters. Generally, the roof absorptivity can vary between clean roof absorptivity up to dust absorptivity value.

5.7.1. Sensitivity to dust particle mean diameter

Dust particles have different diameters which vary from one region to another depending on dust components. In general, dust generated to atmosphere has diameter of less than 20 μm [32]. Therefore, diameters of 5, 10, 15, and 20 μm were tested while using a constant dust density of 2.6 g/cm^3 as shown in Figure 5.4. Results showed that the roof absorptivity increases more quickly with smaller dust particles.
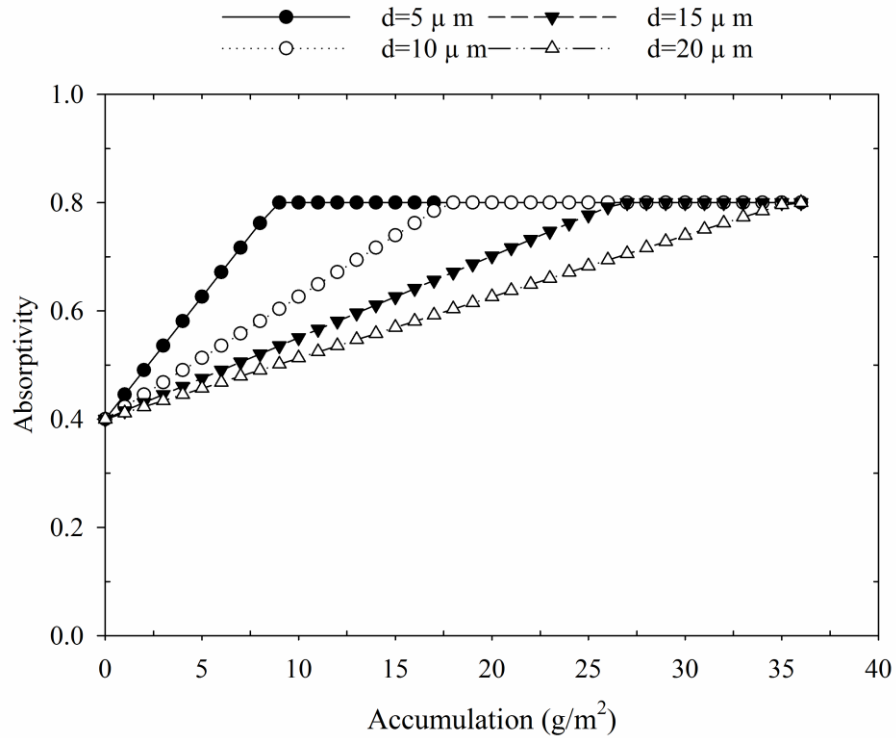
Figure 5.4 Evaluation of roof solar absorptivity with dust accumulation as a function of mean dust diameters using a constant dust density of 2.6 g/cm^3

5.7.2. *Sensitivity to dust particle density*

Dust density varies based on grain size distribution and differs based on environmental characteristics and climate conditions of the site. Generally, dust is classified as a combination of sand, silt, and clay. Modaihsh and Mahjou [17] studied the grain size distribution of fallout dust over 13 different sites located in the country of Saudi Arabia. The study showed silt to be the most dominant grain size. In a similar study, silt and clay shared the representative 63% of the total dust. Hence, knowledge of dust components is significant for determining the dust density [37]. To account for the dust density impact, densities of 1, 1.5, 2, 2.5, and 3 g/cm^3 were tested

108

using a constant dust diameter of 8.5 μm as shown in Figure 5.5. A linear decrease in roof absorptivity as dust density increased was observed.
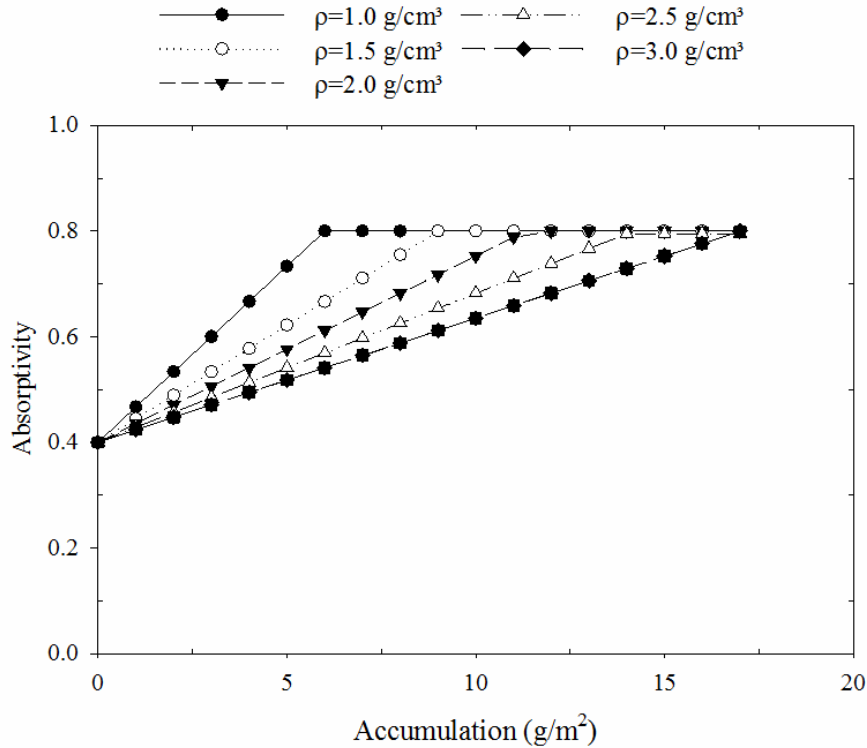
Figure 5.5 Evaluation of roof solar absorptivity with dust accumulation as a function of dust density using a constant dust diameter of 8.5 μm

5.8. Results and discussion

5.8.1. Dust flux prediction

The NMMB online model was used to predict monthly averaged accumulated dust from sixteen different populated locations in the Middle East and North Africa, as shown in Table 5.1. In fact, deserts in the Middle East and North Africa are considered the biggest natural dust sources with a worldwide total of 75% [15]. Results of the model are based on fifteen years of data analysis (2000–2013).

Generally, accumulated dust is the greatest in Saudi Arabia, Kuwait, and Iraq, with a peak accumulation occurring in the summer. In the northern countries of the Middle East (such as Jordan and Syria) and in most of North Africa, moderate accumulated dust is reported with more activity in winter and spring. Therefore, dust accumulation can be classified into four groups based on monthly trends and the amount of accumulated dust: (1) extreme dust accumulation with a summer peak along the west coast of Saudi Arabia, Kuwait, and Iraq, (2) moderate dust accumulation with a summer peak in the southeast of the Middle East, (3) moderate dust accumulation with a spring peak in North Africa and in the northern part of the Middle East, and (4) slight year-long dust fallout in the north of Tunisia and Algeria.

Table 5.1 Sites used in simulation

	Location	
	Latitude (°)	Longitude (°)
Algiers, Algeria	36.8	3.2
Amman, Jordan	31.9	35.9
Baghdad, Iraq	33.3	44.4
Cairo, Egypt	30.1	31.2
Damascus, Syria	33.5	36.3
Doha, Qatar	25.3	51.5
Dubai, UAE	25.0	55.3
ElAuin, West Sahara	27.1	13.2
Jeddah, Saudi Arabia	21.5	39.2
Khartoum, Sudan	15.6	32.5
Khamis Mushait, Saudi Arabia	18.3	42.7
Kuwait, Kuwait	29.4	48.0
Marrakesh, Morocco	31.6	8.0
Riyadh, Saudi Arabia	24.6	46.7
Tripoli, Libya	32.9	13.2
Tunis, Tunisia	36.8	10.2

In the extreme and moderate dust fallout regions, dust accumulation reaches the maximum in June and July and then sharply decreases until it terminates in January, as shown in Figure 5.6

and Figure 5.7. The results show that the maximum averaged monthly dust fallout is 130.1 g/m^2, in Jeddah, the most extreme dust fallout site, due to its frequent severe dust storms. The most moderate accumulation of dust is reported as 34 g/m^2, in Doha.

Figure 5.8 shows monthly averaged moderate dust accumulation (g/m^2) for sites in North Africa and northern of the Middle East. Dust accumulation reaches the maximum during February and March then gradually decreases until late summer. Figure 5.9 shows very slight dust accumulation that may not affect total roof solar properties. The minimum averaged monthly dust fallout is 1.3 g/m^2 in Tunis and 2.1 in Algiers.
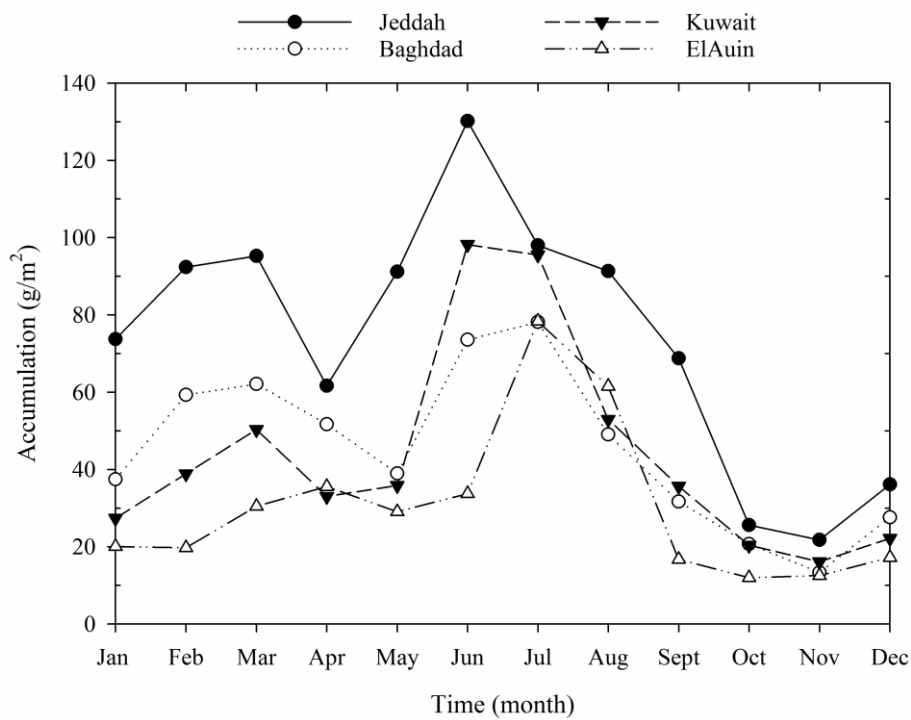
Figure 5.6 Evaluation of extreme monthly averaged dust accumulation within selected sites, during 2000–2013 and by using NMMB model [15]
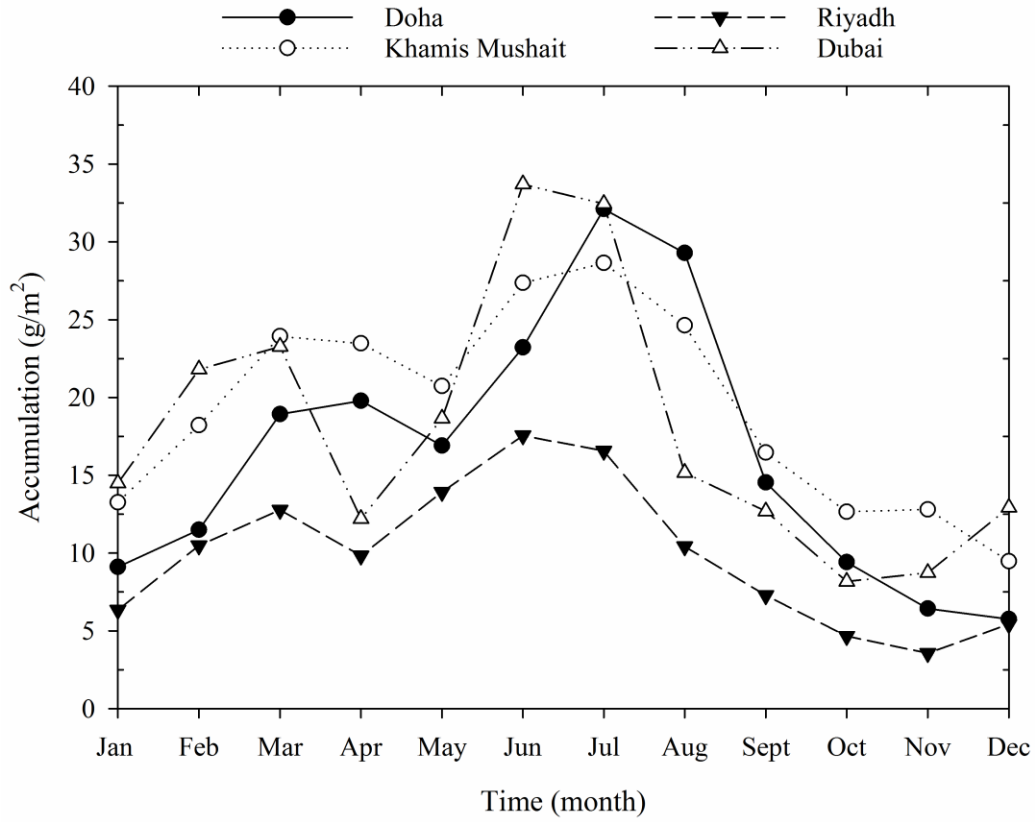
Figure 5.7 Evaluation of moderate monthly averaged dust accumulation within selected sites, during 2000–2013 and by using NMMB model [15]
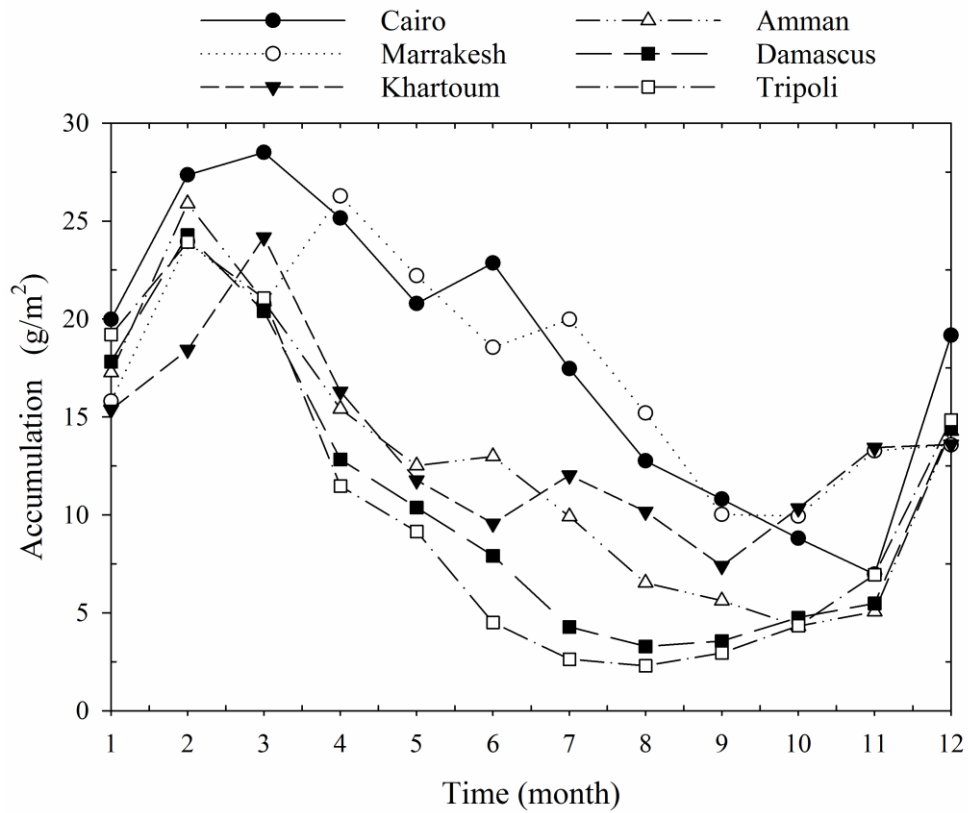
Figure 5.8 Evaluation of spring peak monthly averaged dust accumulation within selected sites, during 2000–2013 and by using NMMB model [15]
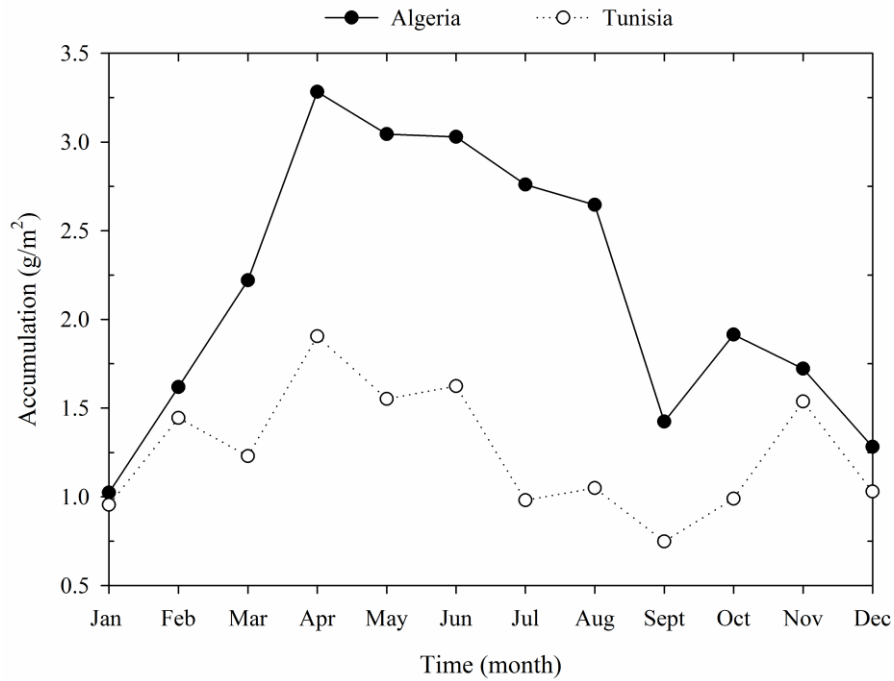
Figure 5.9 Evaluation of slight monthly averaged dust accumulation within selected sites, during 2000–2013 and by using NMMB model [15]

5.8.2. Transient roof thermal performance and heat gain

To study the impact of dust accumulation on building thermal performance, a number of hot-dry sites were selected for building energy simulation as shown in Table 5.1. The impact of dust on building performance was estimated using eQuest 3.65 [38], a building energy simulation program. A single-story residential building (Villa) with an area of 100 m^2 was modeled. Identical building envelopes, equipment, and schedule details were used for all locations as described in Algarni and Nutter [39]. Buildings' walls and roof consist of 0.2 m hollow concrete block with gypsum plastering and 0.15 m concrete slab, respectively. Floor height is 3.5 m and windows are 15% double glazed of wall area. Ventilation and infiltration rates are 0.75 ach. The building operation is 24 hours with various schedule for lighting and equipment. Since horizontal

residential building roofs are the most common traditional architecture in the selected areas, only horizontal roofs were considered in the study. Typical weather data including Typical Meteorological Year 3.0 (TMY3) and International Weather for Energy Calculations 2.0 (IWEC2) were used to simulate the weather for the design building.

Dusty building roof performance compared to that of non-dusty cool and typical roof systems was studied. Cool roof (λ=0.2) and typical concrete roof (λ=0.4) were used in the building simulation. In addition, in order to examine the potential of various roof characteristics under dusty conditions, different roof U-values were also considered. For each site, three roof U-values were used: 0.57, 1.7, and 2.84 (W/m^{2}K), where a lower roof U-value represents an insulated roof.

In the case of dusty conditions, monthly total roof solar absorptivity was calculated as a function of accumulated dust (*M*) using equations. (8) and (9), and results are shown in Table 5.2 for a typical roof (λ=0.4). Similarly, a dusty cool roof (λ=0.2) total absorptivity can be calculated. A long term dust accumulation impact, i.e., a month-to-month dust accumulation, was not considered due to expected periodic cleaning processes such as wind and rain or human cleaning effort. As a result, monthly cooling and heating loads were calculated for the corresponding calculated monthly solar absorptivity and summed for the annual building loads.

Table 5.2 Monthly calculated total roof absorptivity for a typical roof (λ=0.4) in different hot-dry locations using packing factor of 0.91. (Note: 0.8 indicates fully dusty roof absorptivity and 0.4 represents non-dusty roof)

| Site | Monthly calculated total roof absorptivity | | | | | | | | | | | |
	1	2	3	4	5	6	7	8	9	10	11	12
Jeddah	0.8	0.8	0.8	0.8	0.8	0.8	0.8	0.8	0.8	0.8	0.8	0.8
Riyadh	0.7	0.8	0.8	0.8	0.8	0.8	0.8	0.8	0.8	0.7	0.7	0.7
Dubai	0.6	0.7	0.7	0.7	0.8	0.8	0.8	0.7	0.6	0.5	0.5	0.5
Doha	0.8	0.8	0.8	0.7	0.8	0.8	0.8	0.8	0.7	0.6	0.6	0.7
Kuwait	0.8	0.8	0.8	0.8	0.8	0.8	0.8	0.8	0.8	0.8	0.8	0.8
Baghdad	0.8	0.8	0.8	0.8	0.8	0.8	0.8	0.8	0.8	0.8	0.7	0.8
Amman	0.8	0.8	0.8	0.8	0.7	0.7	0.7	0.6	0.5	0.5	0.5	0.8
Damascus	0.8	0.8	0.8	0.7	0.7	0.6	0.5	0.5	0.5	0.5	0.5	0.8
Cairo	0.8	0.8	0.8	0.8	0.8	0.8	0.8	0.7	0.7	0.6	0.6	0.8
Khartoum	0.8	0.8	0.8	0.8	0.7	0.6	0.7	0.7	0.6	0.7	0.7	0.7
Tripoli	0.8	0.8	0.8	0.7	0.6	0.5	0.5	0.5	0.5	0.5	0.6	0.8
Tunis	0.4	0.4	0.4	0.4	0.4	0.4	0.4	0.4	0.4	0.4	0.4	0.4
Algeria	0.4	0.4	0.5	0.5	0.5	0.5	0.5	0.5	0.4	0.4	0.4	0.4
Marrakesh	0.8	0.8	0.8	0.8	0.8	0.8	0.8	0.8	0.7	0.7	0.7	0.7
ElAuin	0.8	0.8	0.8	0.8	0.8	0.8	0.8	0.8	0.8	0.7	0.7	0.8
Khamis Mushait	0.6	0.7	0.8	0.8	0.8	0.8	0.8	0.8	0.8	0.6	0.6	0.4

Based on the above results, annual cooling, heating, and peak roof conduction were calculated for different roof systems. A summary of results is presented in Table 5.3 and discussed below.

It was found that for the selected locations, net building annual cooling was increased and net annual heating was reduced with an overall net annual load increased. Changing roof solar absorptivity from 0.2 to a monthly calculated absorptivity (as shown in Table 5.2), leads to an increase in annual cooling ranging from 44.7 to 181.1 kWh/m^2/yr. in Algeria and in Riyadh, respectively. Similarly, the influence of dust accumulation on a typical roof (λ=0.4) with using a

roof U-value of 2.84 W/m^2 K leads to an annual cooling increase between 49.6 and 126.8 kWh/m^2/yr for the same selected sites. In the case of a well-insulated cool roof, the dust accumulation impact on annual cooling ranges from 18.1 to 44.5 kWh/m^2/yr.

While dust accumulation may present some conserving advantage in the winter—by increasing total roof solar absorptivity which in turn decreases the heating load—in hot-dry climates, winter is a brief concern. The winter heating conservation afforded by dust accumulation in hot-dry climates is only between 0.5 and 13.1 kWh/m^2/yr., a negligible benefit compared to the astronomical annual cooling increase as shown in Figure 5.10.
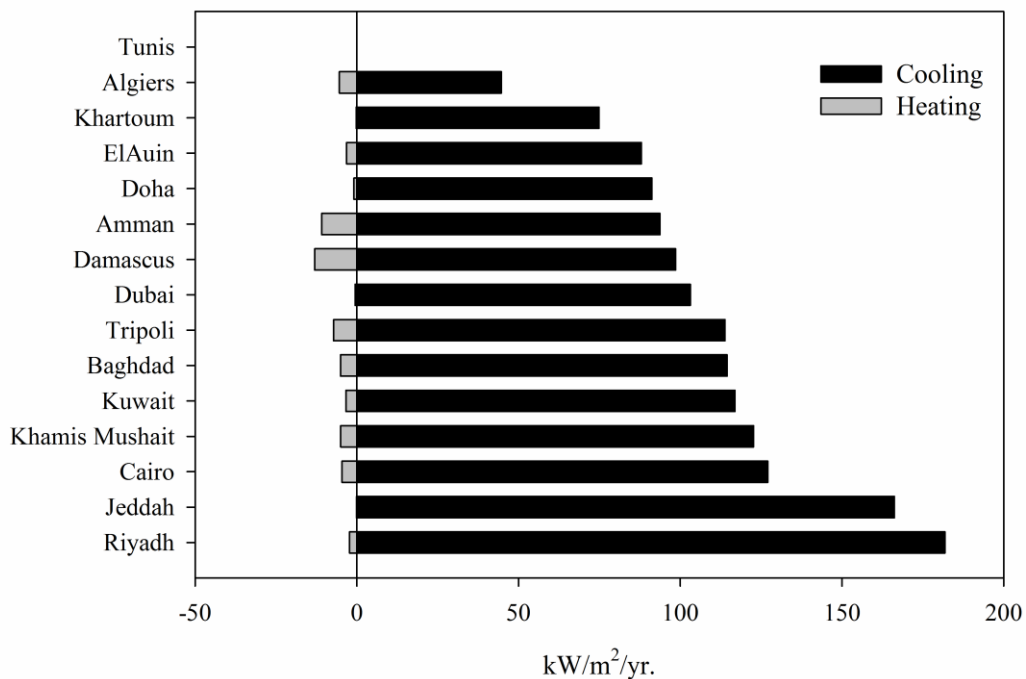
Figure 5.10 Predicted increases in net annual cooling and heating reduction due to dust accumulation over a cool roof (λ=0.2) using a U-value of 2.84 W/m^2 K

Increasing insulation levels reduces the impact of dust accumulation on building roof systems, as shown in Table 5.3. In fact, reducing the roof U-value from 2.84 to 0.57 W/m^2 K

leads to a higher roof performance under dusty roof conditions compared to cool and typical roof systems as follows: in Riyadh, i.e., a 28% cooling space reduction is predicted under a dusty roof compared to 13% and 19% reductions under non-dusty cool and typical roofs for the same site.

Furthermore, net cooling increase in dusty cool and typical roofs for six selected sites with slight to extreme dust storm conditions using three U-values was demonstrated in Figure 5.11.a and 5.11.b. Results indicate the importance of using well insulated roof (lower roof U-values) especially in extreme hot-dry dusty sites and in dusty cool roof as shown in Figure 5.11.a. Also, it can be concluded that net roof cooling increase is not a linear function of roof U-values. It is clear that dust accumulation has a greater impact on poorly insulated buildings. Although the results show that using appropriate insulation is significant for energy saving, most residential buildings in the Middle East and North Africa are poorly constructed. For instance, more that 70% of Saudi Arabian residential buildings are not insulated [39].
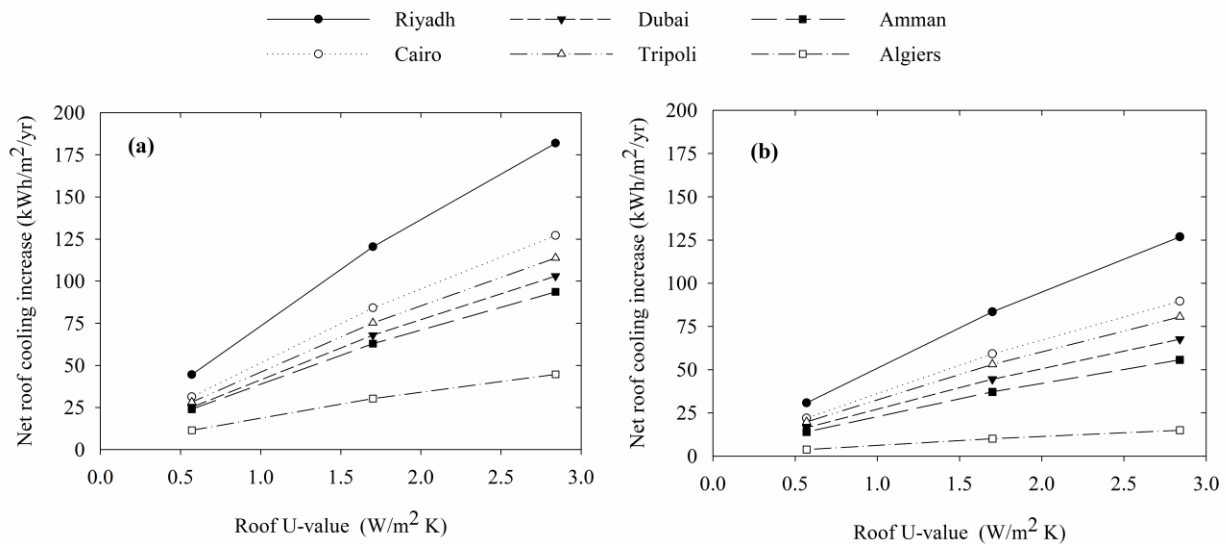
Figure 5.11 Influence of low, medium and high roof U-values on net cooling increase for six selected sites with slight to extreme dust storm conditions under **(a)** a dusty cool roof, and **(b)** a typical dusty roof

Next, the results showed that buildings located in a moderate hot-dry climate have higher corresponding percentage increases in annual cooling. For example, in Khamis Mushait, an increase of 38% in annual cooling was observed as solar absorptivity increases from 0.2 to monthly calculated absorptivity. Similarly, 33% and 32% increases in annual cooling were observed in Amman and Cairo, respectively.

Figure 5.12 depicts the predicted increase in peak roof conduction as a result of dust accumulation on cool and typical roofs. Absorptivity ranges from 0.2 (cool roof) and 0.4 (typical roof) to the corresponding monthly calculated absorptivity (as shown in Table 5.2) with a U-value of 2.84 $W/m^2 K$. Accumulated dust on a cool roof yields a higher increase in peak roof conduction compared to typical roof peak conduction. For cool roof, peak conduction increases by 52% to 71% while the percentage increase in typical roof peak conduction varies between 38% and 53%. Results indicate a cool roof system presents challenges in hot-dry dusty climates.
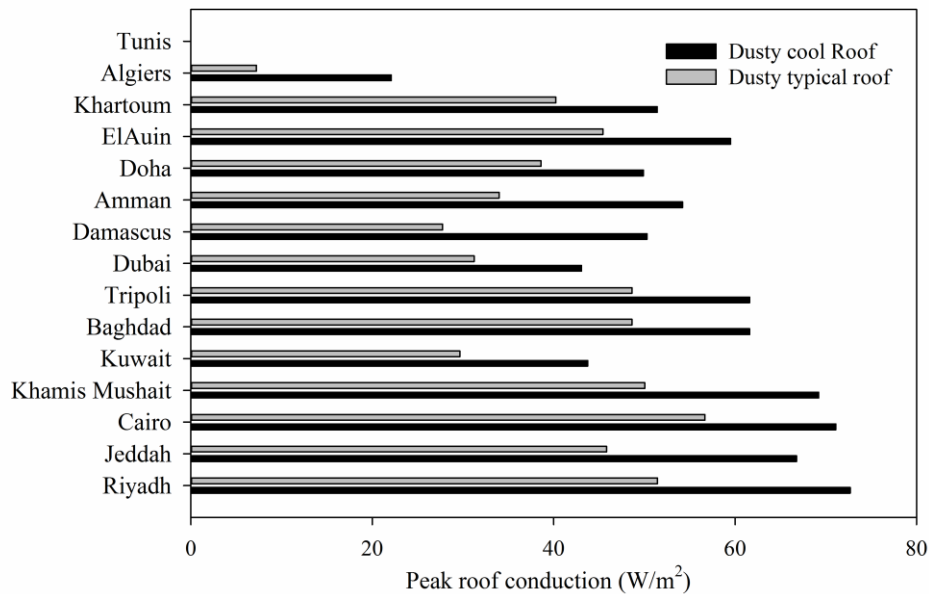
Figure 5.12 Predicted increase in peak roof conduction under cool (λ=0.2) and typical (λ=0.4) roofs due to dust accumulation with a U-value of 2.84 $W/m^2 K$

119

Table 5.3 Calculated annual cooling, annual heating, and peak roof conduction for cool, typical, and dusty roofs using three U-values and the corresponding percentages of annual cooling increasing and annual heating reduction

| | Roof U-values (W/m²K) | Cool Roof λ=0.2 | | | Typical Roof λ=0.4 | | | Dusty Roof λ=f(M) | | | Load Increase % | | | | | |
| | | a | b | c | a | b | c | a | b | c | Dusty roof (a) vs Cool roof (a) | Dusty Roof (b) vs Cool Roof (b) | Dusty Roof (c) vs Cool Roof (c) | Dusty Roof (a) vs Typical Roof (a) | Dusty Roof (b) vs Typical Roof (b) | Dusty Roof (b) vs Typical Roof (c) |
		Annual Cooling (kWh/m²)	Annual Heating (kWh/m²)	Peak Roof Cond.(W/m²)	Annual Cooling (kWh/m²)	Annual Heating (kWh/m²)	Peak Roof Cond.(W/m²)	Annual Cooling (kWh/m²)	Annual Heating (kWh/m²)	Peak Roof Cond.(W/m²)						
Riyadh	2.84	572.4	26.4	57	627.5	25.7	78	754.3	24.1	129	24	-9	56	17	-7	40
	1.7	537.2	19.6	38	574.1	19.3	52	657.6	18.3	85	18	-7	55	13	-5	39
	0.57	496.3	13.0	13	510.1	12.9	17	540.8	12.6	25	8	-3	49	6	-2	33
Jeddah	2.84	571.3	0.9	54	620.4	0.9	75	737.5	0.8	121	23	-13	55	16	-9	38
	1.7	537.4	0.6	32	570.4	0.6	50	647.4	0.5	79	17	-11	59	12	-8	37
	0.57	497.9	0.3	11	510.4	0.3	15	538.7	0.3	25	8	-5	58	5	-4	42
Cairo	2.84	269.9	52.9	36	307.4	51.2	50	397.0	48.2	107	32	-10	67	23	-6	53
	1.7	269.5	37.4	24	294.5	36.6	33	353.7	34.9	55	24	-7	57	17	-5	40
	0.57	271.3	20.9	08	280.7	20.7	11	302.6	20.3	20	10	-3	62	7	-2	47
Khamis Mushait	2.84	204.1	58.6	26	246.2	56.6	45	326.7	53.6	95	38	-9	73	25	-6	53
	1.7	209.0	39.2	15	237.3	38.2	26	290.7	36.6	54	28	-7	73	18	-4	52
	0.57	220.2	19.6	06	230.9	19.4	10	250.8	19.0	17	12	-3	67	8	-2	42
Kuwait	2.84	458.5	40.8	48	492.7	39.5	62	575.4	37.4	92	20	-9	48	14	-5	32
	1.7	444.9	28.8	31	467.6	28.1	38	521.9	26.9	60	15	-7	48	10	-4	37
	0.57	431.1	16.1	06	439.6	16.0	07	459.6	15.6	20	6	-3	67	4	-2	65
Baghdad	2.84	404.4	58.4	46	438.0	56.4	60	518.9	53.4	97	22	-9	52	16	-6	38
	1.7	396.6	43.3	30	419.1	42.2	41	472.6	40.3	64	16	-7	53	11	-5	37
	0.57	389.2	25.8	10	397.7	25.5	12	417.6	25.0	24	7	-3	57	5	-2	48

Tripoli	2.84	248.0	83.2	45	281.2	80.5	58	361.8	76.0	107	31	-9	58	22	-6	46
	1.7	246.5	62.2	28	268.7	60.7	38	321.8	58.0	58	23	-7	52	17	-5	35
	0.57	246.7	39.7	10	255.1	39.3	13	274.8	38.5	20	10	-3	48	7	-2	33
Dubai	2.84	452.0	6.8	43	487.4	6.6	55	555.1	6.2	86	19	-10	50	12	-6	36
	1.7	441.5	3.2	28	465.0	3.1	36	509.5	2.9	56	13	-8	50	9	-5	36
	0.57	430.5	0.7	10	439.2	0.7	13	455.6	0.7	19	6	-4	44	4	-3	29
Damascus	2.84	214.3	155.2	34	254.5	148.8	56	312.9	142.1	84	32	-9	60	19	-5	33
	1.7	213.6	122.8	20	240.8	118.9	38	279.5	114.7	56	24	-7	63	14	-4	33
	0.57	215.6	84.1	08	226.0	82.9	10	240.4	81.4	16	10	-3	53	6	-2	37
Amman	2.84	191.3	122.5	28	229.3	117.2	49	285.0	111.6	83	33	-10	66	20	-5	41
	1.7	194.9	93.9	19	220.7	90.8	33	257.8	87.4	49	24	-7	61	14	-4	34
	0.57	203.0	61.1	06	213.0	60.3	10	226.9	59.2	15	11	-3	60	6	-2	33
Doha	2.84	463.6	12.3	42	494.5	12.0	53	554.8	11.4	92	16	-8	54	11	-5	42
	1.7	451.1	7.6	27	471.5	7.4	35	511.2	7.1	49	12	-6	44	8	-4	29
	0.57	437.8	3.2	10	445.4	3.2	13	460.0	3.1	18	5	-3	44	3	-2	29
ElAuin	2.84	208.3	43.4	37	233.7	42.3	51	296.3	40.2	96	30	-8	62	21	-5	47
	1.7	213.0	30.1	22	229.8	29.6	30	271.0	28.4	63	21	-6	66	15	-4	53
	0.57	221.3	16.4	08	227.6	16.3	10	242.7	16.0	15	9	-3	46	6	-2	33
Khartoum	2.84	547.0	1.9	36	572.3	1.8	47	621.9	1.7	88	12	-13	59	8	-8	46
	1.7	531.2	0.9	24	547.8	0.9	31	580.4	0.8	58	8	-9	59	6	-6	46
	0.57	512.6	0.2	09	518.7	0.2	10	530.6	0.2	16	3	-4	45	2	-3	35
Algiers	2.84	165.2	113.6	33	195.0	109.7	48	209.9	108.2	55	21	-5	40	7	-1	13
	1.7	168.6	85.9	22	188.8	83.8	31	198.8	82.9	36	15	-4	40	5	-1	13
	0.57	175.3	56.8	06	183.0	56.3	08	186.7	56.0	09	6	-1	37	2	0	12
Tunis	2.84	186.4	98.5	35	213.7	95.2	47									
	1.7	188.2	74.5	23	206.5	72.7	31									
	0.57	192.8	48.8	07	199.8	48.3	10									

5.9. Conclusions

This paper endeavors to account for the accumulated dust impact on building roof thermal performance and heat gain. A new model is introduced in an effort to relate building exterior roof solar and thermal properties (absorptivity, reflectivity, and emissivity) to monthly averaged dust accumulation. In this study, the model is a primary function of accumulated dust, dust particle size, density, and packing factor. The NMMB online model was used to predict monthly averaged dust accumulation for the selected sites. The mathematical model was tested to evaluate its sensitivity to the model inputs: mean dust particle diameter and density.

Results showed that smaller dust particles and lower densities tend to cover more roof area, which results in a higher roof absorptivity. The results of the NMMB model were analyzed based on fifteen years of monthly averaged simulation results. The predicted monthly averaged accumulated dust for the studied sites varies between 1.3 and 73.8 g/m^2/month. The impact of dust accumulation on building roof thermal performance was estimated. It was found that dust accumulation reduced annual heating by 0.5 to 13.1 kWh/m^2/yr, while building annual cooling was increased by 44.7 to 181.1kWh/m^2/yr. For all the selected hot-dry locations, it is clear that annual heating reduction is insignificant compared to the greater increase in annual cooling. Finally, improved insulation resulted in improved performance for all roof systems.

The results of this work attempt to provide a physical understanding of accumulated dust impact and to improve the predictive capability of current building simulation models. The results also underscore the ability to implement the new proposed solar absorptivity model (equations 8 and 9) in current building simulation programs instead of using a fixed solar value for a yearly simulation, especially in hot-dry dusty climates or where dust exists. Expanding current building energy weather data to include dust accumulation will improve the accuracy of

122

energy calculation in hot-dry climates. It is furthermore recommended that a periodic dust

removal process could help reduce dust accumulation and sustain original roof solar properties.

In the Middle East and North Africa, the current traditional horizontal building roof design with

extended walls encourages dust accumulation. Alternatively, adopting a different roof design, a

sloped roof, would decrease dust accumulation and restore cost-effectiveness to the cool roof,

thereby reducing energy consumption and improving roof thermal performance.

5.10. References

[1] P. Berdahl, H. Akbari, R. Levinson, W.A. Miller, Weathering of roofing materials–an overview, Construction and Building Materials 22 (4) (2008) 423–433.

[2] H. Suehrcke, E.L. Peterson, N. Selby, Effect of roof solar reflectance on the building heat gain in a hot climate, Energy and Buildings 40 (12) (2008) 2224–2235.

[3] Cool Roof Rating Council (CRRC), 2014, http://coolroofs.org/products/.

[4] M. Sleiman, G. Ban-Weiss, H. E. Gilbert, D. François, P. Berdahl, T. W. Kirchstetter, H. Destaillats, R. Levinson, Soiling of building envelope surfaces and its effect on solar reflectance—Part I: Analysis of roofing product databases, Solar Energy Materials and Solar Cells 95 (12) (2011) 3385–3399.

[5] R.T.A. Prado, F.L. Ferreira, Measurement of albedo and analysis of its influence the surface temperature of building roof materials, Energy and Buildings 37 (4) (2005) 295–300.

[6] J. R. Simpson, E. G. McPherson, The effects of roof albedo modification on cooling loads of scale model residences in Tucson, Arizona, Energy and Buildings 25(2) (1997) 127–137.

[7] S. E. Bretz, H. Akbari, Long-term performance of high-albedo roof coatings, Energy and Buildings 25 (2) (1997) 159–167.

[8] A. Synnefa, M. Santamouris, H. Akbari, Estimating the effect of using cool coatings on energy loads and thermal comfort in residential buildings in various climatic conditions, Energy and Buildings 39 (11) (2007) 1167–1174.

[9]   H. Akbari, S. Bretz, D.M. Kurn, J. Hanford, Peak power and cooling energy savings of high-albedo roofs, Energy and Buildings 25 (2) (1997) 117–126.

[10] P. Berdahl, S.E. Bretz, Preliminary survey of the solar reflectance of cool roofing materials, Energy and Buildings 25 (2) (1997) 149–158.

[11] C.K. Cheung, R.J. Fuller, M.B. Luther, Energy-efficient envelope design for high-rise apartments, Energy and Buildings 37 (1) (2005) 37–48.

[12] M. Dabaieh, O. Wanas, M.A. Hegazy, E. Johansson, Reducing cooling demands in a hot dry climate: A simulation study for non-insulated passive cool roof thermal performance in residential buildings, Energy and Buildings 89 (2015) 142–152.

[13] J. P. Brito Filho, TV Oliveira Santos, Thermal analysis of roofs with thermal insulation layer and reflective coatings in subtropical and equatorial climate regions in Brazil, Energy and Buildings 84 (2014) 466–474.

[14] V. Costanzo, G. Evola, L. Marletta, A. Gagliano, Proper evaluation of the external convective heat transfer for the thermal analysis of cool roofs, Energy and Buildings 77 (2014) 467–477.

[15] C. Pérez, K. Haustein, Z. Janjic, O. Jorba, N. Huneeus, J.M. Baldasano, T. Black, S. Nickovic, R.L. Miller, J.P. Perlwitz, M. Schulz, M. Thomson, Atmospheric dust modeling from meso to global scales with the online NMMB/BSC-Dust model–Part 1: Model description, annual simulations and evaluation, Atmospheric Chemistry and Physics 11 (24) (2011) 13001–13027.

[16] G.E. El-Desoky, M.A. Aboul-Soud, Z.A. Al-Othman, M.Habila, J.P. Giesy, Seasonal concentrations of lead in outdoor and indoor dust and blood of children in Riyadh, Saudi Arabia, Environmental geochemistry and health 36 (3) (2014) 583–593.

[17] A.S. Modaihsh, M.O. Mahjou, Falling dust characteristics in Riyadh city, Saudi Arabia during Winter months, APCBEE Procedia 5 (2013) 50–58.

[18] M. Malakootian, M. Ghiasseddin, H. Akabari, N.A. Jafarzadeh, H. Fard, Urban Dust Fall Concentration and Its Properties in Kerman City, Iran, Health Scope 4 (2013) 195–201.

[19] Z.Y. Offer, D. Goossens, Thirteen years of aeolian dust dynamics in a desert region (Negev desert, Israel): analysis of horizontal and vertical dust flux, vertical dust distribution and dust grain size, Journal of arid environments 57 (1) (2004) 117–140.

[20] Z.Y. Offer, D. Goossens, Ten years of aeolian dust dynamics in a desert region (Negev desert, Israel): analysis of airborne dust concentration, dust accumulation and the high-magnitude dust events, Journal of arid environments 47 (2) (2001) 211–249.

[21] G.H. McTainsh, W.G. Nickling, A.W. Lynch, Dust deposition and particle size in Mali, West Africa, Catena 29 (3) (1997) 307–322.

[22] G.W. Crabtree, Dustfall on the southern high plains of Texas, Doctoral dissertation, Texas Tech University, 2005.

[23] T.L. Péwé, Desert Dust: Characteristics and rates of deposition in central Arizona, Geological Society of America Special Papers 186 (1981) 169–190.

[24] S. Nickovic, G. Kallos, A. Papadopoulos, O. Kakaliagou, A model for prediction of desert dust cycle in the atmosphere, Journal of Geophysical Research: Atmospheres (1984–2012) 106 (D16) (2001) 18113–18129.

[25] G.A. Grell, S.E. Peckham, R. Schmitz, S.A. McKeen, G. Frost, W.C. Skamarock, B. Eder, Fully coupled "online" chemistry within the WRF model, Atmospheric Environment 39 (37) (2005) 6957–6975.

[26] G. Kallos, S. Nickovic, A. Papadopoulos, D. Jovic, O. Kakaliagou, N. Misirlis, L. Boukas, N. Mitikou, G. Sakelaridis, J. Papageorgiou, E. Anadranistakis, M. Manousakis, The Regional Weather Forecasting System SKIRON: An Overview, Proceedings of the symposium on regional weather prediction on parallel computer environments 15(1997) 109–123.

[27] H.L. Noboa, Influence of dust on the emissivity of radiant barriers, Doctoral dissertation, Texas A&M University, 1991.

[28] H.L. Noboa, The influence of dust on the absorptivity of radiant barriers, Doctoral dissertation, Texas A&M University, 1993.

[29] A.Y. Al-Hasan, A new correlation for direct beam solar radiation received by photovoltaic panel with sand dust accumulated on its surface, Solar Energy 63 (5) (1998) 323–333.

[30] R. Williams, The Geometrical Foundation of Natural Structure: A Source Book of Design, Dover, New York, 1979.

[31] W. Slinn, Predictions for particle deposition to vegetative canopies, Atmospheric Environment 16 (7) (1982) 1785–1794.

[32] J.F. Kok, E.J. Parteli, T.I. Michaels, D.B. Karam, The physics of wind-blown sand and dust, Reports on Progress in Physics no.106901, 75, 2012.

[33] L. Zhang, S. Gong, J. Padro, L. Barrie, A size-segregated particle dry deposition scheme for an atmospheric aerosol module, Atmospheric Environment 35 (3) (2001) 549–560.

[34] D. Goossens, J.L. Rajot, Techniques to measure the dry aeolian deposition of dust in arid and semi-arid landscapes: a comparative study in West Niger, Earth Surface Processes and Landforms 33 (2) (2008) 178–195.

[35] DOE, EnergyPlus Engineering Document, Version 8.2., U.S. Department of Energy, Washington, DC, 2014.

[36] K. Haustein, C. Pérez, J. M. Baldasano, O. Jorba, S. Basart, R.L. Miller, Z. Janjic, T. Black, S. Nickovic, M.C. Todd, R. Washington, D. Müller, M. Tesche, , B. Weinzierl, M. Esselborn, A. Schladitz, Atmospheric dust modeling from meso to global scales with the online NMMB/BSC-Dust model–Part 2: Experimental campaigns in Northern Africa, Atmos. Chem. Phys. 12 (6) (2012) 2933–2958.

[37] A.M. Al-Dousari, J. Al-Awadhi, Dust fallout in northern Kuwait, major sources and characteristics, Kuwait Journal of Science, 39 (2A) (2012) 171–187.

[38] DOE, eQUEST the Quick Energy Simulation Tool, Version 3.65, U.S. Department of Energy, 2014.

[39] S. Algarni, D. Nutter, Geospatial Representation of the Residential Energy Use in Saudi Arabia. Proceedings of the 2013 ASME Early Career Technical Conference (ECTC), April 4–6, Tulsa, Oklahoma, USA, 2013.

Appendix 3: Nomenclature of Chapter 5

I_{solar}	= solar flux, (W/m^2)
T_a	= ambient air temperature, (K)
T_s	= outside surface temperature, (K)
T_{sky}	= sky effective temperature, (K)
T_{set}	= indoor set point temperature, (K)
T_{in}	= inside surface temperature, (K)
T_s	= outside surface temperature, (K)
h_{out}	= outside convection heat transfer coefficient, (W/m^{2}K)
h_{in}	= inside combined heat transfer coefficient, (W/m^{2}K)
A	= a percentage of unit area covered by dust
A_{dust}	= roof area covered by dust, (m^2)
A_{roof}	= total roof area, (m^2)
F	= shape factor
f	= packing factor
M	= accumulated dust, (kg/m^2)
N	= number of dust particle
d_p	= mean dust diameter, (m)
r_p	= mean dust radius, (m)
V_p	= dust particle volume, (m^3)
Greek	
β	= a soiling resistance
ε	= thermal emissivity
λ	= solar absorptivity
$\lambda_{new\ roof}$	= new roof solar absorptivity
λ_{dust}	= dust solar absorptivity
ρ	= dust density, (kg/m^3)
σ	= Stefan Boltzmann constant, (W/m^{2}K^4)

6. Conclusion

This study's research objective was to better understand and account for the influence of radiant transient factors such as sky long wave radiation exchange and atmospheric aerosols, with an effort to improve radiative predictive capabilities, which are especially important for hot and dry climates under clean, cloudy, and dusty sky conditions. To that end, one must first, gain an understanding of building energy use and the influence of various energy-related building and system factors. Then, to better quantify the influence of sky long wave radiation exchange on a building's external surface, sky effective temperature models were comprehensively reviewed. Consequently, the influence of transient factors including sky long wave radiation exchange and dust accumulation on buildings were investigated, resulting in improved radiative predictive capabilities, especially important for hot and dry climates under different sky conditions including clear, cloudy, and dusty.

The most significant results in this study are summarized as follows:

1) A focus toward residential building improvements in hot-dry climate is necessary. This is due to the fact that the majority of annual energy use and greatest opportunity for air-conditioning load reduction was identified to be in residential buildings, located in hot- dry climates.

2) Although sky long wave exchange is an effective building energy balance element, it was found that the simplest sky models were the ones most often utilized. Therefore, there is a need for additional data and research that captures additional variables and leads to better sky temperature predictions.

3) A new dusty sky temperature model was introduced as a function of atmospheric aerosol optical depth to better account for dust impact on sky temperature prediction.

4) The recommended sky temperature models, along with their cloudy and dusty sky factors, for a hot-dry site such as Riyadh, Saudi Arabia, are given. These models can be broadly used for sites which have similar sky and climatic conditions.

5) The effect of sky radiative cooling on building roofs was investigated under clear, cloudy, and dusty conditions for extreme hot and dry climates located in several international sites. Similar results were found in the selected global hot-dry sites. For example, in Saudi Aribia, a daily mean of clear sky cooling around 2645 W-hr/m^2 and 2385 W-hr/m^2 was estimated for July and January, respectively. Depending on severity, the average sky cooling heat exchange was found to range between 436 W-hr/m^2 and 1636 W-hr/m^2 for dust storm and scattered cloudy sky conditions, respectively.

6) A new absorptivity model was introduced in an effort to relate a building's exterior roof solar and thermal properties (absorptivity, reflectivity, and emissivity) to monthly averaged dust accumulation.

7) Results from using the new roof absorptivity model demonstrated an annual cooling space increase of 44.7 to 181.1kWh/m^2/yr due to dust high absorptivity. A reduction in the building's heating load was found to be 0.5-13.1 kWh/m^2/yr; therefore, it is clear that annual heating reduction is insignificant compared to the greater increase in annual cooling needs.

The results of this dissertation are an effort to provide a physical understanding of sky long wave radiation exchange interface and dust accumulation impact on building energy usage. Also, the results seek to improve the predictive capability of current building simulation models for an accurate estimation of building annual load sizing.